Nuclear Magnetic Relaxation Dispersion Investigations of Molecular Dynamics in Soft Matter

A Thesis Submitted to
University of Hyderabad
for the award of the Degree of

DOCTOR OF PHILOSOPHY
in Physics

by

M. TRIVIKRAM RAO

School of Physics
University of Hyderabad
Hyderabad - 500046, India

December, 2008

Dedicated to

My Parents

Declaration

I, M. Trivikram Rao, hereby declare that the work presented in this thesis has been carried out by me under the supervision of Prof. V.S.S. Sastry, School of physics, University of Hyderabad, Hyderabad, India, as per the Ph.D ordinances of the University. I declare, to the best of my knowledge, that no part of this thesis has been submitted for the award of a research degree of any other University.

Molugu Trivikram Rao,
Registration No: 02PHPH01.

Certificate

This is to certify that the thesis work entitled **Nuclear Magnetic Relaxation Dispersion Studies of Molecular Dynamics in Soft Matter** being submitted to the University of Hyderabad by **M. Trivikram Rao** (Reg. No. 02PHPH01), for the award of the degree of Doctor of Philosophy in Physics, is a record of *bonafide* work carried out by him under my supervision.

The matter embodied in this report has not been submitted to any other University or Institution for the award of any degree or diploma.

Supervisor,

Dean,

Abstract

The work reported in this thesis is concerned with the investigation of the effect of details of molecular structure on the dynamic processes in liquid crystals and also with denaturant-protein interactions in water solutions through a study of dynamic processes of water molecules. These systems belong to the general class of complex fluids, and the slow time scale of relevant motions is very conveniently accessed through frequency dispersion measurements on the nuclear relaxation processes using field cycling NMR methods.

Role of order director fluctuations in influencing the stability of the nematic phase against the formation of a low temperature layered mesogenic structure has been well recognized. Appearance of differing polymorphism in a given homologous series of liquid crystal system, with only subtle changes in the molecular structure, has been a subject of considerable importance from the point of molecular engineering for application purposes. Investigation of resultant molecular processes, including the collective dynamics, in a well chosen set of such systems with specific focus on a detailed modeling of the relevant dynamics has been made possible with the advent of new technologies to probe relaxation phenomena at very low Larmor frequencies. Such experimentation provides the required dynamic range to attempt the above study over a wide frequency range. Thus the first part of the thesis deals with the experimental studies on two liquid crystal systems.

Another complex phenomena which could be made accessible through such low frequency dispersion studies on spin-lattice and spin-spin relaxation processes has been the dynamics of water molecules which contain large and relatively very slowly tumbling guest molecules, like for example proteins. The dynamics of a given water molecule depends on the region in the solution that it is sampling during the time of observation. In this case it is customary to distinguish three types of dynamic environments that are accessible to the water molecules: water in the bulk with very fast and isotropic dynamics, water meandering near the surface with a restricted dynamics, and finally some water molecules which are captured inside a protein with a certain probability, and experience a vastly different, slow, dynamic environment over

residence times small compared to the time scale of observation. Field cycling NMR techniques have been recently found very valuable in understanding the subtleties of such motions. What is more interesting however is the fact that any changes that can be effected gently to the protein structure, like for example through the introduction of a denaturant, is expected to have a profound effect on the low frequency dispersion of the nuclear relaxation rate. The second part of the thesis reports work on two protein-water systems under controlled perturbation through the introduction of a denaturant.

The thesis is organized as follows: the first Chapter provides a brief introduction to various types of liquid crystals, their physical properties and applications. Introduction to the protein structure also discussed in this chapter. The second chapter provides a brief introduction of nuclear magnetic relaxation theory to the two systems mentioned above, introducing the underlying microscopic dynamic models and relating them to the experimental observables. The third chapter recounts briefly the NMR methodology to appreciate the relaxation measurements, with a summary of the field cycling technique and the details of the instruments used in the investigations.

The next two Chapters deal with two liquid crystal systems. Earlier NMR work on phase diagrams of mixtures of liquid crystals (which do not have inherent nematic phases) with induced nematic phase in certain regions of intermediate relative concentration showed that the molecular organization reported in these nematic phases is qualitatively different. The differences show up in the anisotropy (with respect to their sizes in different directions) of the nematic clusters that form in the medium, and their temperature dependence. Keeping this view, three members in the homologous series (four samples of butyloxy benzylidene alkylanilines 4O.m: 4O.2, 4O.3, 4O.4 and a mixture of 4O.2 + 4O.4) were studied. The frequency dispersion of spin-lattice relaxation of ^{1}H is collected (dispersion profile) as a function of temperature in the nematic region, including a few points just below the nematic-isotropic transition temperature. The focus of the analysis is to figure out the dominant molecular mechanism from among the different contributions relevant in these time scales: low frequency collective modes of director fluctuations, self-diffusion of the molecules, individual molecular reorientations, and possibly diffusion assisted orientation fluctuations. The model for taking into account director fluctuations explicitly incorporates the three elastic coefficients and attempts at estimating the lower and upper cut-off frequencies, and hence the wave lengths, of the available collective modes in the system. The analysis shows that 4O.3 system with no underlying smectic phase is qualitatively different showing the behaviour of what is reported earlier as frustrated

nematic system, with isotropic nematic clusters without temperature dependence. This is to be contrasted with the other members, below and above in the homologous series, with underlying layered structure. This work is reported in the fourth chapter.

The fifth chapter attempts at a different application of field cycling relaxometry to a recent liquid crystal systems (Singly fluorinated iso-thiocianato tolanes : 4OTOLFm and 4OFTOL). These systems have been reported to be well suited for applications due to their low viscosity and wide nematic temperature range, apart from other optical properties. From NMR point of view, the interest in the system arises from the fact that the molecule has a lone ^{19}F nucleus and its relaxation mechanism differs from the dipolar mechanism of the protons. It has been known that in simple fluids the spin relaxation of this nucleus is mediated by its strong spin-rotation coupling. Dispersion profile of such a nucleus in liquid crystal has not been reported before, and one could on general principles expect that its dispersion profile naturally would be different, being sensitive to possibly different molecular mechanisms which modulate this specific interaction on the time scale of experiment. While providing contrasting dispersion behaviour compared to proton relaxation measurements in terms of the novel mechanism of relaxation in operation, the conclusions from the two different studies could provide a richer understanding of the dynamics in the medium. With this motivation, ^{19}F and ^{1}H relaxation dispersions were made on the liquid crystal system 4OTF in the isotropic phase at different temperatures. While the proton dispersions indicate the known and reported behaviour compatible with isotropic phase, fluorine dispersions show the signatures of spin-rotation coupling (increase in the relaxation rate with increase in temperature), a strong dispersion in the sub-MHz region (which is normally absent in proton studies in this phase), and evidence of hetero-nuclear coupling of fluorine with proton at low enough frequencies due to overlapping line-widths which manifest as sudden increase in the relaxation rates at very low frequencies. These studies are also supplemented with detailed temperature dependence measurement of fluorine relaxation rates at different low frequencies. The conclusions of this study are reported in this Chapter.

Studies on denaturant-protein interactions in two protein-water systems are reported in the sixth Chapter. The two proteins, Lysozyme and Bovine Serum Albumin (BSA), are chosen due to different considerations. In the first case, reasonable understanding of the nature and structure of protein, including an estimate of the 'integral waters' that reside in this protein are known. This would enable quantitative evaluation of the contributions from different mechanisms and provides a basis for comparison with other such studies. The second protein is chosen for its size, and hence its contrasting molecular dynamics in the solution. Dispersions are

recorded with varying concentration of a denaturing agent, guanidine hydrogen chloride (GdnHCl) at a fixed temperature. While the bulk and surface water molecules provide differing, but frequency independent, contributions to the observed relaxation rate in the frequency range of the NMR experiment, the dispersion in the sub-MHz region arises due to the contribution coming from this dynamic process experienced by the integral water molecules during their residence time within the protein. The idea of introducing the denaturant is to try to destabilize the tertiary structure of the protein and hence perturb this dynamics. If the destabilization process is to be visualized as a monotonic process with increase in the denaturant concentration, then one should expect that the dispersion profile of the protons at the very low frequencies should gradually decrease and the dispersion should eventually disappear as the process of destabilization is complete. While this proved to be the ultimate result, as expected, the response of the system to the introduction of small amounts of the denaturant is however is different and interesting. The dispersion becomes more pronounced at low concentrations of the denaturant, thereby indicating that the tertiary structure of the protein is more stabilized. It seems to require a critical threshold of denaturant concentration before the tertiary structure of the protein starts getting destabilized. Similar behaviour is also observed with the bigger protein. These results are interpreted as due to the initial stabilization of the tertiary structure of the protein due to the denaturant-protein polar interactions, as a consequence of which the internal orientational disorder of the integral water molecules seem to decrease.

The final Chapter concludes the thesis with a summary of salient observations arising from this experimental work with regard to role of underlying smectic phases on the nematic organizations in a few structurally related liquid crystals, new information available in such systems by probing with nuclei having a differing relaxation mechanism, role of denaturants in initial stabilization of proteins studied, and finally an appreciation of nuclear magnetic relaxation dispersion study as a useful, and sometimes unique, tool to probe environments with separated time scales experienced by molecules in their dynamic evolution in a complex fluid.

Acknowledgements

Contents

List of Figures

List of Tables

Chapter 1

Introduction to Liquid Crystals and Proteins

1.1 Introduction

Soft matter represents materials which are neither simple liquids nor solids, such materials are familiar in everyday life: eg. glues, paints, soaps, much of the food we eat and indeed most of the tissue of our body itself shares the qualities of soft matter. In William Burrough's words we are **soft-machines** *(Burrough 1961)*. These materials include collidal dispersions, where sub-μm particles are dispersed in another liquid, polymer melts, solutions in which the size and connectivity of the molecules lead to strikingly new properties such as viscoelasticity (eg. protein solutions), and liquid crystals where an anisotropic molecular shape leads to states with a variable degree of ordering intermediate between a crystalline solid and a liquid. Many features that they share, such as long-range ordering, molecular aggregation or self-association, and anisotropic molecular interactions make it worth considering them as in the same class.

Study of molecular processes is a very important step in understanding the intermolecular potentials, collective behaviour of the medium as well as factors responsible for the onset of new thermodynamic phases, etc. There are several methods to study the dynamic behaviour including magnetic resonance, dielectric measurements, diffraction, dynamic light scattering experiments, etc. Applications of a specific technique depend on the dynamic aspects of interest, and important time scale of occurrence. Magnetic resonance and relaxation studies are one of the popular methodologies since the dynamics can be probed either by nuclear or electron spin probes, and due to the resonant nature of the probe, one can precisely measure the estimates of parameters as a function of specific time window. In this connection, with the advent of recent new methodology, it has been possible to extend the time

window of NMR relaxation studies over several orders of frequency (10^3 - 10^8 Hz). This range is particularly interesting and suitable for studying many characteristic molecular processes that occur in soft materials, and the present work is concerned with the nuclear spin-lattice relaxation dispersion over a range of resonance frequencies, and at different temperatures, in chosen liquid crystals and protein solutions. In this context, this chapter gives brief introduction to liquid crystals and proteins in next two sections.

1.2 Liquid crystals

1.2.1 Mesomorphic Behavior

Liquid crystals are substances that exhibit a phase of matter that has properties between conventional liquids, and solid crystals. As a rule a substance in this state is strongly anisotropic in some of its properties and yet exhibits a certain degree of fluidity, which in some cases may be comparable to that of an ordinary liquid. For instance, a liquid crystal may flow like a liquid, but have the molecules in the liquid arranged and/or oriented in a crystal-like way. The essential characteristic is the presence of orientational order of the non-spherical molecules, while in addition the positional order of the centers of mass is either absent or reduced. Liquid crystals at a primary level are classified into thermotropic and lyotropic. Single component systems that show mesomorphic behavior in a definite temperature range are called thermotropic liquid crystals whereas lyotropic liquid crystals are multi-component (two or more) systems. They are formed in mixtures of amphiphilic molecules and polar solvents like water. Amphiphiles tend to aggregate so that the polar groups occupy the interface towards solvent. Small aggregates with dimensions comparable to the molecular length are often spherical in shape and exist in micellar solutions. The formation of infinitely extended aggregates or lamellas is characteristic for the most common lyotropic liquid crystalline phases. Thermotropic liquid crystals, depending on the shape of the molecule, are further classified into calamatic (rod like) and discotic liquid crystals. The present work on liquid crystals deals with thermotropics formed by elongated molecules. Their classification, physical properties and applications are discussed in this Chapter.

Mesophases of rod like molecules are classified broadly into three types: nematic, cholesteric and smectic. The nematic liquid crystal has a high degree of long range orientational order of the molecules, but no long range positional order. It is similar to ordinary isotropic liquid except that its molecules are spontaneously oriented with respect to their long axes. The preferred axis of this orientation is referred to

as the director and represented by a (headless) unit vector. This medium is optically birefringent and several physical properties such as diamagnetic susceptibility, dielectric constant and refractive index, are anisotropic. Where in anisotropy is a function of the orientational order parameter of the molecules and is defined as S=$\frac{1}{2}$ $< 3\cos^2\theta - 1 >$, where θ is the angle between the long molecular axis and the director. The angular brackets denote the statistical average. S decreases with increase of temperature in nematics and has a value in the range 0.7 to 0.3. The lack of long range translational order allows the nematic to flow relatively easily. This unique combination of fluidity and high anisotropy plays a key role in many applications. Liquid crystals can also exhibit biaxial symmetry in the nematic phase, meaning that in addition to orienting along their long axis, they also orient along a secondary axis, breaking the rotational symmetry of the system around the director *(Freiser 1970, Alben 1973)*. Biaxial nematics are usually found in liquid crystals with banana shaped molecules. Cholesteric liquid crystals are nematics composed of optically active molecules. As a result the structure acquires a spontaneous twist about an axis perpendicular to the director. The pitch is typically in the range of wavelength of visible light, and thus owing to the periodicity in the structure the cholesteric gives raise to intense reflections of light whose wave length depends on the angle of incidence.

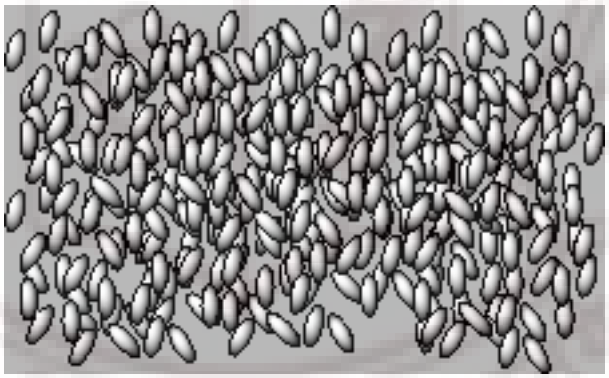

Figure 1.1: Molecular arrangement in a typical nematic liquid crystalline phase.

Below their clearing point anomalous phases appear in many cholesterics which are collectively known as blue phases (BP). In chiral compounds with sufficiently high twist, up to three distinct blue phases appear. The two low-temperature phases, blue phase I (BP I) and blue phase II (BP II), have cubic symmetry, while the highest temperature phase, blue phase III (BP III), appears to be amorphous. These are non-ferroelectric chiral phases with applications in electro-optic switching. *(Collings and Patel 1997, Stegemeyer et al. 1986, Wright and Mermin (1989))*.

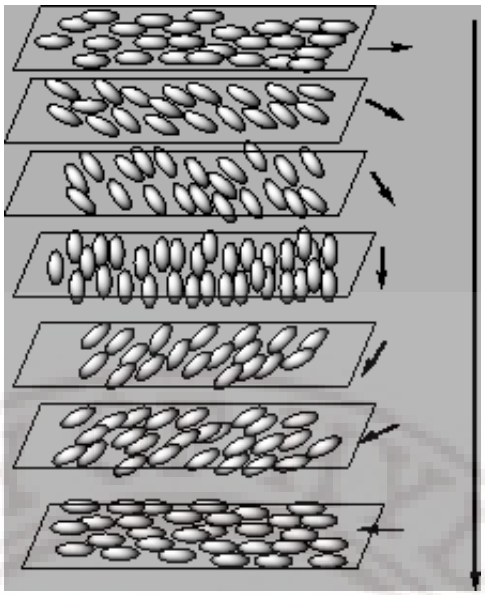

Figure 1.2: Molecular arrangement in a cholesteric liquid crystalline phase

Smectic liquid crystals have layered structure i.e the molecular centres are on average arranged in equidistant planes. Depending on the molecular arrangement there are different sub-classes of smectic liquid crystals (S_A to S_H). In S_A phase the molecules are upright in each layer with the centers randomly spaced in a liquid-like fashion. In S_B phase the molecules are upright but the centers have long range positional order. S_C phase is a tilted form of S_A. S_D mesophase is described as cubic arrangement of rods and hence does not form layers. Orthorhombic packing of molecular centers with upright molecules is named S_E. If the molecules are tilted with pseudo hexagonal packed arrangement, the phase is called S_F. Tilted S_E is S_G and tilted S_B is S_H. Higher order smectics also observed in polymeric liquid crystals (eg. S_I, S_J, S_K, S_L) *(Singh 2000)*. In these smectic phases rotations around the long-molecular axes is strongly hindered. They posses three dimensional long range order and hence known as crystalline smectics. Certain compounds show a second nematic phase that occurs below the smectic phase, and is called re-entrant nematic phase. Apart from these, several polymer systems, that are macro-molecules, also exhibit liquid crystalline properties.

A brief overview of the consequences of molecular anisotropy on various physical properties of liquid crystals is presented below.

1.2.1.1 Anisotropic Physical Properties

The orientational order existing in the liquid crystalline phases introduces anisotropy in the mesomorphic behaviour of the system, manifesting in the elastic, electric, magnetic and optical properties of a mesogenic material. Applications of thermotropic

liquid crystals rely on their anisotropic physical properties and their response to the external variables (eg. temperature, electric or magnetic fieds). The dielectric, diamagnetic, optical, elastic and viscous coefficients are hence the important indicators of anisotropic properties useful in evaluating a LC system for a specific application.

1.2.1.2 Birefringence (Δn)

A mono-domain specimen of nematic medium is optically uniaxial and strongly birefringent. This optical anisotropy, or birefringence, is dependent on wavelength and temperature and defined by the equation

$$\Delta n = n_e - n_0 = n_{\parallel} - n_{\perp}$$

where n_o and n_e are ordinary and extraordinary refractive indices, correspondingly $n_{\perp}$ and $n_{\parallel}$ are the components parallel and perpendicular to the director respectively. For rod-like molecules $n_{\parallel} > n_{\perp}$; Δn is therefore, positive and can have values between 0.02 to 0.4. In the case of discotic molecules $n_{\parallel} < n_{\perp}$ and thus have negative birefringence. In case of chiral nematics the optic axis coincides with the axix of helix which is perpendicular to the local director; $n_e = n_{\perp}$, and n_o is a function of both $n_{\parallel}$ and $n_{\perp}$ and depends on the relative magnitude of the wavelength with respect to the pitch. Usually it happens that $n_{\parallel} < n_{\perp}$, and hence chiral nematics have a negative birefringence. For biaxial liquid crystals, all 3 principal refractive indices are different, but usually one (n_3) is significantly greater (or less) than the other two, and the uniaxial birefringence can be defined as

$$\Delta n = n_3 - \frac{1}{2}(n_2 + n_1)$$

and the biaxiality is $\delta\Delta n = n_2 - n_1$. The value of Δn depends on the structure of the compound, and for a given compound it decreases appreciably with raise of temperature. If the molecules are highly conjugated and made up of groups having strong anisotropy in polarizability Δn is larger. The measurements of the refractive indices are conveniently carried out by the use of Abbe's double prism method.

1.2.1.3 Dielectric Anisotropy ($\Delta\epsilon$)

The response of matter to the application of an electric field is charecterized by dielectric permitivity, ϵ. For a uniaxial liquid crystalline phase, choosing z-axis along the director, the principal elements of ϵ are $\epsilon_{zz} = \epsilon_{\parallel}$ and $\epsilon_{xx} = \epsilon_{yy} = \epsilon_{\perp}$. Then the anisotropy of dielectric permitivity is defined as

$$\Delta\epsilon = \epsilon_{\parallel} - \epsilon_{\perp}$$

If the molecule is non polar or if the net dipolar moment (μ) is zero, $\Delta\epsilon$ arises entirely from the anisotropy of the low frequency molecular polarizability and has a positive value normally between 0.5 and 1. The presence of a strong polar group with μ pointing along the long molecular axis enhances $\Delta\epsilon$. The component of μ perpendicular to the length of the molecule has a dielectric relaxation frequency in the microwave region, arising from the rapid rotation of the molecule about its long axis. On the other hand, the parallel component of μ has to work against the nematic orienting potential as well as the viscous torque, and the relaxation frequency comes down considerably, usually to the MHz region, and in some cases to the kHz region too. Hence $\Delta\epsilon$ drops to a low value beyond certain frequency ν_o, and in some cases even changes sign from a positive to a negative value beyond ν_o. This proves to be a useful property in multiplexed display devices.

1.2.1.4 Diamagnetic Anisotropy ($\Delta\chi$)

The liquid crystals are diamagnetic like most organic materials. The diamagnetism exhibited by these systems is the result of additive contributions of the magnetic properties of the single molecular components. The diamagnetic properties of uniaxial mesophases can be described by the two susceptibilities $\chi_{\parallel}$ and $\chi_{\perp}$, which are the resulting susceptibilities when the magnetic field is applied parallel and perpendicular to the director, respectively. The magnitude of anisotropy in the diamagnetic susceptibility is defined as

$$\Delta\chi = \chi_{\parallel} - \chi_{\perp}$$

The diamagnetic anisotropy of all liquid crystals having an aromatic ring system has been found to be positive and of the order of magnitude 10^{-7} (SI units). The magnitude is found to decrease with every benzene ring which is substituted by a cyclohexane or cyclohexane derivative ring. A negative anisotropy is observed in purely cycloaliphatic liquid crystals. The diamagnetic anisotropy can be used as an order parameter to describe the degree of orientational order of a mesophase.

1.2.1.5 Viscous Properties

The nematic liquid crystal material often appears to flow as easily as a simple Newtonian liquid of similar molecular structure. However, the situation becomes very complicated when the state of molecular alignment in the nematic phase is taken into consideration. In a liquid crystal the viscosity exhibits an anisotropy. For a complete characterization of a nematic liquid crystal, five different viscosity coefficients are necessary *(Leslie 1968.)*. Three of these represent conventional shear flow with different arrangements of the director to the shear direction, while the other

two take director rotation or coupling between the director and the flow pattern into account. When an oriented nematic liquid crystal is placed between two plates which are then sheared, following relevant cases can be observed

η_1 : The director is perpendicular to the flow pattern and parallel to the velocity gradient,

η_2 : The director is parallel to the flow pattern and perpendicular to the velocity gradient,

η_3 : The director is perpendicular to both the flow pattern and the velocity gradient.

These three viscosity coefficients are known as the Miesowicz viscosities. They are difficult to determine. In addition to the coefficients η_1 and η_2 which are antisymmetric with regard to the flow direction and the velocity gradient, a symmetric viscosity coefficient η_{12} is also possible. This refers to the case when director is suspended at an angle of 45° with both the flow pattern and the velocity gradient.

When a rotation of the molecule around an axis perpendicular to the director takes place, an additional viscosity coefficient γ_1 known as rotational viscosity, results. This coefficient is very important when the reorientation of the director in an electric or magnetic field is discussed, for example in determining the on and off times of display devices. In liquid crystal display (LCD) the switching time τ is approximately proportional to $\gamma_1 d^2$ with d representing the cell spacing. The value of γ_1 for technically important nematic materials is found to be in the range 0.02 poise to about 0.5 poise.

For most practical purposes an appropriate average value $\overline{\eta}$ is adequate. As a rule, the longer and stiffer the molecule the greater the value of $\overline{\eta}$. It has a high value for esters and a relatively low value for the biphenyls and an even lower value for the phenyl cyclohexanes *(Pohl et al. 1977)* and cyclohexyl cyclohexanes *(Pohl et al. 1978)*. The value decreases rapidly with increase in temperature.

1.2.1.6 Conductivity Anisotropy ($\Delta\sigma$)

Nematogenic molecules are electrically neutral. However, the presence of ionic impurities, accidentally or deliberately introduced in the liquid crystal, makes the medium electrically conducting. Because of the anisotropic viscosity of the liquid crystal, the ions can flow more easily along the director than in a direction perpendicular to it. The conductivity anisotropy, $\Delta\sigma$ is positive, and the value of $\frac{\sigma_\parallel}{\sigma_\perp}$, is usually about 1.4. The actual value of σ depends on the nature of the liquid crystal, the nature

and concentration of the dopants, and the temperature. The electrical conductivity is measured using the standard methods employed for the dielectric liquids in general. However, these measurements are not trivial due to the problems arising, for example, from electrode reactions, double layers leading to electrode polarization, separation of displacement and resistive currents, etc. The precise measurements of the electrical conductivity of liquid crystals with well controlled concentrations of impurity ions are relatively scarce. No large variations of the ratio $\frac{\sigma_\parallel}{\sigma_\perp}$ are observed for the nematics. Since the anisotropy of the conductivity is the driving force for the hydrodynamic instabilities of a nematic layer in an electric field, this ratio is very important. If the liquid crystal shows both smectic and nematic phases the cybotactic groups build up in the nematic phase close to the transition. In this regime $\Delta\sigma$ changes sign and becomes negative.

1.2.1.7 Elasticity

Nematic liquid crystals exhibit curvature elasticity, i.e. a restoring torque comes into play if the local director changes its orientation at a given point. There are three fundamental types of distortions: splay, twist, and bend *(de Gennes 1974, Priestly et al. 1975)*. These are illustrated in Fig. 1.3. The corresponding curvature elastic constants are denoted by K_1, K_2, and K_3 (Frank elastic constants) *(Frank 1958)*respectively. The free energy density may be approximated a quadratic function of curvature strains in which the analogues of elastic moduli appear as coefficients. The elastic free-energy for the uniaxial nematics can be written as

$$F = \frac{1}{2}\left[K_1\left(\nabla\cdot\hat{n}\right)^2 + K_2\left(\hat{n}\cdot\nabla\times\hat{n}\right)^2 + K_3\left(\hat{n}\times\nabla\times\hat{n}\right)^2\right]$$

The units of K_i are dynes. For normal nematics, the value is around 10^{-6} dyne and $K_3 > K_1 > K_2$. Like all other order-dependent properties ($K_i \propto S^2$ approximately) *(Haller and Litster 1970)* all the three constants decrease with increase in temperature. In the case of cybotactic nematics, anomalous behavior is observed for K_2 and K_3 usually close to the smectic-nematic transition. These two constants increase very rapidly as this transition temperature is approached *(Chenug et al. 1973)*. The elastic properties of smectic materials tend to be more complex *(de Gennes 1969, Group 1971)* as certain types of distortions involve changes in the thickness of the smectic layers and a concomitant high cost in free energy, as well as in simple reorientations of the molecules. In the S_A phase both the twist and bend deformations are practically expelled and the elastic free-energy is expressed as

$$F = \frac{1}{2}\left[K_1\left(\nabla\cdot\hat{n}\right)^2 + \frac{1}{2}B\left(\frac{\partial u}{\partial z}\right)^2\right]$$

where B is bulk or compressional elastic constant.

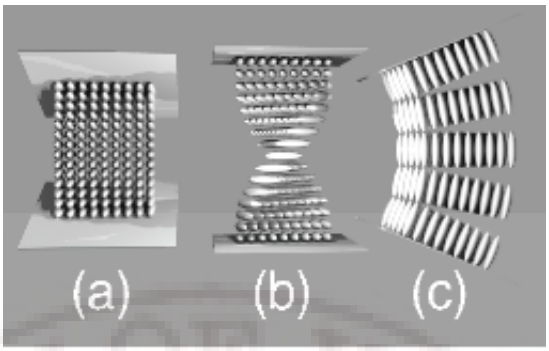

Figure 1.3: Elastic deformations of a nematic liquid crystal: (a) splay, (b) twist and (c) bend.

1.2.1.8 Flexoelectricity

If the molecules are say pear shaped with a permanent dipole moment along the long axis, for geometrical reasons a splay deformation should produce an electric polarization in the liquid crystal. Similarly, if the molecules are banana shaped with a dipole moment along the short axis, a bend should produce the same effect. This is the analogue of piezoelectricity in solids. Later, Prost and Marcerou showed that even quadrupoles can lead to flexo-(or curvature-) electricity under deformation. Experiments have confirmed the existence of both the types of effects. When a homogeneously aligned sample is subjected to a dc or to an ultra low-frequency ac electric field, certain periodic instabilities can be observed owing to the flexoelectric torques produced in the sample. However, even for relatively low frequency of the applied ac voltage, the flexoelectric effects are often masked by the electro-hydrodynamic instabilities and hence pose tougher experimental challenges for finding suitable application.

1.2.1.9 Surface Alignment

Unidirectional rubbing of a nematic with a glass substrate produces a homogeneously aligned medium with its director oriented along the direction of the rubbing. Alignment can also be reproducibly achieved by vacuum-coating the substrate at an oblique angle. In this case, the angle made by the director with the substrate depends on the angle of coating. To produce homeotropic alignment (the director perpendicular to the substrate), a monolayer of a long chain compound with a polar head, e.g. cetyl trimethyl ammonium bromide (CTAB), is coated on the surface. The polar groups attach themselves to the glass plate and, if the density of CTAB is sufficiently high, the alkyl chains stand out of the glass plate and align the nematic normal to the substrate. The anchoring energy, of course depends on the mode of preparation of

the substrate.

1.2.2 Phase Transitions

Liquid crystalline materials exhibit the richest variety of polymorphism. Transitions between different phases correspond to the breaking of some symmetry of the medium. As expected on physical grounds, the most common examples of phase transitions involve a transformation from an ordered (lower symmetry) phase to a relatively disordered (higher symmetry) phase (or vice versa) as the transition temperature is crossed.

The reasons for the continued interest in liquid crystal phase transitions is that they provide numerous examples for many theoretical studies on interesting critical phenomena. Since the mesophase transitions are either weakly discontinuous or continuous, they display behaviour associated with critical points, including strong fluctuations and diverging susceptibility. One of the significant theoretical findings of the theoretical works is that in the vicinity of such a transition the microscopic details of the system become unimportant in describing the details of the transition. Instead, the range of the interactions, the physical dimension of the system, and symmetry of the order parameter and its dimensionality determine the behaviour of the system very close to the transition. Fluctuations are thus expected to be an important feature of LC phase transitions. Understanding of critical phenomena at a first-order phase transition is, such as NI transitions, is relatively blurred as compared to fluctuation-controlled second-order phase transitions. Further, critical phenomena in LC have unique features due to the variety of symmetries of the different phases and coupling of the different order parameters *(Gupta 1995)*. These features call for more involved theoretical considerations and thus require more sophisticated theoretical methods for their interpretation.

The magnitude of the transition enthalpy is proportional to the change in structural ordering of the phases involved. The relatively small enthalpy changes involved in liquid crystalline phase transitions show that these are associated with more subtle structural changes. Typically, a melting transition from a crystalline solid to isotropic liquid phase involves an enthalpy change of around 30 - 50 kJ/mol whereas nematic-isotropic transition usually gives a smaller enthalpy change (1-2 kJ/mol). The S_C to S_A transition is often difficult to detect because the enthalpy change is typically less than 300 J/mol. The enthalpy for S_A - N transition is also fairly small (1 kJ/mol) and the S_C - N transition has enthalpy even less. These changes can be readily detected by optical methods.

The LC phase transitions are not necessarily sharp, but can stretch over a reasonable temperature range. The N-I transition extends over about 0.6-0.8K whereas crystalline smectic or smectic-isotropic liquid transitions are generally even wider. All N-I transitions are observed to be first order and due to the involvement of the small latent heat and volume changes across the transition, it shows a nearly second order nature (weak first order), permitting a description in terms of suitably modified Landau theory *(de Gennes 1974)*. Unlike pure first order transitions, liquid crystals at N-I transition show pre-transtional effects such as fluctuations in the magnitude of the order parameter in the isotropic phase very near T_{NI}, fluctuations in the short range nematic order just below T_{NI} and layer undulations near N-S transition.

Theoretical models for the liquid crystal phase transitions were developed in several directions. The phenomenological theory of Landau and de Gennes *(de Gennes 1972, Sheng and Priestley 1974, Gramsbergen et al. 1986, Landau and Lifshitz 1980, Gordon and Breach 1967, Landau 1937, Stephen and Stratey 1974)*, Faber's continuum theory *(Faber 1982)*, mean field theories by *Onsager (1949)*, Maier-Saupe(MS) *(Maier and Saupe 1959, Maier and Saupe 1960)* and extensions *(Cotter 1977, Krieger and James 1954, Widom 1963, Luckhurst and Zannoni 1977, Luckhurst 1979, and references therein)*, Molecular theory by *Singh (1991)* and several others, explained the liquid crystalline phase transitions theoretically. Many of these theoretical predictions were tested by experimental and computer simulations (Ex. Hard particle model, Lebwohl-Lasher lattice-, and Gay-Berne models *(Lebwohl and Lasher 1972, Gay and Berne 1981, Pacini and Zannoni 1998)* etc.)

1.2.3 Progress and Applications

Liquid crystal technology has had a major effect on many areas of science and engineering, as well as device technology. Applications of this special kind of material are markedly increasing in daily life and novel results are still being discovered. The most common application of liquid crystal technology is the liquid crystal displays (LCD). In 1911, Mauguin *(Mauguin 1911)* discovered and described the twisted nematic structure. This configuration played a crucial role in display research nearly sixty years later. The first true application of liquid crystals was patented in 1936, when researchers developed a liquid crystal light valve *(Company 1936)*. Before the revolution of liquid crystal display applications took place in the 1960s, significant research on the electro-optical properties of liquid crystals carried out in many laboratories. In the 1950s, the first application of cholesteric liquid crystals as temperature sensors was developed. Chiral nematic liquid crystals reflect light with a wavelength equal to the pitch. Because the pitch is dependent upon temperature, the color

reflected also is temperature dependent. Liquid crystals thus make it possible to accurately gauge temperature just by looking at the color of the thermometer. By mixing different compounds, device can be built practically covering any temperature range. After that practical applications have been developed in diverse areas like medicine and electronics. As the electrical and optical properties of stable room-temperature nematic materials became well known, scientists began investigating the possibility of building optical devices. Heilmeier *(Heilmeier et al. 1968, Heilmeier et al. 1969a, Heilmeier and Goldmacher 1969b)*is credited with being the first to consider liquid crystals for display purposes. In the 1960's, he developed guest-host displays, and in 1968 watches were built using the so-called dynamic scattering effect.

Early liquid crystal displays required high voltages in order to switch, and suffered from poor contrast ratios. The twisted nematic field effect display, patented in 1969 by James Fergason, was the first commercially successful display used in pocket calculators and wrist watches, and later in small TV's and laptop computers. This display had the good fortune of being invented at the time the electronics industry was first developing inexpensive integrated circuits. The combination of these two components yielded very effective affordable digital display devices. Following the great amount of research into material properties in the 1970's, researchers were ready to look at other possibilities for displays. In 1980, six years after the discovery of ferroelectric liquid crystals, Noel Clark from the United States and Sven Lagerwall from Sweden developed the Surface Stabilized Ferroelectric Liquid Crystal display (SSFLC), using chiral smectic liquid crystals. This was the first electronic display to exhibit bistability. Also, its switching speed is faster than any other LC display invented so far.

In 1984 Terry Scheffer developed his super twisted birefringent effect (SBE) displays. The OMI, an achromatic modification of the SBE device developed by M. Schadt in 1987, is widely used in laptop displays today. In 1986, J. W. Doane and others developed Polymer Dispersed Liquid Crystal (PDLC) displays, which could operate without polarizers *(Doane et al. 1987)*. A large number of other display techniques using cholesteric, antiferroelectric, absorptive, and other liquid crystalline properties have since been proposed and developed by researchers in many countries. Recently (1996) new liquid crystalline phases were discovered. The individual molecules which form these phases are banana- or bow-shaped, and are not chiral. An application of liquid crystals that is only now being explored is optical imaging and recording. In this technology, a liquid crystal cell is placed between two layers of photoconductor. Light is applied to the photoconductor, which increases the material's conductivity. This causes an electric field to develop in the liquid crystal

corresponding to the intensity of the light. The electric pattern can be transmitted by an electrode, which enables the image to be recorded. This technology is still being developed and is one of the most promising areas of liquid crystal research. Liquid crystals have a multitude of other uses. They are employed for nondestructive mechanical testing of materials under stress. This technique is also used for the visualization of RF (radio frequency) waves in waveguides. They are used in medical applications where, for example, transient pressure transmitted by a walking foot on the ground is measured. Low molar mass (LMM) liquid crystals have applications including erasable optical disks, full color "electronic slides" for computer-aided drawing (CAD), and light modulators for color electronic imaging. More details on display applications of liquid crystals is discussed by Castellano *(Castellano 1991)* in his article. In summary liquid crystals continue to excite scientists working in both fundamental and applied areas, opening up fresh avenues.

1.3 Proteins

Proteins are the most versatile macromolecules in living systems, and play crucial role, essentially in all biological processes. They function as catalysts, they transport and store other molecules, (for example oxygen), they provide mechanical support and immune protection, they generate movement, they transmit nerve impulses, and they control growth and differentiation. In this context, this section will present a brief overview on the current understanding of proteins and their functionality.

Proteins are macromolecules; synthesized by polymerizing amino acids or, by constructing a vast array of macromolecules formed by a limited number of monomer building blocks. They are synthesized in *vivo* at the ribosome by the linear addition of amino acids to the C-terminus of the growing polypeptide chain (Fig. 1.4). There are twenty main species of such amino acid residues. The number of residues in protein chains ranges from a few dozens to many thousands. The number of amino acid residues, and their position in a given protein chain is purely gene-encoded. A set of rules called the genetic code uniquely determines the protein sequence, provided the DNA sequence of the encoding gene, or the corresponding m-RNA, is known.

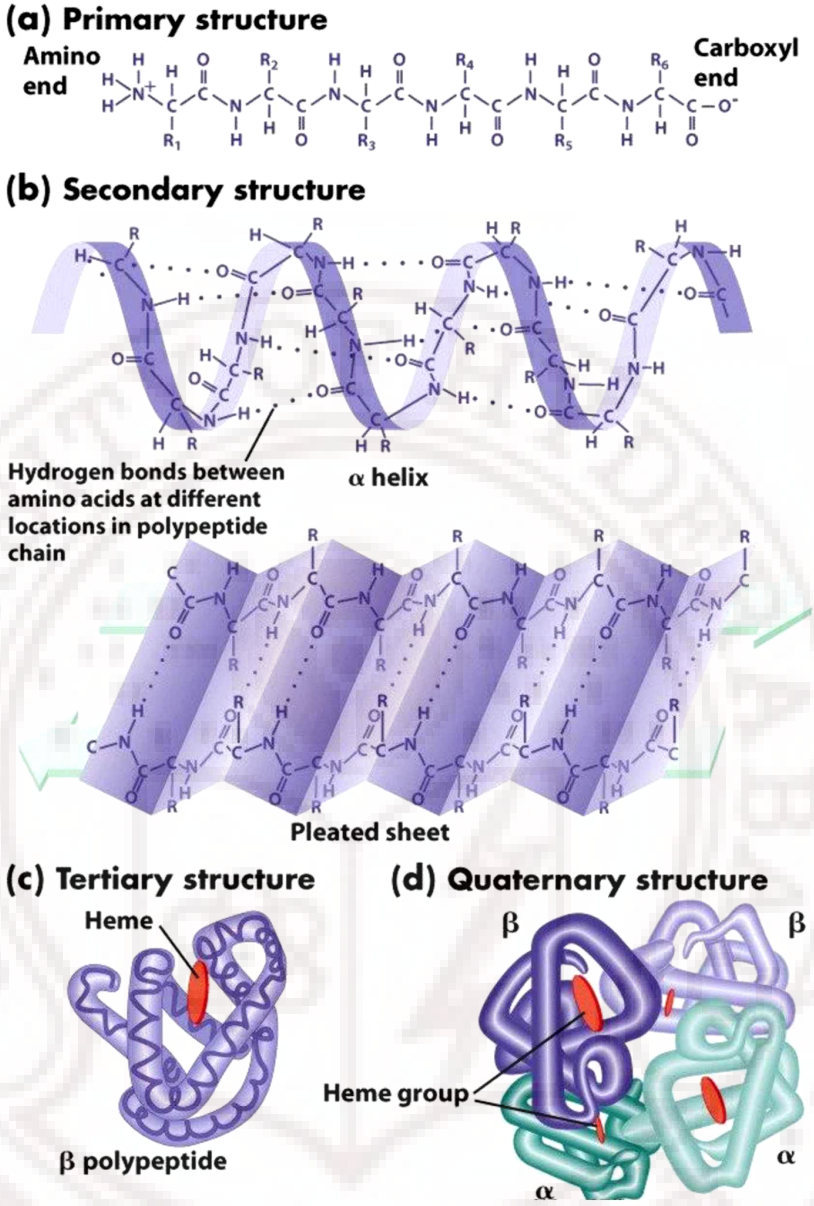

Figure 1.4: Hierarchy of protein structure.

The specific physiological activity of the protein, however, does not arise from this sequence, i.e. the primary structure in itself. Remarkably, proteins spontaneously fold up into subsequent higher ordered (three-dimensional) structures that are determined by the sequence of amino acids in the primary structure. Though the number of possible conformations to get into three dimensional forms is astronomical, a unique conformation, the native tertiary structure, provides the biological activity. Thus, proteins are the embodiment of the transition from the one-dimensional world of sequences to the three-dimensional world of molecules capable of diverse activities.

Four levels of structural hierarchy is known for the protein architecture *(Bruce*

et al. 2002). The primary structure is the amino acid sequence, and secondary structure refers to the spatial arrangement of amino acid residues that are nearby in the sequence. Some of these arrangements are of a regular kind, giving rise to a periodic structure. The α-helix and β-strand are elements of secondary structure *(Pauling and Corey 1951, Pauling et al. 1951)*. Tertiary structure refers to the spatial arrangement of amino acid residues that are far apart in the sequence and to the pattern of disulfide bonds to get a globule like structure. A few proteins contain more than one polypeptide chain. Such proteins exhibit a fourth level of structural organization. Each polypeptide chain in such a protein is called a subunit. Quaternary structure refers to the spatial arrangement of these subunits and the interaction among them. The simplest form of quaternary structure is a dimer, consisting of two identical subunits. More complicated quaternary structures also are common and more than one type of subunit can be present in variable numbers. Proteins are able to perform numerous functions relying solely on the versatility of their 20 amino acids. However, many proteins are covalently modified, through the attachment of groups other than amino acids, to augment their functions. For example, acetyl groups are attached to the amino termini of many proteins, a modification that makes these proteins more resistant to degradation. Usually the water soluble proteins attain their compact tertiary structure due to the presence of non-polar residues in the chain. This is known as hydrophobic effect, and is considered to be the major driving force for the folding of globular proteins. It results in the burial of the hydrophobic residues in the core of the protein. Protein folding is essential for the conversion of genetic information into biological activity. The failure of proteins to fold, or to fold incorrectly can result in diseases (eg. Creutzfeldt-Jakob disease, mad cow disease(bovine spongiform encephalopathy), amyloid-related illnesses such as Alzheimer's disease and familial amyloid cardiomyopathy or polyneuropathy, as well as intracytoplasmic aggregation diseases such as Huntington's and Parkinson's disease). Hence the study of protein folding emerged as an important research field.

1.3.1 Protein Folding Studies

Proteins can be denatured by heat, or by chemical denaturants such as urea or guanidinium hydrogen chloride. For many proteins, a comparison of the degree of unfolding as the concentration of denaturant increases has revealed a relatively sharp transition from the folded, or native, form to the unfolded, or denatured form, suggesting that only these two conformational states are present to any significant extent. A similar sharp transition is observed if one starts with unfolded proteins and removes the denaturants, allowing the proteins to fold. Protein folding and unfolding is thus largely an "all or none" process that results from a cooperative transition. For example,

if a protein is placed in conditions under which some part of the protein structure is thermodynamically unstable, the interactions between it and the remainder of the protein will be disturbed resulting in destabilization of the remaining structure. Thus, conditions that lead to the disruption of any part of a protein structure are likely to unravel the protein completely. The structural properties of proteins provide a clear rationale for the cooperative transition. The consequences of cooperative folding can be illustrated by considering the contents of a protein solution under conditions corresponding to the middle of the transition between the folded and unfolded forms. Under these conditions, the protein is folded. Yet the solution will contain no half-folded molecules but, instead, will be a 50/50 mixture of fully folded and fully unfolded molecules. Thus structures that are partly intact and partly disrupted are not thermodynamically stable and exist only transiently. Cooperative folding ensures that partly folded structures that might interfere with processes within cells do not accumulate.

A strategy for studying the folding of proteins is to unfold the protein molecules in high concentrations of a chemical denaturants and then dilute the solution rapidly until the denaturant concentration is lowered to a level where the native state is thermodynamically stable again. Afterwards, the structural changes of the protein folds may be observed. Several techniques are used to investigate structural changes during the refolding process. Circular dichroism (CD), nuclear magnetic resonance (NMR), dual polarization interferometry (DPI), mass spectrometry and high time resolution studies, include a few of such techniques. Computational prediction of protein tertiary structure is a distinct field (*Bioinformatics*) of protein folding studies. In this, the complex folding processes are simulated, from the knowledge of amino-acid sequence, and information on statistically-probable and reproducible (energetically favorable) folding pathways were obtained. X-ray diffraction-interpretation of protein structure also well known. Despite dramatic progress in biophysical protein engineering and computational techniques to study protein folding, it is still not possible to predict how extended polypeptide sequences will fold to a native protein and thus left the understanding of protein folding as an important challenge.

Chapter 2

Concepts and Theoretical Framework of Nuclear Magnetic relaxation

2.1 Introduction

The applications of nuclear magnetic resonance (NMR) methods provide a versatile tool to explore structure, dynamics and function of materials. As the methods are fully noninvasive and produce no dose of ionizing radiation they are readily used in probing invivo biological functions too. The weak interaction of nuclear spins with non-spin degrees of freedom greatly facilitates the use of nuclear spin systems as microprobes in the condensed matter physics. In a typical magnetic relaxation experiment, the system under investigation is disturbed from equilibrium and allowed to relax towards thermal equilibrium with the heat reservoir called lattice. The rate at which the nuclear spins reach the equilibrium is measured experimentally. These relaxation rates are connected to the dynamics of the lattice provided the spin-lattice coupling interactions are known. Thus relaxation experiments allow one to determine the spectral densities as a function of frequency and temperature.

A brief introduction to the magnetic relaxation theory and the interactions involved in the process are explained in the first part of this chapter. Theoretical models developed for spin-lattice relaxation process in liquid crystals and proteins are discussed in the second part.

2.2 Magnetic Resonance

When a system of nuclei with nonzero spin $\boldsymbol{I}$ is subjected to static magnetic field H_o, degeneracy of spin eigenvalues is lifted (Zeeman interaction). Taking the field to

be H_o along the z direction, the interaction Hamiltonian $\mathcal{H}_o$ is written as

$$\mathcal{H}_o = -\gamma\hbar H_o I_z \tag{2.1}$$

where γ represents the gyro magnetic ratio of the nucleus involved. Nuclear spins occupy the $2\boldsymbol{I}$ $+1$ energy levels, and follow Boltzman's distribution at the thermal equilibrium. As the lower energy levels are preferentially occupied an equilibrium magnetization builds up in the system. Each magnetic moment vector (μ_i) of spins precesses around H_o (Larmor theorem). This precessional frequency is called Larmor frequency (ω_o) and defined as

$$\omega_o = \gamma H_o \tag{2.2}$$

A non-equilibrium state in the populations can be created either by a sudden change in H_o or by applying an alternating magnetic field perpendicular to H_o (in the x-y plane), with angular frequency equal to ω_o, causing transitions between the energy levels (the phenomenon is known as magnetic resonance). The process by which the total magnetization vector $\mathbf{M}$ (vectorial sum of all μ_i) approaches thermodynamic equilibrium in the absence of external oscillating fields is called magnetic relaxation. For a system of non-interacting spins there can be two relaxation processes commonly known as spin-lattice and spin-spin relaxations characterized by time constants T_1 and T_2 respectively. T_1 process occurs due to the time modulation of other than spin degrees of freedom called lattice. The spin-lattice relaxation rate constant describes the recovery of the longitudinal magnetization to thermal equilibrium or, equivalently, return of the populations of the energy levels of the spin system to the equilibrium Boltzmann distribution. T_2 is due to the presence of interactions among the individual spins. The spin-spin relaxation rate constant describes the decay of the transverse magnetization to zero, or equivalently, the decay of transverse quantum coherences. Non-adiabatic processes contribute to both spin-lattice and spin-spin relaxation. Adiabatic processes only contribute to spin-spin relaxation; spin-lattice relaxation is not affected because adiabatic processes do not change the populations of stationary states.

In the simplest theoretical approach to spin relaxation, the relaxation of isolated spins is characterized in the Bloch equations by two phenomenological first order rate constants, namely the spin-lattice and the spin-spin relaxation rate constants *(Bloch 1946)*. The Bloch formulation provides qualitative insights into the effects of relaxation on the NMR experiment, and the phenomenological rate constants can be measured experimentally. The Bloch formulation does not provide a microscopic explanation of the origin of the relaxation rate constants, nor it is extendable to more

complex, coupled spin systems.

2.3 Spin Lattice Relaxation Process

The total Hamiltonian for a spin system in a static field H_o can be written as

$$\mathcal{H} = \mathcal{H}_0 + \mathcal{H}_1(t) \tag{2.3}$$

Where $\mathcal{H}_0$ is large time-independent interaction due to applied Zeeman field in the z-direction. $\mathcal{H}_1(t)$ consists of interactions between the nuclear spins and the space variables affected by microscopic motions at the molecular level and hence $\mathcal{H}_1(t)$ is time-dependent. A nucleus in the system will experience a fluctuating field due to the magnetic moments and electric quadrupole moments (in case $I > \frac{1}{2}$) of nuclei in other molecules as they execute Brownian motion pertaining to the temperature (thermal bath or lattice). This random fluctuating field may be resolved by Fourier analysis into oscillating at different frequencies and may be further subdivided into components perpendicular and parallel to H_o. The component perpendicular to the static field which oscillates with the Larmor frequency induces transitions between the levels in a similar way to an electromagnetic field. This gives rise to a non-adiabatic contribution to relaxation of both the longitudinal and transverse components of **M**. The very many lattice variables, interacting among themselves as well as affecting $\mathcal{H}_1(t)$, make this interaction nondeterministic. A convenient method of description of its time dependence is to model the molecular dynamics modulating the spin system as a stochastic process with certain prescribed characteristics. A time dependent perturbation treatment yields an expression for the transition probability $P(m|k,t)$, connecting the eigenstates and of the Zeeman term, $\mathcal{H}_0$, as

$$P\left(m\left|k,t\right.\right) = \frac{1}{\hbar^2}\left[\int_{-\infty}^{\infty} \overline{\left\langle m\right|\mathcal{H}_1\left(t\right)\left|k\right\rangle}^2 \exp\left(-i\omega_{mk}t\right)dt\right] \tag{2.4}$$

where $\omega_{mk} = \frac{E_m - E_k}{\hbar}$ and E_m, E_k are the energies of Zeeman levels.
Ensemble averaged transition probability per second $W_{mk} = \langle P\left(m,k|t\right)\rangle$ is related to T_1 as

$$T_1 = \frac{1}{W_{mk}} \tag{2.5}$$

This W_{mk} is given by the Fourier transformation of a correlation function $G_{mk}(\tau)$ (Abragam 1961) as

$$W_{mk} = \frac{1}{\hbar^2}\int_{-\infty}^{\infty} G_{mk}\left(\tau\right)\exp\left(-\omega_{mk}\tau\right)d\tau \tag{2.6}$$

where

$$G_{mk}(\tau) = \overline{\langle m|\mathcal{H}_1(t)|k\rangle \langle m|H_1(t+\tau)|k\rangle} \tag{2.7}$$

and bar denotes the average over the ensemble of spins.
For a typical physical system the perturbing term $\mathcal{H}_1(t)$ varies in time owing to some physical movement creating random fields B_{loc}. $G_{mk}(\tau)$ quantifies the correlation between the random function $B_{loc}(t) = H_1(t)$ at time t and $t+\tau$. B_{loc} is considered as stationary random function (invariant under time translation) and approximated to a Markoff process in time. Then the correlation function can be written as

$$G_{mk}(\tau) = \left\langle |B_{loc}(0)|^2 \right\rangle exp(-\tau/\tau_c) \tag{2.8}$$

where τ_c is the correlation time corresponding to the molecular motions. Further, the Fourier transform of a correlation function gives the spectral density $J(\omega)$ (the power available from the fluctuations at transition frequency) ω, consequently equations 2.4 and 2.5 give

$$\frac{1}{T_1} \propto J(\omega) \tag{2.9}$$

Thus the spin-lattice relaxation rate T_1^{-1} is proportional to the spectral density functions $J(\omega)$ of the local random fields and these $J(\omega)$ are frequency dependent and related to the correlation times corresponding to the molecular motions. This is a semi classical treatment (spins considered as quantum and lattice as classical varibables) *(Wagsness and Bloch 1953, Redfield 1965, Slichter 1978)* of approach to an expression for spin lattice relaxation rates. There are different approaches developed to understand the way molecular motions cause spin-lattice relaxation viz., quantum mechanical time-dependent perturbation theory *(Bloembergen et al. 1948, Abragam 1961)*, spin temperature concept *(Goldman 1970, Wolf 1979)*, density matrix formalism *(Wagsness and Bloch 1953, Redfield 1965, Slichter 1978)* etc. All these approaches have the same objective of obtaining the expression for the spectral density.

The main theoretical problem now is to connect these spectral density functions to the characteristics of the molecular motions of interest. For a given model of the molecular motion, it is in principle possible to calculate the appropriate probability distribution and correlation functions. The Fourier transform of these correlation functions gives spectral density functions and hence the relaxation rates. On the other hand, the experimental investigations of these molecular motions begin with the measurement of relaxation rates as a function of temperature, frequency, etc. Spectral density values corresponding to the local field fluctuations, which fit the experimental data, are then deduced. In order to connect these results to specific molecular models, as well as to account for all the details of the observable features, it is necessary to

consider the different magnetic interactions in the system as well as their sensitivity to different molecular motions. It can readily be seen that correlation functions and spectral density functions define the central problem in the connection between the characteristics of Brownian system and relaxation. A schematic representation of this methodology is shown in Fig. 2.1.

If different molecular motions are present in a system, each one mediating the relaxation process with its own individual spectral density function, and which are statistically independent of each other, the total relaxation rate is obtained as a sum of individual relaxation rates i.e.

$$T_1^{-1} = \sum_{\lambda} \left(T_1^{-1}\right)_{\lambda} \tag{2.10}$$

where λ denotes the type of mechanism. Thus in any system, estimate of the total relaxation rate involves modeling different molecular motions and computing the corresponding contribution from each mechanism to the relaxation.

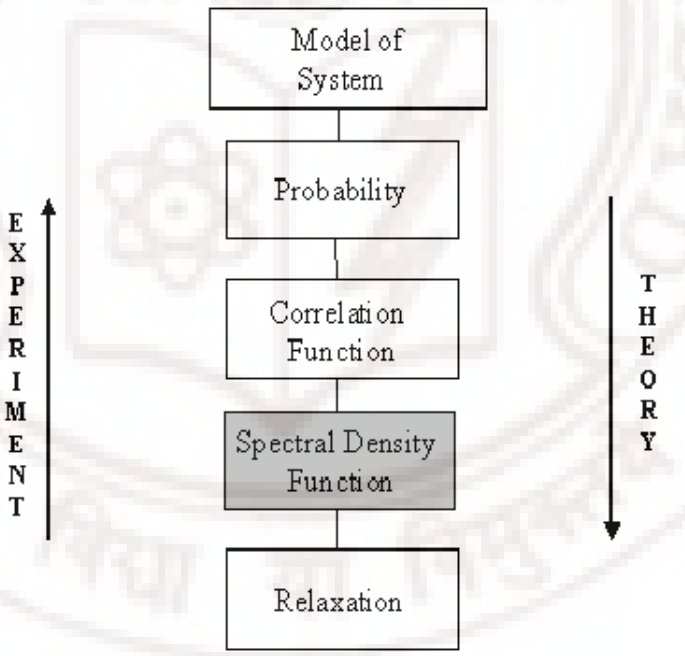

Figure 2.1: Schema of treatment of spin relaxation in Brownian systems.

2.4 Nuclear Magnetic Interactions

The various nuclear magnetic interactions mediating relaxation mechanisms are classified into two groups 1. Magnetic interactions and 2. Electric interactions. The

nuclear magnetic moment, in a diamagnetic material, can couple with (i) the external magnetic field H_o (ii) other nuclear spins in the sample, and (iii) the total angular momentum of the molecule J. There are five types of such couplings, which are magnetic interactions, namely Zeeman (Z), dipolar (D), J-coupling (J), chemical shift (CS) and spin-rotation (SR) interactions. In NMR only one spin dependent electric interaction need to be considered. That is the coupling of the nuclear quadrupole moment with the electric field gradient tensor at the nuclear site. This is relevant only in case of spin $> \frac{1}{2}$ nuclei. These interactions can also be classified depending on whether they are single spin interactions (Z, CS, Q and SR) or pair-wise interactions (D and J).

In order to connect the spectral densities to the molecular processes the various nuclear magnetic interactions and their sensitivity to the molecular motions have to be considered. In this connection and in view of the present work, involving NMR studies of spin $\frac{1}{2}$ nuclei in the wide-line regime, dipole-dipole interaction and spin-rotation interaction mediated by different molecular processes provide the requisite relaxation mechanism. These are discussed in detail here.

2.4.1 Dipolar Interaction

The dipolar Hamiltonian for N spins I_i for i = 1 to N is written as

$$\mathcal{H}_{\mathcal{D}} = \frac{1}{2}\sum_{i=1}^{N}\sum_{j=1}^{N}\left[\frac{\mu_i \cdot \mu_j}{r_{ij}^3} - \frac{3\left(\mu_i \cdot r_{ij}\right)\left(\mu_j \cdot r_{ij}\right)}{r_{ij}^5}\right] \tag{2.11}$$

where μ_i is the magnetic moment associated with the spin I_i and is given by $\mu_i = \hbar\gamma_i I_i$. r_{ij} is the radius vector from μ_i and μ_j. If we express the components of spin operator (I_x and I_y) in raising and lowering operators I^+ and I^- and express r interms of spherical coordinates r, θ and ϕ, for pair of spins I_1 and I_2 we may write the Hamiltonian in a form that is particularly convenient for computing matrix elements

$$\mathcal{H}_{\mathcal{D}} = \frac{\gamma_1\gamma_2\hbar^2}{r_{12}^3}\left(A + B + C + D + E + F\right) \tag{2.12}$$

where $A = I_{1z}I_{2z}\left(1 - 3\cos^2\theta\right)$

$$B = -\tfrac{1}{4}\left(I_1^+ I_2^- + I_1^- I_2^+\right)\left(1 - 3cos^2\theta\right)$$

$$C = -\tfrac{3}{2}(I_1^+ I_{2z} + I_{1z} I_2^+)sin\theta cos\theta e^{-i\theta}$$

$$D = -\tfrac{3}{2}(I_1^+ I_{2z} + I_{1z} I_2^-)sin\theta cos\theta e^{i\theta}$$

$$E = -\tfrac{3}{4} I_1^+ I_2^+ sin^2\theta e^{-2i\phi}$$

and $$F = -\tfrac{3}{4} I_1^- I_2^- sin^2\theta e^{2i\phi}$$

were the term A connects the states $|m_1 m_2\rangle$ with $\langle m_1 m_2|$. On the other hand, B connects to states $|m_1 m_2\rangle$ to states $\langle m_1 + 1, m_2 - 1|$ or $|m_1 - 1, m_2 + 1\rangle$. It simultaneously flips one spin up and one spin down. The terms C and D flip one spin only which differ in energy by $\hbar\omega_o$. Finally E and F flip both spins up or both spins down connecting the states that differ by $2\hbar\omega_o$. Here C, D, E and F are off-diagonal terms. They produce slight admixture of zero order and first order states and the results can be computed by second order perturbation theory. The dipolar Hamiltonian can also be written in terms of irreducible spherical tensor operators as *(Abragam 1961)*.

$$\mathcal{H}_D = C^D \sum_{m=-2}^{2} (-1)^m T_{2,m}^D R_{2,-m}^D \tag{2.13}$$

where $$C^D = -\gamma_1 \gamma_2 \hbar^2$$

$$T_{2,0}^D = \left[-\tfrac{2}{3} I_z^1 I_z^2 + \tfrac{1}{6}\left(I_+^1 I_+^2 + I_-^2 I_+^J\right)\right]$$

$$T_{2,\pm1}^D = \left[I_z^1 I_\pm^1 + I_\pm^2 I_z^2\right]$$

$$T_{2,\pm2}^D = \tfrac{1}{2} I_\pm^1 I_\pm^2$$

$$R_{2,0} = ((1 - 3cos^2\theta)/r^3)$$

$$R_{2,\pm1} = \tfrac{sin\theta cos\theta}{r^3} e^{\pm i\theta}$$

$$R_{2,\pm2} = \tfrac{sin^3\theta}{r^3} e^{(\pm 2i\phi)}$$

The functions $T_{2,m}^D$ contain the spin and $R_{2,m}^D$ describe the orientation operators. The effect of random molecular motions (i.e. of the vector r_{ij}) is to make this interaction time-dependent, and so the time correlation function of $R_{l,m}^D$ is relevant here. For an isotropic random motion

$$\left\langle R_{2m}^D(t)\, R_{2m'}^D(t+\tau)\right\rangle_{ave} = \delta_{m,m'} \mathrm{G}_m(\tau) \tag{2.14}$$

with the spectral density, $J^m(\omega)$ at any frequency defined as

$$J^m(\omega) = \int_{-\infty}^{\infty} G^m(t)\, e^{-i\omega\tau} d\tau \tag{2.15}$$

Bloembergen, Purcell and Pound (BPP) *(Bloembergen et al. 1948)* showed for like spins, that the relaxation rate due to the dipolar interaction is

$$\frac{1}{T_1} = \frac{3}{2}\gamma^4\hbar^2 I(I+1)[J_1(\omega) + \frac{1}{2}J_2(2\omega)] \tag{2.16}$$

Kubo and Tomita *(Kubo and Tomita 1954)* and Solomon *(Solomon 1955)* modified the equation 2.16 by taking into account the additional non-secular broadening effects, as

$$\frac{1}{T_1} = \frac{3}{2}\gamma^4\hbar^2 I(I+1)[J_1(\omega) + J_2(2\omega)] \tag{2.17}$$

where $J_1(\omega)$ and $J_2(2\omega)$ are given by equation 2.15 for m = 1 and 2 respectively and ω is the angular Larmor frequency of the nuclear spins in the presence of applied static field H_o. Dipolar interaction can be further divided as arised from intra and inter-molecular interactions. Usually in liquids inter-molecular dipolar interactions are motionally averaged to small leading to negligible contribution. Intra-molecular dipolar interactions are motionally averaged to their isotropic values. Spin rotation interaction is purely intra-molecular.

2.4.2 Spin Rotation Interaction

The interaction of a nuclear magnetic moment with the magnetic field produced at the position of the nucleus by the rotation of the molecule containing the nucleus is called the spin-rotation interaction. If the molecule rotates at an angular velocity ω we shall describe the rotation by

$$I\omega = \mathbf{J}\hbar \tag{2.18}$$

where I is the moment of inertia of the molecule, $\mathbf{J}$ is angular momentum operator. The spin rotation interaction Hamiltonian for a nucleus with spin $\mathbf{S}$ can be written as *(Brown et al. 1963)*

$$\mathcal{H}_{sr} = -\hbar\mathbf{S}.\mathcal{C}.\mathbf{J} \tag{2.19}$$

Here $\mathcal{C}$ is a dyadic or a tensor quantity known as the spin-rotation interaction constant. Expression for spin lattice relaxation time due to spin rotation is given as *(Hubbard 1963, Green and Powles 1965)*

$$\frac{1}{T_1} = \frac{2}{9}\frac{\hbar^{-2}(I_x + I_y + I_z)\left(2\mathcal{C}_\perp^2 + \mathcal{C}_\parallel^2\right) k_B T \tau_{sr}}{(1+\omega^2\tau_{sr}^2)} \tag{2.20}$$

where I is moment of inertia of the molecule, $\mathcal{C}_\perp$ and $\mathcal{C}_\parallel$ are the components of the spin rotation interaction tensor, τ_{sr} is molecular angular velocity correlation time, T is absolute temperature and k_B the Boltzman's constant. It was shown *(Hubbard 1963, Green and Powles 1965)* that for a spherical molecule undergoing isotropic Brownian motion in liquid state, the correlation time for molecular angular velocity, τ_{sr}, is closely related to the correlation time for molecular re-orientation, τ_D as

$$\tau_{sr}\tau_D = \frac{I}{6k_BT} \tag{2.21}$$

provided that $\tau_{sr} \ll \tau_D$. The correlation time τ_D is usually determined from the dipolar contribution to the spin-lattice relaxation. It is then possible to estimate the value of τ_{sr} and root mean square value of the spin-rotation interaction constant $\left(\overline{\mathcal{C}^2}\right)^{\frac{1}{2}}$ (where $3\overline{\mathcal{C}^2} = 2\mathcal{C}_\perp^2 + \mathcal{C}_\parallel^2$) using equation 2.21 and 2.20 respectively. No independent experimental method for determining the correlation time τ_{sr} seems to be available however knowledge of the magnitude of the spin-rotation interaction constant $\mathcal{C}$ enables us to derive values for τ_{sr} using the equation 2.20. These values may be combined with estimates of τ_D to examine the relation given in equation 2.21 *(Deverell 1970)*.

Spin-rotation interaction constant $\mathcal{C}$ can be independently calculated from the estimated paramagnetic term in the magnetic shielding using molecular beam experiments *(Deverell 1969, Deverell 1970)*. Ramsey *(Ramsey 1950, Ramsey 1956, Ramsey 1961)* derived an expression for the magnetic shielding of the nucleus in a molecule which results from the induced motion of surrounding electrons produced by an external magnetic field and showed that for a linear molecule the second-order paramagnetic term is directly related to the experimentally measurable spin-rotation interaction constant.

2.5 Spin Lattice Relaxation Processes in Liquid Crystals

The molecular processes which affect NMR relaxation in mesophases are collective and non-collective in nature. Pre-transitional effects due to short-range nematic clusters near isotropic-nematic transition ($T > T_{NI}$), nematic order parameter fluctuations just below isotropic-nematic transition ($T < T_{NI}$), nematic director fluctuations (in mid nematic phase), diffusion-assisted director fluctuations, pre-transitional effects due to cybotactic clusters near N-S_A transition ($T > T_{NA}$) and layer undulations in the S_A phase (mid smectic phase) are the collective motions while the

non-collective motions encompass translational self-diffusion and molecular reorientations about molecular axes, in particular along short axis, which are common to the all mesophases.

2.5.1 Collective Motions

2.5.1.1 Near the Isotropic-Nematic Transition ($T > T_{NI}$)

The nematic - isotropic transition in liquid crystals is a weak first order change and may be described in terms of an extension of the Landau theory *(de Gennes 1974)* of second order phase transition. Although the long-range order vanishes abruptly at the nematic - isotropic transition T_{NI}, there is evidence to indicate that a short-range order analogous to the nematic order persists in the isotropic phase just above the transition *(Blinc et al. 1969)*. A measure of the local anisotropy is given by the 'coherence length' ξ i.e. average nematic cluster size. The pre-transitional effects, which are manifested as critical anomalies in magnetic relaxation measurements, are caused by fluctuations in the order parameter appropriate to the particular transition *(Freed 1977)*. Fluctuations in the local order increase rapidly as this almost second-order phase transition is approached from above. The critical temperature, at which a second-order phase transition would occur, is usually within 1°C below T_{NI}. The short-range order effects in the isotropic phase of nematics and cholesterics were discussed *(de Gennes 1974)*. These remarkable effects had been observed and studied by NMR *(Blinc et al. 1969, Cabane 1972, Ghosh et al. 1980)*, and by light scattering experiments *(Stinson and Litster 1970, Stinson and Lister 1973)*. The frequency of the fluctuations in the magnitude of the local anisotropy can be determined reliably from the Rayleigh linewidth and lies in the frequency range of NMR *(Dong 1994)*. Just above $T > T_{NI}$, the fluctuations in the orientation of the local nematic order contributes to the relaxation rate. The fluctuations in the short-range order i.e. aggregation and segregation of the nematic clusters, modulate the dipolar interaction between the spins. The relaxation rate due to short-range nematic order is given by *(Dong 1994, Chavez et al. 2000)*

$$\frac{1}{T_{CF}} = A_3 \left[\frac{\tau_1}{1 + \sqrt{1 + \omega^2 \tau_1^2}} \right]^{\frac{1}{2}} \tag{2.22}$$

Here $A_3 = A' T \sqrt{\eta}$ is a temperature dependent parameter, but A' is a temperature independent quantity, τ_1 is the average correlation time of the short-range nematic order. It is expressed as

$$\tau_1 = \frac{\eta \xi^2}{L}$$

η is the effective viscosity, ξ is the correlation length that measures the distance over which the local order persists in the isotropic phase and is given by,

$$\xi = \sqrt{L/(a\,(T - T^*_{IN})^{\gamma})} \tag{2.23}$$

($a > 0$ is temperature independent and $\gamma = 1$ in the mean field approximation), T^*_{NI} is the critical temperature slightly below T_{NI} and L is related to elastic constants. Assuming an Arrhenius-like behavior for η, its temperature dependence is expressed as

$$\eta = \eta_0 \exp\left(\frac{E_{CF}}{RT}\right) \tag{2.24}$$

where E_{CF} is the activation energy for this process. Thus, the complete dependence of τ_1 and the CF term on T is given by

$$\tau_1 = \tau_{10} \frac{\exp\left(\frac{E_{CF}}{RT}\right)}{(T - T^*_{NI})} \tag{2.25}$$

where τ_{10} is a constant. And

$$\frac{1}{T_{1CF}} = A_2 T \exp\left(\frac{E_{CF}}{RT}\right) \left[\frac{\tau_1}{1 + \sqrt{1 + \omega^2 \tau_1^2}}\right]^{1/2} \tag{2.26}$$

For small frequencies *(Blink 1976)*, if the condition $\omega\tau_1 \ll 1$ is fulfilled for the whole temperature range,

$$\frac{1}{T_1} = \frac{AT \exp\left(\frac{E_{CF}}{RT}\right)}{(T - T^*_{NI})^{1/2}} \tag{2.27}$$

$$T_1 \propto \xi^{-1} \propto (T - T^*_{NI})^{\gamma/2} \neq f(\omega)$$

Hence we are not making anything about γ and its mean field value, but we say so in the $T < T_{NI}$. Thus T_1 is strongly dependent on temperature but independent of frequency. Whereas in case of large Larmor frequencies i.e. $\omega\tau_1 \gg 1$. Thus

$$\frac{1}{T_1} \propto \frac{1}{\sqrt{\omega}}$$

and is weakly dependent of temperature. This situation is close to T_c where T_1 becomes large *(Blink 1976, Ghosh et al. 1980)*.

2.5.1.2 Near the isotropic-nematic transition ($T < T_{NI}$)

In contrast to short range nematic order fluctuations in the isotropic phase ($T > T_{NI}$), just below T_{NI}, fluctuations in the magnitude of the nematic order parameter S are effective in relaxing nuclear spins. i.e. the fluctuations in long-range orientational

order modulates the dipole-dipole interactions between nuclear spins and influence the NMR spin relaxation. In particular, if these order parameter fluctuations (OPF) are significant in comparison to the director fluctuations (DF), then the following spectral density model due to OPF is adiquate to account for the observed relaxation process. The spectral density due to the OPF is *(Dong 1994)*

$$J_{m_L}(m_L\omega) = A_0 \left[\frac{\tau_0}{1+\sqrt{1+(m_L\omega\tau_0)^2}}\right]^{1/2} \tag{2.28}$$

where

$$A_0 = \frac{k_B T}{4\sqrt{2}\pi L_N}\sqrt{\frac{v_N}{L_N}}\left|\kappa(0,m)\right|^2.$$

Here $|k(0,m)|^2$, is the mean square average of the Wigner rotation matrices expressed as power series in the order parameter S. These κ values are needed to reduce the importance of the order parameter fluctuations, as the orientational ordering increases far below T_{NI}

$$\tau_0 = \frac{\nu_N \xi_N^2}{L_N}, \tag{2.29}$$

and ν_N, L_N and ξ_N are the values of corresponding nematic viscosity elastic constant and coherence length. We may now distinguish two different cases

Case 1. In case of small Larmor frequencies i.e. $\omega\tau_0 \ll 1$

$$T_1 \propto \xi_N^{-1} \propto \left(T_{NI}^{+} - T\right)^{\nu'} \neq f(\omega)$$

where the critical exponent ν has a mean field value of $\frac{1}{2}$. However, ν has been found *(Lei 1982)* to be temperature dependent and takes an effective value of $\frac{2}{5}$

Case 2. In case of large Larmor frequencies i.e. $\omega\tau_o \gg 1$

$$\frac{1}{T_1} \propto \frac{1}{\sqrt{\omega}}$$

Thus

$$T_1 \propto \sqrt{\omega} \neq f(T)$$

In this case, T_1 is proportional to the square root of frequency but is weakly dependent on temperature.

2.5.1.3 In the Mid Nematic Phase

The nematic mesophase is characterized by long range correlations in molecular orientation though there is no positional order. The director which represents the

average direction of the orientation of the molecules fluctuates due to the thermally stimulated fluctuations in the local directors. These can be visualized as cooperative reorientations of the molecules around their short axes. Among the several motional processes that take place simultaneously and may cause spin relaxation, director fluctuations (DF) are unique to liquid crystals. In the mid nematic phase DF is the dominant spin relaxation mechanism. There was much effort paid in the development of relaxation models to interpret the nuclear spin relaxation due to these director fluctuations. The non-applicability of BPP theory for nematic liquid crystals i.e. Lorentzian frequency dependence of relaxation rate, led Pincus *(Pincus 1969)* to derive the first expression for relaxation due to director fluctuations. Starting from this early model to take into account DF mechanism to cause spin relaxation under one elastic constant approximation ($K_1 = K_2 = K_3$; the Frank elastic coefficients), several improvements were made. Blinc and co-workers *(Blink 1976)* extended Pincus treatment to include upper cut off frequencies and anisotropy in the visco-elastic properties. But their formulae do not reduce to those of Pincus under one constant approximation. Vold and Vold *(Vold and Vold 1988)* modified these expressions further by considering ellipsoidal volume of integration for the q-modes, which allows asymptotic approach to Pincus model under one elastic constant approaximation. Corresponding to the q-mode cut off values introduced in the q-space interpretation there are lower and upper cut off frequencies. The dispersions of relaxation rates are discussed in distinct regions of frequency, relative to these cut off values. For example, this model predicts that below upper cut-off frequencies $\omega^{-0.5}$ behavior of T_1^{-1} is observed where as above the cut-off frequencies the frequency dependence may reach up to ω^-2 behavior depending on the value of the K_3 relative to K_1 and K_2. Struppe and Noack derived an expression including both upper and lower cut-off frequencies under single constant approximation.

The application of the above theoretical formalisms *(Blink 1976, Vold and Vold 1988)* could be further sharpened to extract useful information on visco-elastic properties of the medium. The initial model of Pincus *(Pincus 1969)* was already reformed in two different directions as indicated above: (1) introduction of anisotropy of visco-elastic constants, however incorporating only the upper cut-off frequencies for the DF modes (Vold and Vold 1988); and (2) introduction of both lower and upper cut-off frequencies, but within the single constant approximation *(Struppe and Noack 1996)*. These modifications describe DF adequately in two situations: (1) nuclear magnetic relaxation dispersion (NMRD) in many nematics for which visco-elastic properties are nearly isotropic($K_1 \simeq K_2 \simeq K_3$); and (2) NMRD in the high frquency region available from conventional spectrometers. However the situation is typically more complex in nematics with underlying smectic phases: the visco-elastic properties are percep-

tibly more anisotropic on one hand; and the presence of cybotactic clusters (smectic organizations) may impose restrictions on the wavelengths of director fluctuations modes leading to the upper and lower cut-off frequencies *(Venu and Sastry 1998)*. Thus it becomes necessary to incorporate both upper and lower cut-off frequencies, as well as anisotropy in elastic coefficients in the DF contribution to spin relaxation. Accordingly we follow the model proposed in this respect *(Venu and Sastry 1998)*, the details of which are briefly presented below. A more comprehensive account of this model was discussed elsewhere *(Satheesh 2000)*. Incorporating these two effects, one obtains proportional to the spectral density $J_m(p\omega)$ as

$$J_m(p\omega) = \frac{3}{16\pi^2}\frac{3}{4}k_B T S^2 \sum_{\alpha=1}^{2} \eta_\alpha \int_{q_{zcl}}^{q_{zch}} dq_z \int_{q_{\perp cl}}^{q_{\perp ch}\left(1-\left(\frac{q_z}{q_{zch}}\right)^2\right)^{1/2}} \frac{q_\perp dq_\perp}{(K_3 q_z^2 + K_\alpha q_\perp^2) + \eta_\alpha^2 \omega^2} \tag{2.30}$$

The upper limit for the integration over q in Eqn. 2.30 is chosen to represent an ellipsoidal volume of integration *(Vold and Vold 1988)*. Performing the integration, results in

$$J_m(p\omega) = C_m(\Delta) \sum_\alpha \frac{\sqrt{\eta_\alpha}}{K_\alpha \sqrt{K_3 p\omega}} \left[f(D_{\alpha h}, A_{\alpha h}) - f(D_{\alpha l}, A_{\alpha h}) - f(B_{\alpha h}, A_{\alpha l}) + f(B_{\alpha l}, A_{\alpha l}) \right] \tag{2.31}$$

where

$$f(D,A) = B\tan^{-1}\left(D^2 + A^2\right) + \frac{B\sqrt{\sqrt{1+A^4}+A^2}}{2\sqrt{2}D} \ln\left| \frac{\sqrt{1+A^4}+\sqrt{2}\sqrt{\sqrt{1+A^4}-A^2}D + D^2}{\sqrt{1+A^4}-\sqrt{2}\sqrt{\sqrt{1+A^4}-A^2}D + D^2} \right|$$
$$- \frac{B_\alpha \sqrt{\sqrt{1+A^4}-A^2}}{\sqrt{2}D} \left\{ \tan^{-1}\left(\frac{\sqrt{2}D - \sqrt{\sqrt{1+A^4}-A^2}}{\sqrt{\sqrt{1+A^4}+A^2}} \right) + \tan^{-1}\left(\frac{\sqrt{2}D + \sqrt{\sqrt{1+A^4}-A^2}}{\sqrt{\sqrt{1+A^4}+A^2}} \right) \right\} \tag{2.32}$$

and $f(B,A)$'s can be obtained by replacing D by B, in equation 2.32.
Hence $D_{\alpha h}^2 = B_{\alpha h}^2 - A_{\alpha h}^2$, $D_{\alpha l}^2 = B_{\alpha l}^2 - A_{\alpha h}^2 \left(\frac{q_{zcl}}{q_{zch}}\right)^2$

$A_{\alpha h(l)}^2 = \frac{K_\alpha q_{\perp ch(l)}^2}{\omega \eta_\alpha}$, $B_{\alpha h(l)}^2 = \frac{K_z q_{zch(l)}^2}{\omega \eta_\alpha}$

$q_{\perp ch(l)} = \frac{2\pi}{\lambda_{\perp cl(h)}}$, $q_{zch(l)} = \frac{2\pi}{\lambda_{zcl(h)}}$

and

$$C_m(\Delta) = f(\Delta)\frac{2S^2 k_B T}{(2\pi)^2} \tag{2.33}$$

where $f(\Delta)$ describes the angular dependence *(Blink 1976)*. Here $\lambda_{zch(l)}$ and $\lambda_{\perp ch(l)}$ are the upper (lower) cut-off wavelengths for the DF modes along and perpendicular

directions of the director. The corresponding cutoff frequencies are given by

$$\omega_{zch(l)} = \frac{K_3 q^2_{zch(l)}}{\eta_\alpha}$$

$$\omega_{\perp ch(l)} = \frac{K_\alpha q^2_{\perp ch(l)}}{\eta_\alpha} \tag{2.34}$$

The expression for the spectral density function due to director fluctuations, given by Eqns. 2.30 - 2.32, now takes into consideration the influence of anisotropic elastic properties as well as upper and lower cut off wavelengths. The corresponding spin-lattice relaxation rate, due to the dipolar interaction between a pair of nuclei having spin I separated by a distance r is given by *(Abragam 1961, Bloembergen et al. 1948)*.

$$R_1 = \frac{3\gamma^4 h^2}{2r^6} I(I+1)[J_1(\omega) + J_2(\omega)] \tag{2.35}$$

The spectral densities $J_1(\omega)$ and $J_2(2\omega)$ can be computed from the Eqn. 2.30. However, for small angle fluctuations of the nematic director in a medium of well aligned long rod like molecules $J_2(2\omega)$ is very small and in that case it is necessary to compute only $J_1(\omega)$. Then the spin-lattice relaxation rate due to director fluctuations can be written as

$$R_{1DF} = A_{DF} \sum_\alpha \frac{\sqrt{\eta_\alpha}}{K_\alpha \sqrt{K_3 p\omega}} \left[f\left(D_{\alpha h}, A_{\alpha h}\right) - f\left(D_{\alpha l}, A_{\alpha h}\right) - f\left(B_{\alpha h}, A_{\alpha l}\right) + f\left(B_{\alpha l}, A_{\alpha l}\right) \right] \tag{2.36}$$

where A_{DF} for protons in a liquid crystal (with its director parallel to the applied magnetic filed) is given by

$$A_{DF} = \frac{9\gamma^4 h^2 k_B T S^2}{16\pi^2 r^6} \tag{2.37}$$

Eqn. 2.35 reduces to $\omega^{-0.5}$ dependence of T_1^{-1} under one elastic constant limit in the regions lying between the upper and lower cut-off frequencies. Further, above the lower cut-off frequencies the above expression results in exactly the same relaxation rate as the one obtained earlier *(Vold and Vold 1988)*. The principal difference between R_{1DF} computed here and earlier calculations is in the low frequency behavior. The Eqn. 2.35 results in a T_1^{-1} dispersion that shows a low frequency plateau due to the imposition of upper cutoff value to the wavelength of DF as expected *(Blink 1976)* and the effect of this low frequency cutoff is shown in Fig. 2.2. Corresponding effect due to variation in the lower cutoff wavelengths on the spectral density function is shown in Fig 2.3. Here the spectral density given by Eqn. 2.35 is plotted for a frequency region spanning over nine decades. Various parameters involved in this expression are chosen at typical values expected in a nematic phase made up of a two-benzene ring compound. The values chosen are $K_1 = K_2 = 10^{-6} dyn$, $\eta_1 = \eta_2 = 0.5P$,

$\lambda_{zcl} = \lambda_{\perp cl} = 30\mathring{A},$, $\lambda_{zch} = \lambda_{\perp ch} = 10^4\mathring{A}$ and $C^1 = 510^{-3}s^{\frac{-3}{2}}$ and $J_1(\omega)$ is plotted for different values of K_3 in the range $10^{-10} - 10^{-3}dyn$. The present model allows for the anisotropy in elastic properties as well, resulting in somewhat complex behavior of the R_{1DF}. The functional dependence of R_{1DF} on ω in different regions in relation to the cutoff frequencies can be understood by examining appropriate limiting cases of the Eq. 2.35. keeping the earlier model also in view *(Vold and Vold 1988)*

Case 1 $\omega_{zcl}, \omega_{\perp cl} \ll \omega \ll \omega_{zch}, \omega_{\perp ch}$:
In this limit $A^2_{\alpha h}, B^2_{\alpha h} \gg 1$ and $A^2_{\alpha l}, A^2_{\alpha l} \ll 1$ resulting in

$$R_{1DF} = A_{DF} \sum_{\alpha} \frac{\pi\sqrt{\eta_\alpha}}{\sqrt{2}K_\alpha\sqrt{K_3}\sqrt{\omega}} \tag{2.38}$$

Equation 2.38 shows that the R_{1DF} has classical $\omega^{-0.5}$ behavior in a region in between upper and lower cutoff frequencies and also far away from the cutoff frequencies. Further, R_{1DF} has weak temperature dependence in this region.

Case 2 $\omega \ll \omega_{zcl}, \omega_{\perp cl} \ll \omega_{zch}, \omega_{\perp ch}$:
In this region $A^2_{\alpha h}, B^2_{\alpha h}, A^2_{\alpha l}$ and $B^2_{\alpha l} \gg 1$. Consequently

$$R_{1DF} = A_{DF} \sum_{\alpha} \frac{\sqrt{\eta_\alpha}}{K_\alpha\sqrt{K_3 p\omega}} \left[\frac{\sqrt{\omega_{\alpha zcl}}}{\omega_{\alpha\perp ch}} - \frac{\sqrt{\omega_{\alpha zcl}}}{\omega_{\alpha\perp cl} + \omega_{\alpha zcl}} - \frac{\pi}{\sqrt{2}} \frac{1}{\sqrt{\omega_{\alpha\perp cl}}} \right] \tag{2.39}$$

Eq. 2.39 shows that in a region below the lower cutoff frequencies R_{1DF} is independent of Larmor frequency reaching a plateau. In fact it is sufficient if the Larmor frequency is below one of the lower cutoff frequencies for R_{1DF} to show frequency independent behavior. In this case it can be shown that

$$R_{1DF} = A_{DF} \sum_{\alpha} \frac{\sqrt{\eta_\alpha}}{K_\alpha\sqrt{K_3 p\omega}} \left[\frac{\sqrt{\omega_{\alpha zcl}}}{\omega_{\alpha\perp ch}} - \frac{1}{\sqrt{\omega_{\alpha\perp cl}}} \right] \tag{2.40}$$

resulting in a frequency independent R_{1DF}.

Case 3 $\omega_{\perp cl} \ll \omega \ll \omega_{zcl} \ll \omega_{zch}, \omega_{\perp ch}$:
The situations, when the Larmor frequency is above one or all upper cutoff frequencies are already discussed earlier *(Vold and Vold 1988)*. In this region the R_{1DF} varies as $\omega^{-1.5}$ to ω^{-2}. Thus to sum up, the R_{1DF} is frequency independent below any of the lower cutoff frequencies, varies as $\omega^{-0.5}$ in the intermediate region between upper and lower cut off frequencies and varies as $\omega^{-1.5}$ to ω^{-2} above upper cut off frequencies. The values of the cutoff frequencies vary due to differences in the visco-elastic properties of the medium (Eq. 2.32).

Case 4 $\omega_{zcl} \ll \omega \ll \omega_{\perp cl} \ll \omega_{zch}, \omega_{\perp ch}$:

This scenario also results in a frequency independent R_{1DF} as

$$R_{1DF} = A_{DF} \sum_{\alpha} \frac{\sqrt{\eta_\alpha}}{K_\alpha \sqrt{K_3 p \omega}} \left[\frac{\sqrt{\omega_{\alpha z c l}}}{\omega_{\alpha \perp c h}} - \frac{\sqrt{\omega_{\alpha z c l}}}{\omega_{\alpha \perp c l}} + \frac{\pi}{\sqrt{2}} \frac{1}{\sqrt{\omega_{\alpha \perp c l}}} \right] \tag{2.41}$$

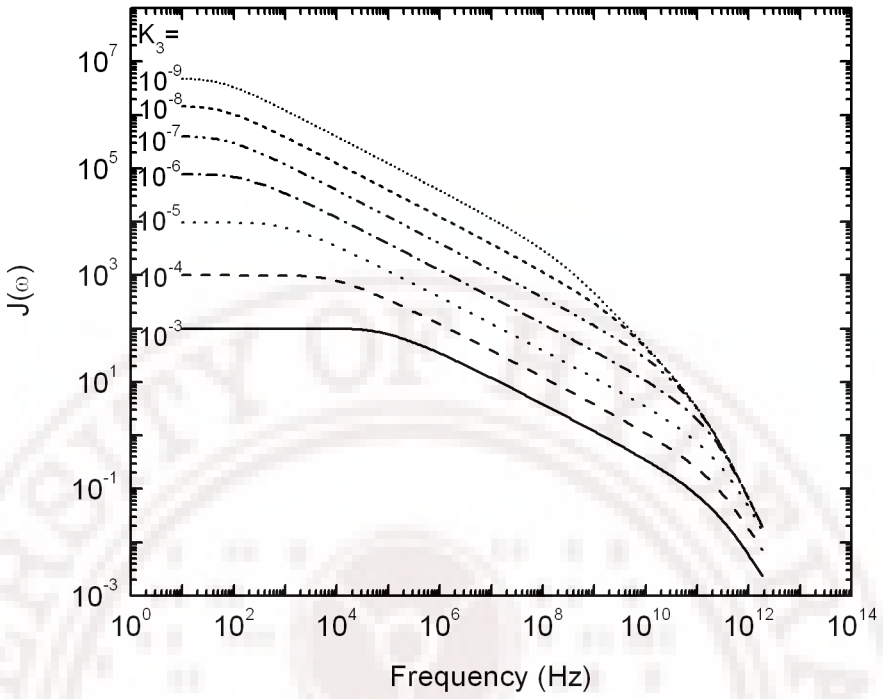

Figure 2.2: Computed variation of the spectral density $J_1(\omega)$ with K_3 based on Eq. 2.31 (other parameters are chosen as explained in the text).

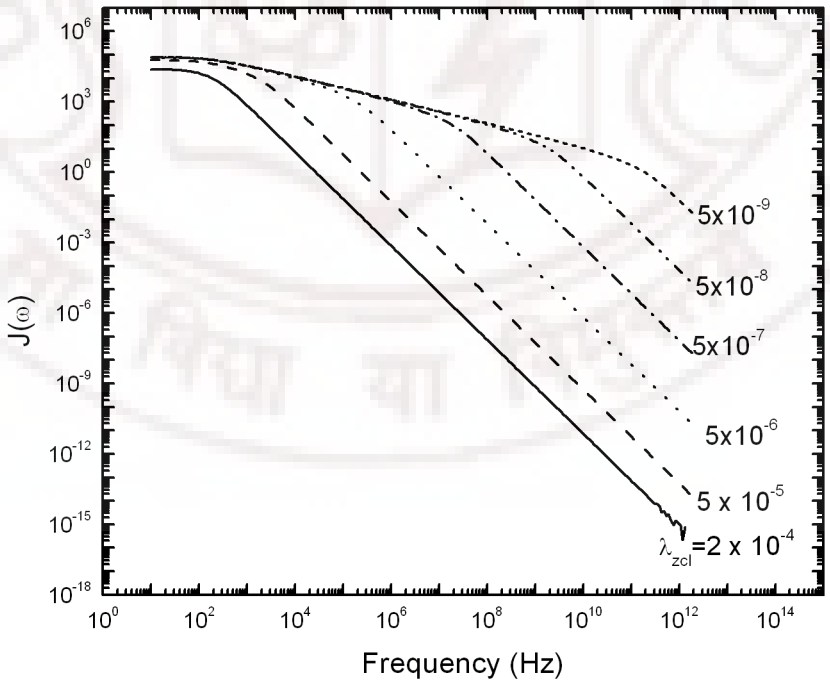

Figure 2.3: Computed variation of the spectral density $J_1(\omega)$ with λ_{zcl} based on Eq. 2.31 (other parameters are chosen as explained in the text).

2.5.2 Individual Molecular Motions

2.5.2.1 Self-Diffusion

Diffusion is molecular mass transport usually by thermally activated particle motions, and is a property of liquid crystals, which is relatively poorly, understood both experimentally and theoretically. Self-diffusion *(Chandrasekar 1943)* or translational displacement of molecules is a consequence of Brownian motions. The translational diffusion constants can be determined by several methods *(Kruger 1982)*. For normal liquids, the spin-spin relaxation is dominated by the translational diffusion and the application of this method to nematics is difficult because of strong magnetic dipole-dipole interactions making T_2 rather short.

NMR methods were applied quite extensively to study the diffusion in mesophases. They are divided into two classes: direct and indirect methods. In general any direct measurement of a diffusion coefficient requires a labelling of the diffusing species. In an NMR experiment labelling is achieved by the introduction of a gradient of the magnetic field B_o, in which the magnetic resonance is observed. By this gradient the magnetic field becomes inhomogeneous in the sample and hence the nuclear spin precession frequency (Larmor frequency) changes in a well-defined way with the position of the spins in the sample i.e. a frequency-space relation is generated by the application of pulse gradient of the magnetic field B_o. Diffusing spins, therefore, undergo Larmor frequency changes in time, caused by the diffusional motions of the molecules, to which they belong. The effect of these frequency changes on the amplitude of the nuclear spin echo can be calculated and hence the diffusion coefficient can be obtained *(Abragam 1961)*. Such a measurement correspond to determination of the mean square displacement of the diffusing spins in the gradient field during a certain time. Spin-echo methods are completely insensitive to other types of molecular motions, as rotations or oscillations; they do not disturb at all the diffusing system, and are particularly suited for the determination of self-diffusion coefficients. Using a special sequence of spin echoes, that removes most of the dipolar interaction, Blinc and coworkers had measured self-diffusion constants in the nematic phase of MBBA *(Blinc et al. 1973, Zupancic et al. 1974)* and this method has been used by the others to study self-diffusion in liquid crystals *(Noack 1984)*.

The indirect NMR methods involve measurements of spin-lattice relaxation times $(T_1, T_{1D}, T_1\rho)$ *(Wade 1977, Dong 1983)*. From their temperature and frequency dependences, one can look for the information on the self-diffusion. In favorable cases, where detailed models of spin relaxation based on diffusion mechanism exist, such attempts are fruitful.

The dipole-dipole interaction between protons on different molecules gets modulated as the molecules diffuse from one site to other and this can lead to considerable contribution to the spectral densities at typically the Larmor frequencies and thus an important mechanism for spin-lattice relaxation in liquid crystals. Torrey *(Torrey 1953)* derived an expression for spin lattice relaxation rate T_1^{-1} for an isotropic liquid using random-flights model. The basic idea is to use the probability distribution of the random flights mode. To calculate the correlation functions of the spatial parts of the dipolar Hamiltonian. With an assumed isotropy of space for flights, the diffusion coefficient D obeys the relation

$$D = \frac{\langle r^2 \rangle}{6\tau_D} \tag{2.42}$$

where $< r^2 >$ is the mean-square flight distance of the molecule and τ_D is the average time between two flights. But this treatment is to be extended in the case of liquid crystals where the anisotropy of the medium is translated to anisotropic diffusion, i.e. different diffusion coefficients for the two directions - parellel and perpendicular to the director. Zumer and Vilfan *(Zumer and Vilfan 1978)* extended Torrey's theory for isotropic liquids to anisotropic medium by taking into account the anisotropy of molecular diffusion, the simplifying cylindrical shape of molecules and a specific distribution of protons along the long molecular axis to obtain the relaxation rate from self-diffusion. Its contribution is given by *(Zumer and Vilfan 1978)*

$$T_1^{-1} = \frac{9}{8}\gamma^4\hbar^2\frac{n\tau}{d^3}Q\left[\omega\tau_D, \frac{< r_\perp^2 >}{a^2}, \frac{D_{||}^0}{D_\perp^0}\right] \tag{2.43}$$

where Q is dimensionless and numerically obtainable function. a is the diameter of the cylinder. Here $D_{||}^0$ and $D_\perp^0$ are the macroscopic self-diffusion constants. These constants correspond to perfectly aligned liquid-crystalline phase and are given by,

$$\begin{aligned} D_\perp^o &= \frac{< r_\perp^2 >}{4\tau_\perp} \\ D_{||}^o &= \frac{< r_{||}^2 >}{2\tau_{||}} \end{aligned} \tag{2.44}$$

The value of $\frac{D_\perp^o}{D_{||}^o}$ does not differ significantly for different compounds *(Kruger 1982)*. The results in nematic compounds were found to reduce to the familiar Torrey's equation *(Torrey 1953)* in the limit $\omega\tau_D < 0.3$

$$T_1^{-1}(\omega) = C - F\omega^{1/2} \tag{2.45}$$

where C and F are the constants related to the average diffusion coefficient D as

(Harmon and Muller 1969)

$$F = -4.88 \times 10^{-14} p\,(1+\delta)\,D^{-3/2} \quad and \quad C \propto D^{-1} \tag{2.46}$$

In the frequency region of interest to NMR experiment spin lattice relaxation rate in the nematic and smectic phases can be shown to follow the Torrey's model (valid for the isotropic phase) but for a scalar factor of 1.4 *(Zumer and Vilfan 1978, Vilfan and Zumer 1980)*. The T_{1SD}^{-1} can thus be written as

$$T_{1SD}^{-1} = \frac{1}{1.4} T_{1Torrey}^{-1} \tag{2.47}$$

In the limit $\omega\tau_D < 1$ the relaxation rate R_{1SD} can be written as (isotropic approximation) *(Zumer and Vilfan 1978)*

$$T_{1SD}^{-1} \;=\; \frac{B}{\omega}\left(f(x) + f(\sqrt{2}x)\right) \tag{2.48}$$

where

$$f(x) = \left(\frac{2}{x^2}\right)\left\{v\left[1 - \frac{1}{(u^2+v^2)}\right] + \left[v\left(1 + \frac{1}{(u^2+v^2)}\right) + 2\right] e^{-2v}\cos 2u + u\left[1 - \frac{1}{(u^2+v^2)}\right] e^{-2v}\sin 2u\right\} \tag{2.49}$$

$$\begin{pmatrix} u \\ v \end{pmatrix} \;=\; \frac{\left(\omega a^2/2D\right)^{1/2}}{\left(4+\omega^2\tau_D^2\right)^{1/4}}\left\{1 \pm \frac{\omega\tau_D}{\left(4+\omega^2\tau_D^2\right)^{1/2}}\right\}^{1/2} \text{and}\, x \;=\; \left(\omega a^2/D\right)^{1/2}$$

Here D is the average diffusion coefficient with a correlation time τ_D given by $\frac{a^2}{6D}$ and a is the closest distance of approach of two molecules (taken to be the diameter of the molecules, $\simeq 5\mathring{A}$). In the limit, $\omega\tau_D \gg 1$, the relaxation rate reduces to the ω^{-2} law.

2.5.2.2 Reorientations

Liquid crystals having anisotropic molecular shape can be visualized to have three types of rotational motions due to (a) fast reorientations around the long axis (b) rotations about the short axes and (c) the isotropic tumbling of the end chains *(Blinc et al. 1978)*. The rotations around the long molecular axis are usually very fast and do not contribute significantly towards relaxation in nematics and high temperature smectics. In low temperature smectic phases on the other hand, rotations around the long axis may become important. For the case that the director makes an angle with the direction of the external magnetic field, one finds for fast rotations ($\omega\tau_l \ll 1$)

around the long molecular axis

$$T_{1RL}^{-1} = \frac{9}{8}\gamma^4\hbar^2 r^{-6}\frac{18}{32}\left(\frac{\tau_l}{8}\right)\left(1+3\cos^2\Delta\right) \tag{2.50}$$

In the above case normally only alkyl chain protons contribute to the relaxation with only marginal effect from benzene ring protons. The relaxation rate for reorientations around the short molecular axes in various mesophases follows a BPP relation *(Bloembergen et al. 1948)* written as

$$T_{1RS}^{-1} = \varepsilon C\sum_{p=1}^{2} p^2\frac{\tau_s}{1+\left(p\omega\tau_s\right)^2} \tag{2.51}$$

where $C = \epsilon C_1$ and ϵ measures the anisotropy of local reorientations around the short axes. The constant C_1 for a molecule consisting of aliphatic groups in the core and aromatic groups in the end chains is given by

$$C_1 = \frac{9}{8}\gamma^4\hbar^2\frac{1}{15}\sum_k \frac{u_k\left(3l_k^2-1\right)^2}{r_k^6} \tag{2.52}$$

where u_k stands for the ratio of protons belonging to k^{th} group, to the total number of protons in the molecules, l_k's are cosines of angle between internuclear vector r_k of k^{th} group and the long axis. In the limit $\omega\tau_s \ll 1$ the relaxation rate due to reorientations around short axis gives rise to frequency independent contribution given by,

$$T_{1RS}^{-1} = 5\varepsilon C\tau_s \tag{2.53}$$

Usually, Arrhenius-type of temperature dependence is assumed for τ_s since the reorientations are thermally activated, i.e.

$$\tau_s = \tau_o\exp\left(\frac{E_{as}}{k_B T}\right) \tag{2.54}$$

here τ_0 is the pre-exponential factor and E_{as} is the activation energy associated with the motional process (k_B is the Boltzmann constant). Thus, a plot of $ln(T_1)$ vs T will have two straight lines with slopes $\frac{-E_{as}}{k}$ and $\frac{E_{as}}{k}$ at higher and lower temperature respectively.

2.5.3 Both Collective and Non-Collective Motions

2.5.3.1 Diffusion Assisted DF

Intermolecular interactions can also influence the intramolecular interactions. For example, molecule diffusing in a nematic medium adjusts its long axis according to the

local director, n(r,t), which is space dependent owing to order director fluctuations. In favourable conditions, this coupling between orientational and diffusive modes could be observed, and the correlation function for director fluctuations will then have dependence on the diffusion coefficient as well. When we include the contribution of translational diffusion to the director fluctuations (also known as *diffusion assisted director fluctuations*), Eqn. 2.36 gets modified. The term $\frac{K}{\eta}$ in equation for spectral density (Eqn. 2.33) is changed to $\frac{K}{\eta} + D$ *(Dong 1994)* i.e,

$$A^2_{\alpha h(l)} = \left(\frac{K_\alpha}{\omega\eta_\alpha} + D\right) q^2_{\perp ch(l)}, \text{ and } B^2_{\alpha h(l)} = \left(\frac{K_z}{\omega\eta_\alpha} + D\right) q^2_{zch(l)} \tag{2.55}$$

The diffusion assisted ODF also has the same angular and frequency dependencies as nematic ODF, but with a different temperature dependence. This is essentially determined by the diffusion coefficient, i.e. the temperature dependence of T_1 arising from ODF mechanism now becomes thermally activated *(Blinc et al. 1975)*.

2.6 Spin-lattice Relaxation Processes in Protein Solutions

Studies of biomolecular hydration via the water nuclei is one of the well established applications of NMR to biological systems *(Halle et al. 1999, and references therein)*. Spin lattice relaxation rate in aqueous protein solutions has long been known to exhibit dispersion in the MHz frequency range. Since the early NMRD studies *(Koenig 1969, Blicharska et al. 1970, Kimmich and Noack 1970)* it took several revolutionary methodological, instrumental and application oriented, advancements in the investigation of protein solutions. In this section we discuss the progress of NMRD, as a potential tool to study protein solutions, and the relevant theory used in the typical analysis of NMRD of these systems.

2.6.1 NMR Properties of Water Nuclei

Three different hydrogen isotopes, ^{1}H, ^{2}H, and ^{3}H as well as the magnetic oxygen isotope ^{17}O are sources for NMR studies of protein hydration. Longitudinal relaxation is predominantly due to fluctuating magnetic dipole-dipole couplings in case of ^{1}H and due to fluctuating electric field gradients in case of the quadrupolar nuclei ^{2}H and ^{17}O. Among these, ^{1}H nucleus has highest sensitivity and widest accessible frequency range followed by deuteron (^{2}H). ^{2}H nucleus has two orders of magnitude lower receptivity and one order of magnitude faster relaxation than ^{1}H. For this reason until recently vast majority of NMRD studies of protein solutions employed ^{1}H

relaxation experiments to investigate protein solutions. Though ^{1}H has several such advantages, experimental ^{1}H relaxation data appears to have been weighed down by interpretational controversies for many decades, for the reasons:

i. Assuming that the dynamic coupling between the water and protein ^{1}H spin systems brought about by cross relaxation (via intermolecular dipole coulings) and is primary to analyze NMRD data.

ii. ^{1}H relaxation generally contains a potentially confounding contribution from labile protein protons and this contribution is more pronounced away from neutral pH and in the presence of buffers *(Liepinsh and Otting 1996)* mostly due to proton exchange catalysis *(Eigen 1964)*

iii. Water protons are engaged in intramolecular as well as intermolecular dipole couplings. The intermolecular couplings are quite different in bulk water and for a water molecule buried inside a protein and thus complicate the interpretation of ^{1}H NMRD data *(Venu et al. 1997)*.

Due to the shorter intrinsic relaxation time, ^{2}H is less susceptible than ^{1}H to labile hydrogen exchange averaging. Neverthless, rapidly exchanging biopolymer deuterons can dominate water ^{2}H relaxation at low and high pH values *(Woessner and Snowden 1970, van der Klink et al. 1974, Piculell and Halle 1986, Denisov and Halle 1995b)*. Initially these problems were successfully overcome by measuring ^{17}O relaxaton rates, for the reason that, unlike the hydrogen nuclei ^{17}O reports exclusively on water molecules *(Halle and Wennerstrom 1981, Piculell and Halle 1986, Denisov and Halle 1995b)*. At the stage where, ^{17}O NMRD was establishing its roots into bio-NMR field, a more recent work has shown that the effect of labile proton exchange is negligible for protein solutions and ^{1}H can be effectively used for NMRD studies *(Venu et al. 1997)*.

2.6.2 Quantitative Analysis and Parametrization of NMRD Data

Recent ^{17}O investigations in the form of difference NMRD experimets (where the NMRD profiles obtained from two structurally related proteins are compared), in support of high resolution studies on protein crystal structures, revealed that there exist small number of crystallographically identifiable internal waters, essentially buried within the protein. These water molecules have residence times in the range 0.01-1μs *(Denisov and Halle 1994, Denisov and Halle 1995a, Denisov and Halle 1995b, Denisov and Halle 1995c, Denisov and Halle 1996)*. It was then concluded that these internal molecules are responsible for the dispersion in the MHz region. To completely

account for the T_1 dispersion of water-protein system the water molecules present in the protein solution are, spatially and temporally resolved into three catagories:

i. Water molecules which are unpertubed by protein or bulk water, which are usually in extreme narrowing regime.

ii. Water molecules that are dynamically pertubed by the protien but remain sufficiently mobile that, their effective correlation times are much shorter than the tumbling time of the protein. These are essentially comprise the hydration layer i.e water molecules in contact with the protein surface.

iii. The long lived water molecules which are usually buried in cavities inside the protein or trapped in deep surface pockets with low accessibility to exteral water.

Then a simple phenomenological description of the effect of exchange averaging on the water longitudinal relaxation rate ($R_1(\omega_o)$), in a protein solution is given as *(Halle et al. 1999)*

$$R_1(\omega_o) = (1 - f_s - f_I) R_{1bulk} + f_s R_s + \sum_k \frac{f_k}{\tau_k + 1/R_{1k}(\omega_o)} \tag{2.56}$$

The first term refers to the fraction 1-f_s-f_I of water molecules that are in the fast exchange regime (bulk water) with relaxation rate R_{1bulk}. The second term refers to the fraction f_s of water molecules (surface waters) with relaxation rate R_s. These water molecules are responsible for the excess relaxation at frequencies above the dispersion. The third term comes from the contribution of fraction of ling-lived internal waters f_I. Each of these water molecules has a distinct residence time τ_k and intrinsic longitudinal relaxation rate R_{1k} and, taken together, they account for a fraction $f_I = \Sigma_k f_K$ of all water molecules in the sample. Third term also contains relaxation rate contributions generally from labile protein hydrogens which exchange slowly compared to the tumbling of the protein.

The dispersion of the spin-lattice relaxation rate, R_1 of the water nuclei in a protein solution is accurately described by *(Denisov and Halle 1996)*.

$$R_1 = R_{1bulk} + \alpha + \beta\tau_c F_1(\omega_o) \tag{2.57}$$

Here, $F_1(\omega_o)$ is a normalized dispersion function decreasing monotonically from 1 at $\omega_o \ll \omega_c$ to 0 at $\omega_o \gg \omega_c$ with ω_c as the dispersion frequency. Usually in case of ^{1}H relaxation,

$$R_1(\omega_o) = R_{bulk} + \alpha + \beta_{intra}\tau_c F_{1intra}(\omega_o) + \beta_{inter}\tau_c F_{1inter}(\omega_o).$$

for the simplest case where all water nuclei contributing to the dispersion exchange with bulk water rapidly compared to the intrinsic spin relaxation but slowy compared to the protein rotational diffusion

$$F_{1inter}\left(\omega_o\right) = 0.1 + \frac{0.3}{1+\left(\omega_o\tau_c\right)^2} + \frac{0.6}{1+\left(2\omega_o\tau_c\right)^2} \tag{2.58}$$

$$F_{1intra}\left(\omega_o\right) = \left(\frac{0.2}{1+\omega_o^2\tau_c^2} + \frac{0.8}{1+4\omega_o^2\tau_c^2}\right) \tag{2.59}$$

This dispersion can be represented by F_{1intra} negleting small shift of the dispersion frequency and by adjusting the α and β vlues as

$$\alpha = \alpha_{true} + 0.1\beta_{inter}\tau_c$$

and

$$\beta = \beta_{intra} + 0.9\beta_{inter}$$

Further more, α is the excess relaxation rate on the high-frequency plateau above the dispersion:

$$\alpha \equiv R(\omega_o \gg \omega_c) - R_{bulk}.$$

β is the dispersion amplitude parameter. It contains information about the number of rapidly exchanging internal water molecules with residence times τ_w obeying $\tau_R \ll \tau_w \ll [R_{1I}]^{-1}$ and about their orietational order, where τ_R is protein rotational correlation time and hence given by

$$\beta = f_I\omega_D^2 S_I^2 \tag{2.60}$$

where ω_D is rigid lattice dipole coupling constant given by *(Abragam 1961)*

$$\omega_D = \left(\frac{3}{2}\right)^{1/2}\left(\frac{\mu_o}{4\pi}\right)\frac{\hbar\gamma^2}{r_{HH}^3} \tag{2.61}$$

with r_{HH}, the H-H seperation in the water molecule. S_I is the generalized second-rank orientational order parameter for internal water molecule.*(Denisov and Halle 1995c, Halle and Wennerstrom 1981, Lipari and Szabo 1982, Halle et al. 1999)* τ_c is effective correlation time, given by

$$\frac{1}{\tau_c} = \frac{1}{\tau_R} + \frac{1}{\tau_w} \tag{2.62}$$

since $\tau_R \ll \tau_w$ usually $\tau_c \simeq \tau_R$ *(Denisov et al. 1997)* The rotaional correlation time of the protein can also be estimated for sufficiently dilute protein solutions from the

Debye-Stokes-Einstein relation

$$\tau_R = \frac{\eta V}{k_B T} \tag{2.63}$$

with V the hydrodynamic volume of the protein and η the viscosity of the solvent. This relation is strictly valid only for a protein that behaves as a smooth rigid sphere. $\beta\tau_c$ measures the magnitude of the dispersion step.

$$\beta\tau_c \equiv R(\omega_o \ll \omega_c) - \alpha - R_{bulk}$$

α, β and τ_c are operationally defined in Fig.2.4 By knowing accurately determined

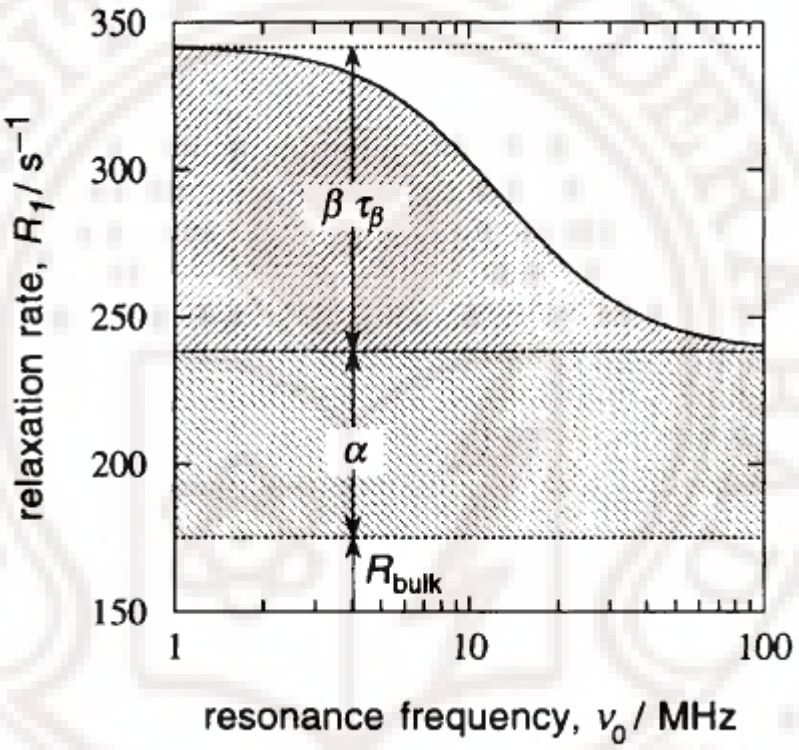

Figure 2.4: Typical water NMRD profile in a protein solution, with the parameters in eqn. 2.57

concentrations of protein samples one can have a quantitative reliable analysis of NMR motional parameters. Thus the identification of internal water molecules as the source of relaxation dispersion has transformed the NMRD method into a quantitative tool for investigating specific water molecules of structural and funcutional significance and for exploiting internal water molecules as noninvasive pobes of protein structure and dynamics.

Chapter 3

Pulsed and Field Cycling NMR Relaxometry

NMR experiments can be carried out either in frequency domain or in time domain. In the early days of its development, continuous wave (CW) spectrometers were used to perform frequency domain experiments where one sees the frequency dependence of the real and imaginary parts of the susceptibilities either by sweeping rf frequency or the static field through the resonance. These were better suited for direct observation of static aspects of the microscopic environment. With the advent of pulsed rf techniques, time domain experiments were possible which readily focus on dynamic aspects aswell. In a typical pulsed experiment one measures the time evolution of magnetization followed by an rf pulse. With the development of fast Fourier transform (FFT) algorithm, such a classification is only of acadamic interest, since the two out comes of these two experiments are closely related by FT as

$$f(t) = \frac{1}{2\pi} \int_{-\infty}^{\infty} F(\omega) e^{-i\omega t} dt \tag{3.1}$$

$$F(\omega) = \frac{1}{2\pi} \int_{-\infty}^{\infty} f(t) e^{i\omega t} d\omega \tag{3.2}$$

Hence the same spectral information can in principle be obtained from both the methods. However the large majority of NMR experiments currently are best performed with pulse spectrometers owing to their advantages over the CW type. There are three principal advantages of pulsed over CW-swept excitation.

i. In the pulsed experiment nuclei within the frequency band width of the pulse are excited simultaneously so that the spectral information obtained per unit time is enhanced.

ii. As the signal detection takes place in the absence of rf excitation, NMR signal is free from oscillator noise, leading to an improvement of the signal-to-noise

ratio $\frac{S}{N}$.

iii. The measurement of signal becomes easier as signal followes by a pulse which provides the phase coherence.

Despite these advantages, applications of pulse experiments are limited due to poor $\frac{S}{N}$ as the signal strength weakens with the decrease in applied static field ($\frac{S}{N} \propto H_0^{\frac{3}{2}}$) for proton typically about 4 MHz Larmor frequency. The significance of field-cycling technique emerges here. In this technique the nuclei are polarized at suitably high static fields and allowed to relax at the desired low field by switching the static field suddenly. The magnetization remaining after a delay time is detected again at a higher field, providing a good signal to noise ratio since the detection system operates under the favourable conditions of high enough frequency. The advent of fast field-cycling NMR (FFCNMR) technique practically leveled the low field limit of NMR experiments only limited by the earth's field. Thus field-cycling relaxometry enables one to investigate the frequency dependence of NMR phenomena covering several decades of frequency with the same instrument. This feature makes it a most powerful tool for the study of molecular dynamics in complex systems. To cover Larmor frequencies ranging from 60 MHz to 10 kHz we augmented the commercial FFCNMR relaxometer (Spinmaster, Stelar, Italy) covering the range 10 kHz to 20 MHz, with a conventional field variable pulsed spectrometer (10 - 60 MHz).

This chapter provides briefly the principles and methodology of pulsed NMR measurements, including field cycling technique. This also gives certain technical detailes of the instruments useful to appreciate the results reported in this thesis.

3.1 Conventional Pulsed NMR Methodology

The equation of motion of the total nuclear magnetic moment $\mathbf{M}$, in the presence of a magnetic field $\mathbf{H}$ can be written, as *(Abragam 1961, Slichter 1978)*

$$\frac{d\mathbf{M}}{dt} = \gamma \left(\mathbf{M} \times \mathbf{H}\right) \tag{3.3}$$

In order to solve the equation readily, it is convenient to transform the reference to a rotating coordinate system. It can be shown that the time derivative of any time dependent vector $\mathbf{M}$(t), computed in the laboratory frame (say, {x,y,z}) is related to such a derivative computed from a rotating frame with an angular velocity ω, (say, {x',y',z'}) as

$$\frac{d\mathbf{M}}{dt} = \frac{\delta\mathbf{M}}{\delta t} + (\omega \times \mathbf{M}) \tag{3.4}$$

where $\frac{\delta \mathbf{M}}{\delta t}$ describe motion of $\mathbf{M}$ in the rotation coordinate system or in detail rate of change of $\mathbf{M}$ with respect to {x',y',z'} frame. Combining Eqns. 3.3 and 3.4 the equation of motion of $\mathbf{M}$ in the rotating frame can be written as

$$\frac{\delta \mathbf{M}}{\delta t} = \gamma M \times \left(H + \frac{\omega}{\gamma} \right) \tag{3.5}$$

Thus in the rotating frame the magnetic moment experiences an effective field which is the sum of the applied field H and a fictitious field $\frac{\omega}{\gamma}$. Considering a special case appropriate to our experiments, where a dc magnetic field H_o is applied along z-direction and a rotating field H_1 around x-axis, the corresponding equation in a rotating frame, where H_1 appears stationary, is given by

$$\frac{\delta \mathbf{M}}{\delta t} = \gamma \mathbf{M} \times \left[\left(H_o + \frac{\omega}{\gamma} \right) \mathbf{k} + H_1 \mathbf{i} \right] \tag{3.6}$$

where $\mathbf{i}$ and $\mathbf{k}$ are the unit vectors along x' and z' axes, respectively, in the rotating frame. (Here x' axis in the rotating frame is chosen to be along H_1). If H_1 is applied at Larmor frequency equation 3.6 becomes

$$\frac{\delta M}{\delta t} = \gamma \left(M \times H_1 \right) \tag{3.7}$$

Thus at resonance, the effective field seen by the nuclear magnetic moment, from the frame where the applied rf field is stationary, is only due to H_1 and hence it precesses around H_1 with a frequency $\omega_1 = \gamma H_1$. Then the angle, through which $\mathbf{M}$ precesses in a time t is

$$\theta = \gamma H_1 t \tag{3.8}$$

If the rf pulse is applied for a chosen time so that $\theta = \frac{\pi}{2}$, then the pulse is called $\frac{\pi}{2}$ pulse. Similarly, if the pulse width is long enough to rotate the magnetization by an angle π (i.e. to flip the total magnetization into -z direction), then the pulse is called π pulse. The total magnetization, thus flipped into transverse plane by a $\frac{\pi}{2}$ pulse is stationary in the rotating frame. But, because of the spin-spin interaction there is a spread (ΔH) in the net magnetic field experienced by the individual magnetic moments. This results in a spread in the Larmor frequencies ($\Delta\omega = \gamma \Delta H$) of individual magnetic moments and they start dephasing resulting in the decay of the net magnetic moment as observed from the x'-y' plane. An rf pick-up coil, in the laboratory frame, outputs an oscillatory emf at the Larmor frequency corresponding to the net magnetization. After rf detection, the envelope of this signal is a decaying curve (Free induction decay, FID), with a time constant of T_2 (spin-spin relaxation time). But in practice, there are two contributions to the spread in the Larmor frequency:

the first due to the spin-spin interaction and the second due to the inhomogeneity in the applied magnetic field. Hence one always finds that the FID decays with a time constant T_2^* which is shorter than T_2.

3.2 Measurement of Relaxation Times

To measure various relaxation times (T_1 and T_2), different pulse sequences, corresponding to the different initial non-equilibrium conditions required to be created, are necessary. The details of such pulse sequences used in the present studies are given below.

3.2.1 T_1 Measurements

3.2.1.1 Saturation Recovery Sequence ($\frac{\pi}{2} - \tau - \frac{\pi}{2}$)

In this sequence the first $\frac{\pi}{2}$ pulse makes the magnetization, in the z-direction, zero. The magnetization, developed after a time τ is again sampled by another $\frac{\pi}{2}$ pulse *(Farrar and Becker 1971, Fakushima and Roeder 1981).* Magnetization recovery after the first $\frac{\pi}{2}$ pulse is described by

$$M_z(t) = M_o \left[1 - \exp\left(-\frac{t}{T_1}\right)\right] \tag{3.9}$$

The amplitude, A(t) of the FID observed after the second $\frac{\pi}{2}$ pulse applied after a time τ (see Fig. 3.1), is represenatative of the instantaneous M_z component developed till that instant as a result of spin-lattice relaxation process. The time evolution of this FID amplitude is thus provided by the above equation. (Eqn.3.9), and hence T_1 value can be computed.

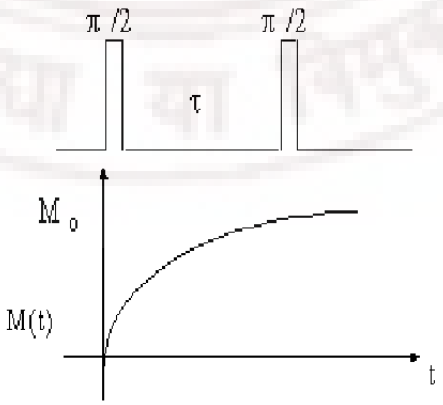

Figure 3.1: Saturation recovery sequence

3.2.1.2 Inversion Recovery ssequence $(\pi - \tau - \frac{\pi}{2})$

This sequence is also used for T_1 measurements. The first π pulse flips the magnetization to -z direction, which is allowed to evolve for a time τ and then sampled by another $\frac{\pi}{2}$ pulse. (Farrar and Becker 1971, Fakushima and Roeder 1981). The amplitude of the FID, A(t), after this sampling pulse, representing the instantaneous $\mathbf{M}-z$ component, increases from a negative value to its equlibrium value covering the zero value in the process. The detected amplitude of the FID evolves as

$$A(t) = A(\infty)\left[1 - \exp\left(-\frac{t}{T_1}\right)\right] \tag{3.10}$$

as shown in the Fig. 3.2. Using this sequence, it is convenient to make a rough estimation of the T_1 value by observing the zero crossing point.

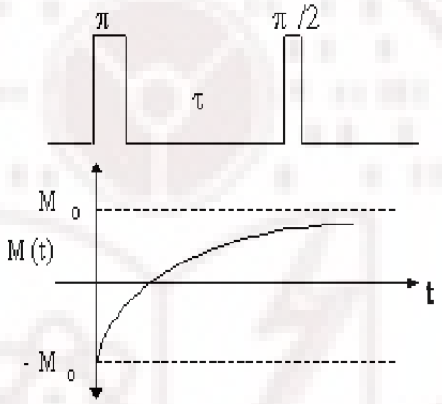

Figure 3.2: Inversion recovery sequence

The advantage of this sequence compared to the saturation recovery sequence is the apparent increase in the signal to noise ratio. The total variation of the magnetization is M_o in the saturation recovery sequence whereas it is $2M_o$ in the inversion recovery sequence. But this sequence assumes that before the first pulse (preparation pulse) is applied the spin system is completely in equilibrium and hence the magnetization is M_o along z-direction. So before repeating the sequence, it is necessary to wait until complete equilibrium is achieved, usually for a period of about $5T_1$. This will become very time consuming if T_1 is more than few hundreds of ms. Saturation recovery sequence does not have this problem since the preparation pulse only has to make the magnetization in the z-direction zero and it does not matter what the magnetization is before this pulse. One disadvantage of these two sequences is that, if the preparation pulse width is not exactly (π or $\frac{\pi}{2}$), the initial conditions of the magnetization ($-M_0$ or zero, respectively) are not met.

3.2.1.3 Saturation Burst Sequence

This sequence employs a number of $\frac{\pi}{2}$ pulses (say, n) (usually $5 < n < 10$) followed by a sampling ($\frac{\pi}{2}$) pulse. The spacing between two $\frac{\pi}{2}$ pulses in the burst (τ) is so chosen that the T_2 process is complete but T_1 process has not effectively taken place (i.e. $T_2 < \tau \ll T_1$). This burst generates zero magnetization in the x-y plane even if the pulses slightly deviate from $\frac{\pi}{2}$ and even if H_1 is slightly inhomogeneous. The magnetization recovery again satisfies Eqn. 3.9 and T_1 can be calculated as explained above. Since the FID amplitude is measured after saturating the spin system, it is not necessary to wait till the spins completely relax to equilibrium, before the next sequence is applied. The sequence can be repeated immediately after recording the FID amplitude. In fact, in an actual experiment, the first pulse in the next burst can be used as the sampling pulse. The recovery of the magnetization, in this experiment, is shown in Fig. 3.3.

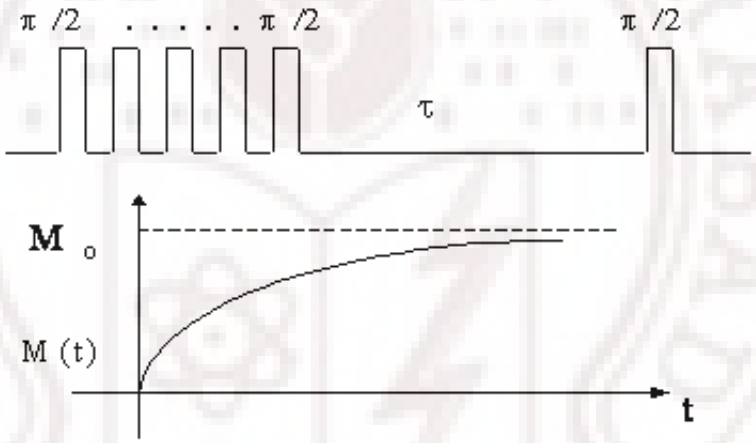

Figure 3.3: Saturation burst sequence

3.2.2 T_2 Measurements

3.2.2.1 Spin-Echo Method

Due to the spatial inhomogeneity in the applied dc field, the time constant associated with the FID decay (T_2^*) is shorter than T_2 and hence the FID after a single $\frac{\pi}{2}$ pulse can not be used to measure T_2. Instead, the spin echo method with a $\frac{\pi}{2} - \tau - \pi$ sequence (Hahn 1950) is used. The effect of this pulse sequence on the spin system is shown in Fig. 3.4, which can be understood as follows. The first $\frac{\pi}{2}$ pulse puts the magnetization in the transverse plane (say along x'-axis, if the pulse is applied along y'-axis). The magnetization starts de-phasing due to the spread in the Larmor frequencies. Next π -pulse (along the same y'-axis) at time τ inverts all individual magnetic moments (to lie along -x' axis) thereby inverting the sequence of dephasing

as shown in Fig. 3.4.

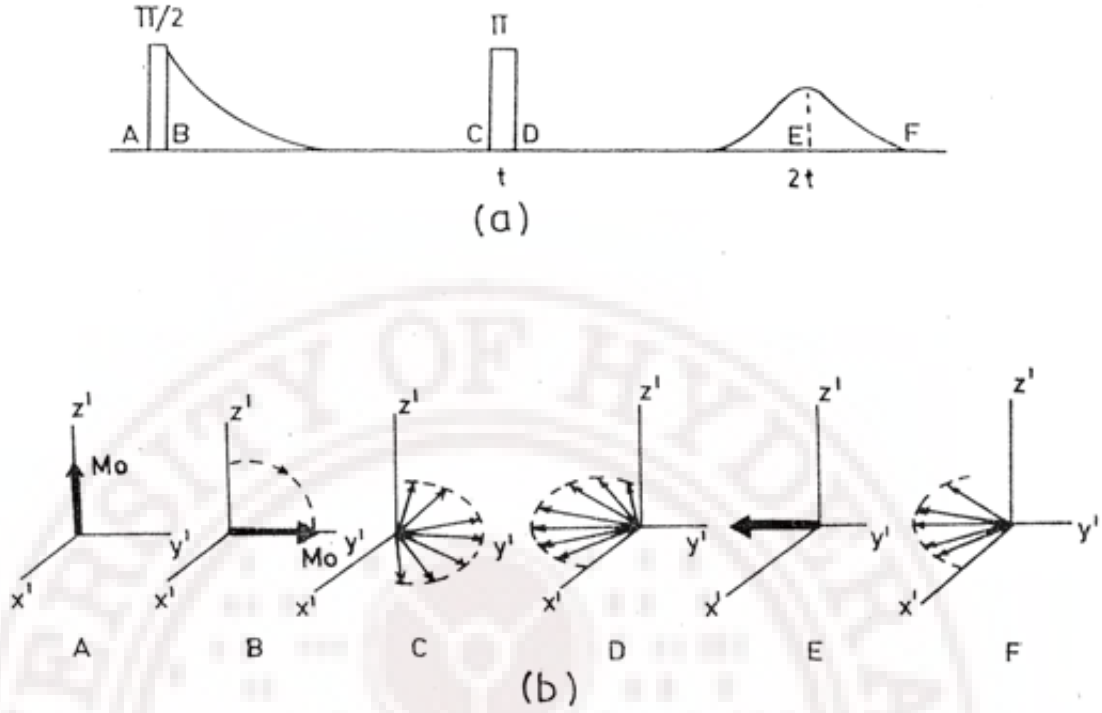

Figure 3.4: Spin-Echo Sequence

Therefore the spins refocus again after the time interval τ from the π pulse forming an echo. If the π pulse can invert the direction of the dephasing of all spins then the echo will have same magnitude as that of the FID. This means that the phase relations among these spins have not changed during the time 2τ. But these phase relations may change for some spins during the time 2τ (e.g., if the dephasing is due to time varying local fields) and such spins do not coalesce with the other spins and so their contribution to spin echo will be missing. Thus any process which causes individual spins dephase in a irreversible manner will reduce the amplitude of the echo, and one obvious example of such process is spin-flip due to spin-spin interaction. Thus by measuring the amplitude of the echo as a function of τ one can measure T_2 since the spin echo amplitude decreases as $\exp\left(-\frac{\tau}{T_2}\right)$.

3.2.2.2 Carr Purcell Sequence

If there is a rapid diffusion in the inhomogeneous magnetic field, the spin echo amplitude is further reduced *(Slichter 1978)* and the above sequence is not useful for measuring T_2. A sequence suggested by *Carr and Purcell (1964)* is well suited in such cases. This sequence consists of a $\frac{\pi}{2}$ pulse followed by a series of π pulses at t,

3t, 5t etc. The spin echoes arising out of this sequence is shown in Fig.3.5. It can be shown *(Ailion 1983)*

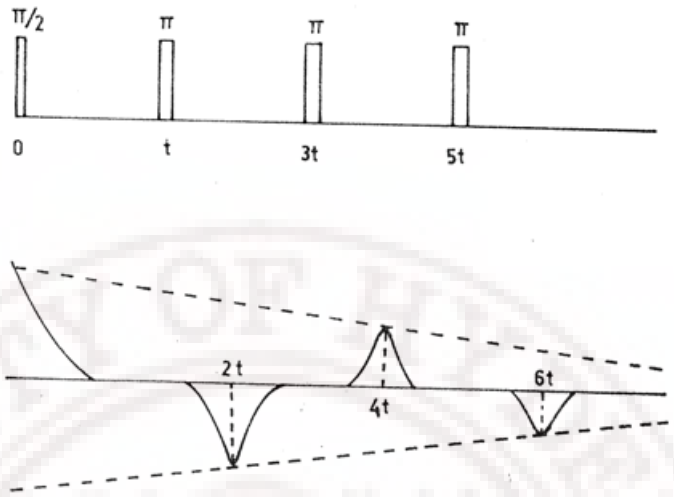

Figure 3.5: CPMG Pulse sequence.

that this sequence makes the contribution of diffusion due to the field inhomogeneity negligible. In this sequence error in setting the width of pulse does lead to some error in T_2 but this can be rectified by the insertion of a 90^0 phase shift between the $\frac{\pi}{2}$ pulse and successive π pulses, as suggested by *Meiboom and Gill (1958).*

3.3 Fast Field-Cycling NMR (FFCNMR) Methodology

Molecular processes in complex fluids, for example the collective motions in liquid crystals are very slow in nature. Typical range of such motional frequencies fall in sub MHz to kHz regime. At such low frequencies conventional pulsed NMR methods are technically impracticable or even impossible. The difficulties are primarily due to the related well-known weakening of the NMR induction signal, which goes approximately as $H_o^{3/2}$. In this context field-cycling (FC) technique is very effective and overcomes this limit extending the scope of field dependent measurements to very low Larmor frequencies while still allowing the convenience of high field signal detection. Thus field-cycling NMR (FCNMR) complements and enables one to extend investigations of molecular processes over a wide band width spacing several decades, in conjunction with conventional pulsed NMR technique.

3.3.1 FC Principle

In a FC experiment sample generally undergoes three evolution phases namely polarization period (P), evolution or relaxation period (E) and detection period (D). Fig. 3.6 illustrates these three periods. The cycle starts with τ where samples are polarized at relatively high fields (B_{oP}) and allowed to relax at a lower field (B_{oE}). The remaining magnetization after pre-defined delay is detected at a higher field B_{acq}. The field switching rate must be large enough to avoid excessive relaxation losses of the magnetization during the switching process and also it should be slow enough to permit adiabatic field changes in case the relaxation field is perceptibly superimposed by local fields (of arbitrary directions other than that of the polarizing field). For this purpose in early FC experiments sample shuttling technique was used. In this, the sample under study is shuttled fast from B_{oP} to B_{oE} and further to B_{acq} mechanically normally pneumatically. Even though this mechanical field-cycling is very simple, it has considerable drawbacks.

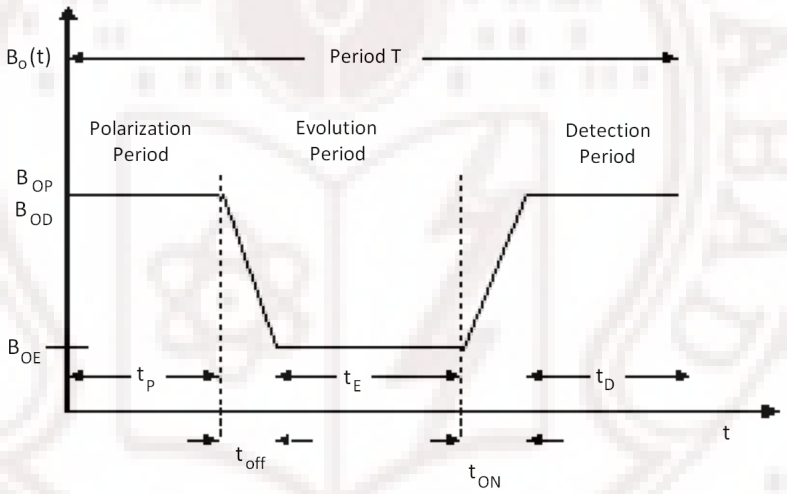

Figure 3.6: Typical field cycle, with polarization, evolution and detection periods separated by the transit intervals t_{ON} and t_{OFF}

The switching is relatively slow and cannot be applied if the T_1 is shorter than 100 ms. In addition, reliable temperature control seems to be almost impossible. In these circumstances the electronic field switching emerged, where the magnetic field cycling takes place by controlling the electrical current through the magnet coil fast compare to the relaxation times. In this technique field switching takes place within 3 ms or even less. For this reason it is often called fast field-cycling (FFC) NMR technique. For achieving this fast switching, one uses energy storage principle discussed in detailed in a review article *(Noack 1986, Kimmich and Anardo 2004)*

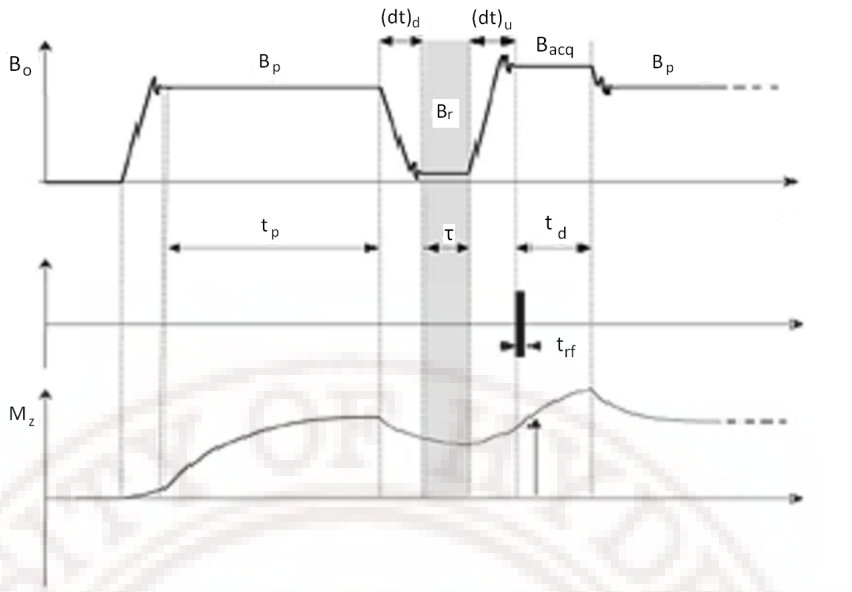

Figure 3.7: Field cycle for low relaxation fields (pre-polarization).

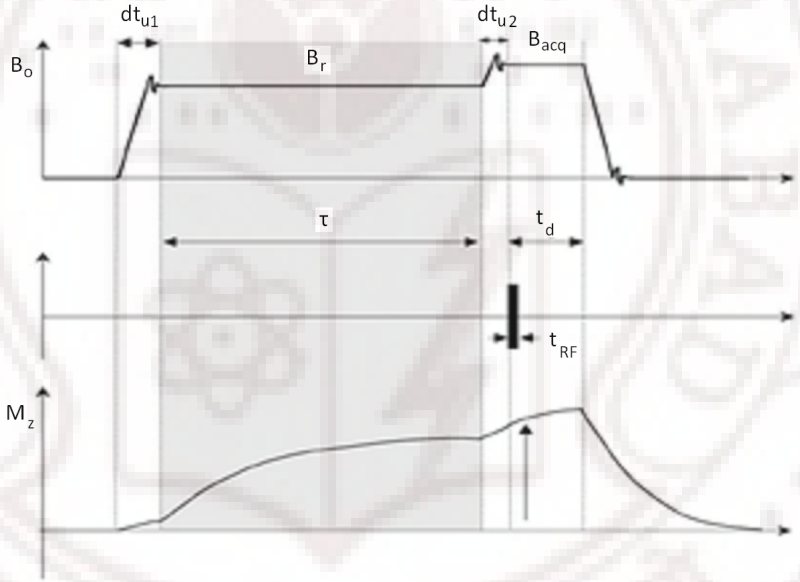

Figure 3.8: Field cycle for high relaxation fields (non-polarization). Shaded part shows the variable relaxation interval. Vertical arrow indicates the time when signal is detected. The 'down' and 'up' field switching times are indicated by the intervals (dt)d and (dt)u respectively. (Kimmich 2004).

3.3.2 T_1 measurements using FCNMR

On FCNMR instrument T_1 measurements are made using two standard protocols: pre-polarized sequence and non-polarized sequence. Pre-polarized sequence is used for operation with below the magnetic fields corresponding to 4 MHz of proton Larmor frequency while non-polarized sequence is used for operating at Larmor frequencies equal to or above 4 MHz. The two pulse sequences are shown in Figs. 3.7 and 3.8. In a pre-polarized sequence nuclei are polarized at sufficiently high field (B_{oP})

up to 4 or 5 times the expected T_1. Then the magnetic filed is switched suddenly to a value at which relaxation measurement is intended to be made. Nuclear spins are allowed to relax for a time period say, τ sec. The magnetization remained after τ sec is then detected at higher field (B_{acq}) by applying a $\frac{\pi}{2}$ pulse. In a non-polarized experiment on the other hand a non equilibrium state is created by switching the field to the desired value and spins are allowed to evolve towards thermal equilibrium for a time period τ and the resulting magnetization is again detected at B_{acq}. In both the cases experiments are repeated by varying τ up to 4 or 5 times the expected T_1.

3.4 The NMR Spectrometer

The NMR spectrometer broadly consists of three units (i) transmitter (ii) matching network or probe and (iii) receiver. The block diagram of the experimental setup used in the field variable pulsed NMR spectrometer is given in Fig. 3.9. The transmitter generates appropriate pulsed rf radiation, amplifies and delivers it to the matching network (probe). The probe consists of passive elements including the sample coil. The receiver picks up the weak signal from the NMR coil and amplifies it in stages. This amplified signal is detected by the phase sensitive detector and processed through a low pass filter and a video amplifier. Finally a signal averager is used to improve the $\frac{S}{N}$.

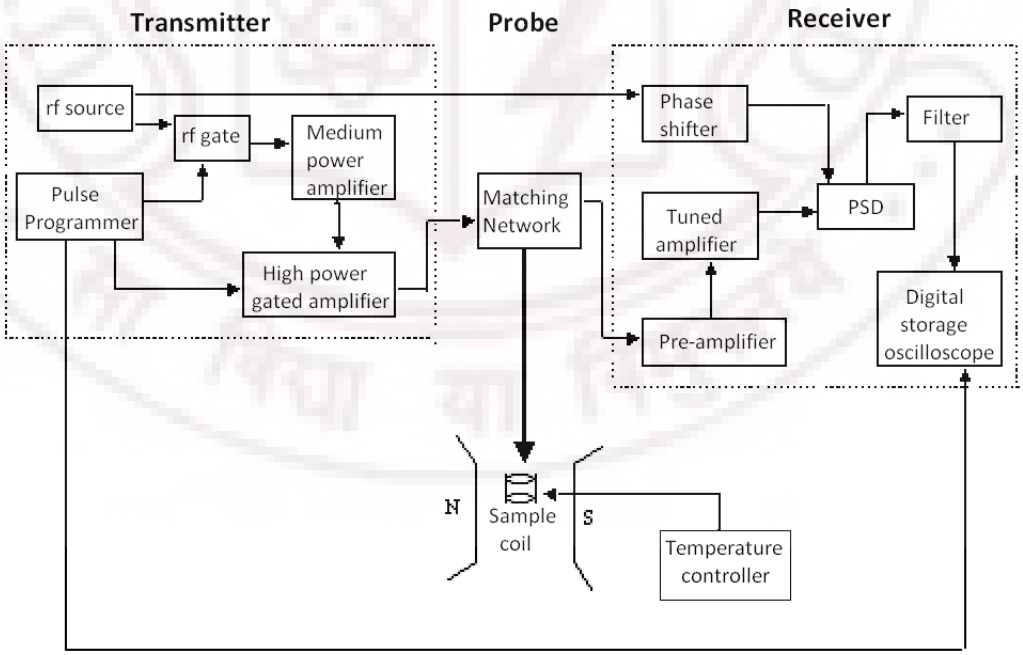

Figure 3.9: Block diagram of NMR set up

Here we employed an automated NMR hardware, (Spinmaster from Stelar, Italy) to take care of all rf operations. Spinmaster encapsulates transmitter and receiver

parts of the NMR spectrometer into a single console. It consists of RF and Digital unit, power supply and variable temperature controller. The variable magnetic field in this instrument is generated by a commercial magnet (Bruker make, model Bruker B-E 25), with a variable pole gap. The pole pieces are 12" in diameter providing a good spatial homogenity. The time stability of the field is better than one point in 10^6. The magnet is cooled by circulating chilled water under pressure. The probe assembly was supplied by Bruker covering the range of 4 - 90 MHz. The temperature is controlled by a home-built facility with an estimated stability of with in ± 0.1°C. Block diagram of the setup of Stelar's fast field-cycling NMR relaxometer is shown in Fig. 3.10. Details of these instruments are briefly prosecuted below.

3.4.1 RF and Digital Unit

The latest generation of direct digital synthesizers (DDS), programmable logic and fast A/D and D/A converters are implemented in the RF electronics of Spinmaster. The unit operates in the 2.2 to 80 MHz band and all pertinent settings are under digital control. The RF and digital unit further consists of

1. Direct digital synthesizer (DDS) rf unit
2. RF power transmitter
3. RF receiver unit
4. Acquisition Manager (AQM)

The direct digital synthesizer (DDS) rf unit consists of (i) clock generator (ii) a digital synthesizer with its control circuitry and (iii) an rf modulator. The clock generator sends a sinusoidal reference signal at 80 MHz as output. This clock output is divided by a factor of 2 and the resultant 40 MHz clock output is available for Acquisition Manager. The DDS controller is used to control the system frequency and phase difference between two channels. RF and pulse modulator produce the pulsed rf output which is to be fed to the transmitter. The level of this pulsed RF output can be varied from 0.25 V to 2.5 V. The rf power transmitter of Spinmaster delivers up to 300 W in the pulse mode. The maximum power level can be adjusted through the Acq NMR software. The receiver amplifies the emf induced by the nuclear magnetization from its initial level (of order microvolt) to the level required for data handling and display (of order volts). In the process, the nuclear signal is demodulated (i.e., the rf frequency removed) by an appropriate detector (normally a phase-sensitive detector).

The receiver is capable of withstanding overloaded voltages and also recovers fast from these overload voltages (due to leakages during pulse ON periods). This is a quadrature receiver with an additional diode detection channel and programmable amplifier filters. Acquisition manager (AQM) is the heart of the Spinmaster. It is connected to a standard PC parallel port which transmits logical commands called interface primitives. It has an inbuilt CPU (Z180) which decodes the instructions into a set of commands to be sent to the hardware interface at planned time intervals. Furthermore, this CPU, reports the current status of the hardware and of the experiment to the PC, programs the hard ware units through a proprietary parallel, bi-directional 8-bit bus (Stelar bus) and sends the acquired data to the host PC. At boot time, the Z180 executes a configuration routine and establishes communication with the PC. In practice, the time-critical instructions are executed by the pulser, which are loaded by the Z180. The host may stop/start the Z180 and the flow of instructions under its control, but the AQM executes the instructions related to configuration and sequence independently.

3.4.2 Probe

The probe or the matching network which houses the sample coil plays an important role in the performance of the spectrometer. An ideal probe must effectively couple the sample coil to the transmitter during pulse ON time and to the receiver during pulse OFF time for signal detection. It should also decouple the receiver from the transmitter during the pulse ON period. For the present experiments we used a single-coil probe. The single-coil probe arrangement is simpler and has many advantages and some disadvantages with respect to the crossed-coil probe. Probably the main advantage of the single-coil is its much high power efficiency since the coil can be tightly wound around the sample, in contrast to the crossed-coil probe in which the transmitter coil must be considerably larger and adjusted for minimum coupling to the receiver coil. Probe is tuned to desired frequency by adjusting tuning and matching capacitors. If the probe is not properly tuned and/or matched, rf power is not optimally transferred, thus lengthening the 90 pulse width and worsening signal to noise. Tuning a probe is obviously necessary when a different nucleus is to be observed. Not so obviously, it is often necessary after changing the sample. This is due to the sample's rf-properties. To tune a probe, directional coupler is used as an impedance sensor. The output is displayed on a dip meter.

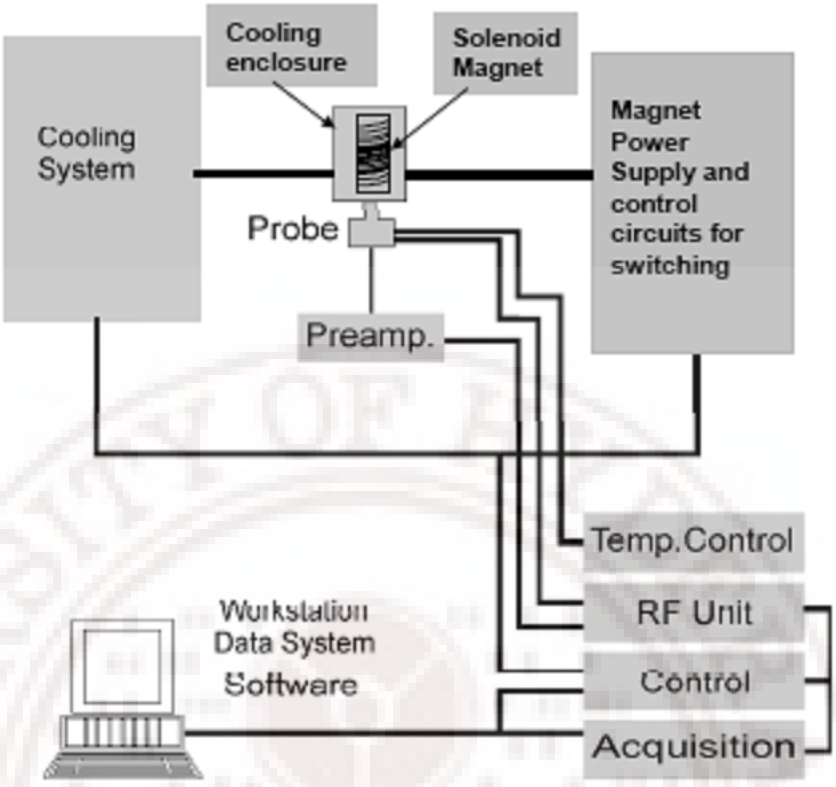

Figure 3.10: Block diagram of field cycling NMR relaxaometer.

3.5 Specifications of Pulsed NMR Spectrometer

Operating frequency range	3.5 MHz to 60 MHz
Field stability	1 in 10^6
Field homogeneity	1 in 10^{-6}
Bandwidth	2 MHz at a given frequency
Pulsed rf power	up to 300 W
ON/OFF ratio of the gated pulse	100 dB modulator
Typical $\frac{\pi}{2}$ pulse width	2-4μ s for proton
Pulse sequence used	Inversion recovery, Saturation burst
Method of detection	Single coil parallel resonance type
Transmitter isolation	60 dB minimum
Recovery time	15 μs
rf gain of the receiver	typically 80 dB, adjustable over a range of 40 dB
Temperature range	25℃ to 120℃ (with 0.2 ℃ stability over one hour)

Table 3.1: Specifications of pulsed NMR spectrometer

3.6 Specifications of FFCNMR Relaxometer

Magnet	Aluminum air coil system
Maximum operating frequency	21 MHz
Field switching time	< 0.15 ms/MHz
Field stability	1 in 10^5
Field homogeneity	1 in 10^4 over 1 cm^3
Bandwidth of the rf spectrometer	2 MHz
Pulsed rf power	up to 300 W
ON/OFF ratio of the gated pulse	100 dB modulator
Typical $\frac{\pi}{2}$ pulse width	5-10 μs for proton
Method of detection	Single coil parallel resonance type
Transmitter isolation	60 dB minimum
Recovery time	20 μs
Interface bus with PC	LPT
rf gain of the receiver	typically 80 dB, adjustable over a range of 40 dB
Temperature controller	Gas flow type PID, VTC90 (Stelar made)
Temperature range	-140℃ to 140oC with 0.1℃ stability over a day

Table 3.2: Specifications of FFCNMR relaxometer

Chapter 4

PMRD Investigations of Nematic Phases of Single Component and Binary Mixture of 4O.m Liquid Crystals

4.1 Introduction

Liquid crystals (LC) are usually formed by long molecules with a rigid core. In the formation of LC phase rigid core plays the significant role. There are evidences where long molecular conformations which are flexible without any rigid core don't exhibit liquid crystal phase of thermotropic kind *(Gray 1979)*. Further it is observed that the liquid crystal properties are very sensitive to molecular structure. Even minor changes in the rigidity or flexibility of the molecules could lead to dramatic effects on the polymorphism exhibited by these systems. From chemical studies it has long been known that the end-chains of the molecules play a significant part in the stability of the mesophases. The nematic-isotropic transition temperature and a number of other properties (e.g. the order parameter, the excess specific heat, the transition entropy, the splay elastic constants, etc.) show a pronounced alternation as the number of carbon atoms in the end-chain is changed. One such efect is the odd-even effect. Many experimental results were reported on different homologous series, mainly by changing the chain length systematically and observing differing physical properties. Investigations on different homologous series are carried out with typical objectives such as:

i. effects of molecular structure on polymorphism;

ii. changes in molecular static/dynamical parameters with additional molecular parameters, as one runs through the homologous series;

iii. discovery of suitable mesogenic phases for different technological applications; and finally,

iv. to look for physical systems to test the validity of theoretical models built to explain static and dynamic features of liquid crystals.

4.2 Review of Literature on nO.m Liquid Crystals

Alkyloxybenzylidine alkylaniline (no.m series) are one of the families of liquid crystals which are well investigated. They have rich polymorphism and also the mesophases are in convenient temperature regions to work with. The first experimental result was reported by *Smith and Gardlund (1973)*. They used calorimetry and optical microscopy, and reported transition temperatures and different mesophases for n=1 to 7 and m=4 to 8. Later *Goodby et al. (1980), Takahashi et al. (1987a) and Takahashi et al. (1987b)* did exhaustive study on odd-even effects of volume changes at I/N and N/S_A transitions and birefrengence study of N/S_A transition in different homologous series of nO.m. Pisipati and group *(Pisipati et al. 1987, Alapati et al. 1988, Potukuchi 1989, Rannavare et al. 1987, Rannavare et al. 1988)* used density, ultrasonic, calorimetry and ESR techniques, respectively, to study various transitions in nO.m series. High-resolution ac calorimetric measurements were carried out on 4O.7, 7O.6 and 7O.4 near the S_A to S_C transition by *Miechle and Garland (1983)*. Apart from these, many experiments were also done on individual members of the nO.m series. Magnetic birefringence studies on 9O.4 by *Rosenblatt and Ho (1983)*, light scattering studies on 6O.9 by *Mahmood et al. (1985)*, 6O.3 and 9O.4 by *Potukuchi (1989)* and dielectric studies on 4O.8 by *Nagabhushan et al. (1988)* are a few examples of such studies. Neutron scattering experiments were used to study the cooperative nature of the molecular motions in S_B and S_G phases of 5O.7 *(Richardson et al. 1984)* and molecular rotational motions in 4O.4, 4O.8 and 5O.6 *(Mitra et al. 2000, Mitra et al. 2004)*.

Magnetic resonance technique is extensively used to investigate both molecular structure and dynamics in liquid crystals and were also carried out on a few homologous members of this series. *Moore et al. (1980)* carried out relaxation and line width measurements on alkoxyazoxybenzenes (PAA) . Relaxation times and self diffusion coefficients were measured in a series of p-Alkonyl-Benzylidene-p Aminoazobenzenes by *Kruger and Spiesecke (1973)*. Various relaxation measurements were made on homologous series p-alkoxybenzoic acids by *Thompson et al. (1977)*. Proton spin relaxation dispersion studies were done on nematic homologous of PAA by *Nagel et al. (1983)*. Studies on isolated systems were also reported: Limmer and group reported line width measurements on three nO.m compounds 5O.6, 7O.5 and 7O.6 *(Limmer et al. 1984)*. *Schmiedel et al. (1980)* measured line shapes to get information on molecular order and intermolecular motions, ESR studies were also done by

this group. *Garland and Stine (1987)* carried out line width measurements on 4O.6. Results on 4O.4 *(Pushnik et al. 1975, Pushnik and Schara 1976)*, 8O.1 *(Bermann et al. 1973, Fryburg et al. 1972)* and line width measurements on 4O.6 *(Garland and Stine 1987)* are a few more contributions.

Information on molecular dynamics can be obtained from nuclear magnetic relaxation measurements *(Wade 1977, Dong 1983, Norrido and Segre 1979, Vold and Vold 1989)*. Blinc and Mugele *(Blinc et al. 1975, Blink 1976, Blinc et al. 1978, Mugele et al. 1980)* investigated the molecular dynamics in TBBA using T_1 relaxation dispersion. Recent proton T_1 relaxation studies on 4O.m series (varying m values from 2 to 9) include the work of *Venu (1985), Ravindranath (1991)*, and *Sailaja (1994)* covering the frequency range of 5 MHz to 50 MHz. These studies showed that in 4O.2, 4O.8 and 4O.9 the ODF contribution is extending up to tens of MHz whereas in 4O.4 and 4O.5 self diffusion was the main mechanism mediating the relaxation above a few MHz while director fluctuations (ODF) were found to be confined to lower frequencies.

The study of molecular dynamics in liquid crystals was originally promoted by the interest in collective dynamic processes associated with orientational fluctuations of the local molecular order. NMR relaxation due to ODF as a manifestation of collective dynamics was first worked out for the nematic phase by Pincus *(Pincus 1969)* (characteristic $\omega^{\frac{1}{2}}$ Larmor frequency dependence for the spin-lattice relaxation time T_1) and later developed by several poineers *(Blink 1976, Vold and Vold 1988, Struppe and Noack 1996, Venu and Sastry 1998)*. Theoretical expressions for these contributions to spin-lattice relaxation rate are given in Chapter 2. Experimentally $\omega^{\frac{1}{2}}$ dependence of ODF on T_1 was first verified in the kHz regime by *(Wolfel et al. 1975)*. However these theoretical predictions were not substantiated until the revolutionary advent of field-cycling technique *(Noack 1986)* ruling out the early pneumatic sample shifting technique. Since then, field-cycling relaxometry has been applied to many different liquid crystalline compounds *(Schweikert and Noack 1989, Pusiol and Chavez 1999, Satheesh 2000, Phanikumar 2003, and references therein)*.

Recently several single-component liquid crystals as well as liquid crystalline mixtures were studied using this technique *(Venu and Sastry 1999, Satheesh et al. 1999, Satheesh 2000, Phanikumar 2003)*. Apart from the dominant ODF, self diffusion (SD) molecular reorientations (R), critical fluctuations near the transition temperatures (CF), diffusion assisted ODF and layer undulations (LU) are the other interesting mechanisms studied *(Pusiol and Chavez 1999, Phanikumar 2003)*. These studies showed that MRD technique can be used to obtain qualitative information

regarding the elastic properties as well as about the presence of smectic clusters in nematic phases. These studies also brought out an interesting difference in the dynamic environment of the nematic phases with and without an underlying smectic phase. For example, observation of an interesting nematic state having small smectic clusters which donot grow as the temperature decreased, and hence not leading to the formation of smetic phase, is attributed to the charetaristic elastic properties of the medium. *(Satheesh et al. 1999).* In this context, detailed PMRD on a chosen set of 4O.m compounds, with the objective of investigating the end chain length influence on the collective motions in different mesophases, and possible odd-even effects in the series should prove to be rewarding.

In the present work field-cycling NMR relaxometric investigations of molecular processes in 4O.2, 4O.3, 4O.4 and a binary mixture of 4O.2 and 4O.4 are carried out. In this chapter Section 4.3 deals with the R_1 dispersions in deep nematic phase while Section 4.4 is concerned with dispersions just below T_{IN}.

4.3 PMRD Investigations of Nematic Phases of 4O.m Liquid Crystals

4.3.1 Butyloxy Benzilidene Ethylaniline. (4O.2)

The first system of 4O.m series studied in this work is butyloxy benzilidene ethylaniline (4O.2). The system has the following structure and phase sequence*(Murase 1971).*

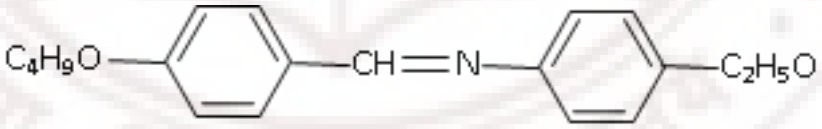

Figure 4.1:

K 43℃ **S_B** 51℃ **N** 65.5℃ **I**

It has a nematic phase over a temperature range of 14.5℃and an ordered smectic phase over 9°C.

4.3.1.1 Experimental Results and Analysis

Spin-lattice relaxation rate (R_1) profile over the frequency range 50 kHz to 50 MHz at a mid nematic temperature 60℃ is collected using fast field cycling NMR relaxometer and a home built, conventional field-variable pulsed NMR spectrometer as

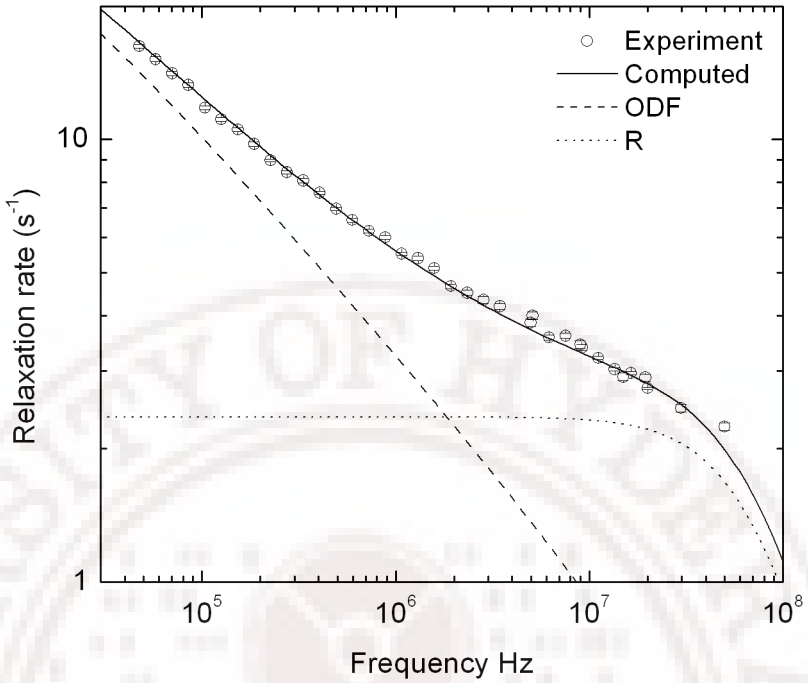

Figure 4.2: PMRD of 4O.2 in the nematic phase at 60°C.

explained in Sections 3.2 and 3.3 of Chapter-3. Fig. 4.2 illustrates the R_1 dispersion. The error in data is less than 3% and temperature stability is within 0.2°C. The spin lattice relaxation times (T_1) measured here are single exponential fits to the magnetization recovery. Data show dispersions over a wide frequency range (50 kHz-50 MHz). Earlier, temperature dependent relaxation data were collected at three different frequencies (9 MHz, 29.8 MHz and 40 MHz) *(Sailaja 1994)* and Fig. 4.3 depicts the temperature variation so obtained. It can be seen from this data that in the nematic phase relaxation times are essentially temperature independent ruling out self diffusion(SD) as the major contributing mechanism for relaxation. The possible mechanisms are thus the order director fluctuations (ODF) and reorientations (R). Data were analyzed considering ODF and R as the contributing mechanisms towards this relaxation. i.e.

$$R_{1Total} = R_{1ODF} + R_{1R} \tag{4.1}$$

R_{1ODF} and R_{1R} are given by Eqns. 2.35 and 2.55 respectively.

The motional parameters of both the mechanisms are extracted from the dispersion by means of a non-linear least squares fitting of the dispersion data to the Eqn. 4.1 using the procedure based on Levenberg-Marquart algorithm which was already explained in Chapter 2. K_1 and K_2 were fixed at 10^{-6} dyne and K_3 was varied in the fitting process. The data doesn't show low frequency plateau indicating that the

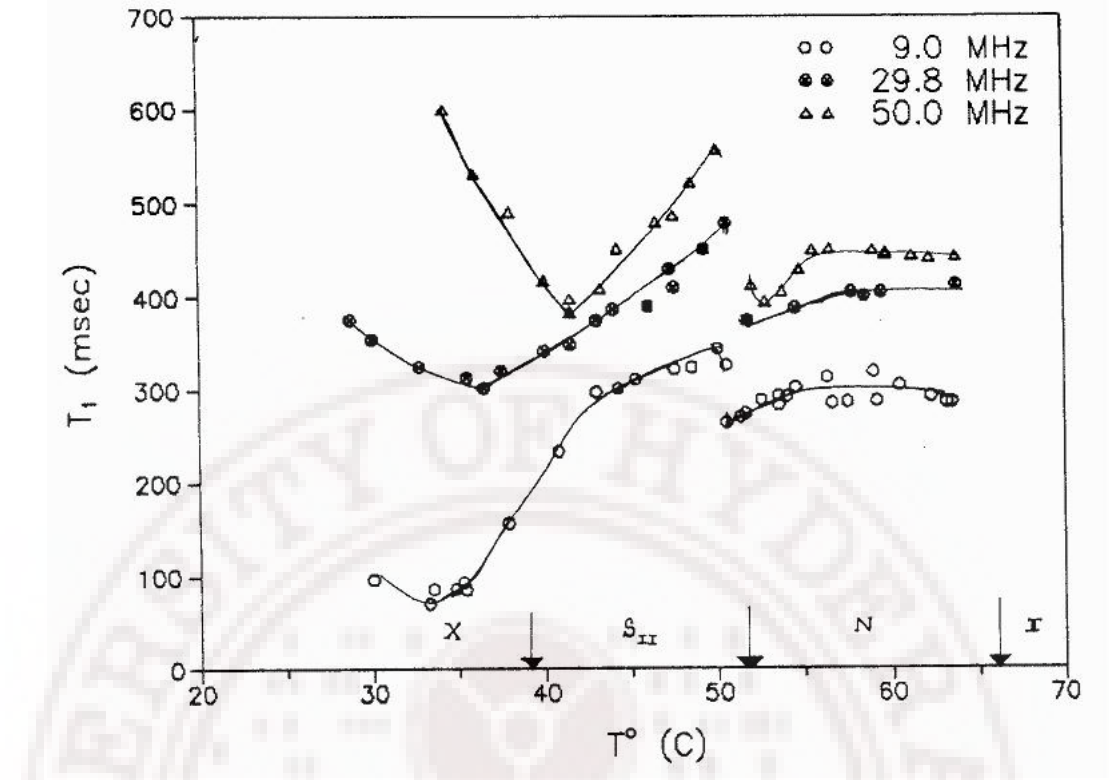

Figure 4.3: Proton Spin lattice relaxation time T_1 as a function of temperature T at three frequencies in 4O.2. Solid lines are drawn as a guide to the eye. The vertical lines denote the transition temperatures. T_1 is temperature independent in the nematic phase (T > 55℃).

low frequency cut off of the ODF contribution is below the lowest frequency of study (50 kHz).

4.3.2 Butyloxy Benzilidene Propylailine (4O.3)

The second system studied in the series of 4O.m is butyloxy benzylidene propylaniline (4O.3), with one CH_2 group more compared to 4O.2. The system has the following phase sequence (Murase 1971)

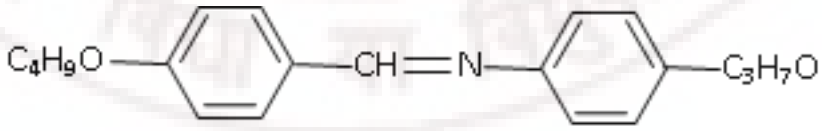

Figure 4.4:

K 54.5℃ **N** 82.5℃ **I**

This system has nematic mesophase over a range of 30℃and no underlying smectic phase.

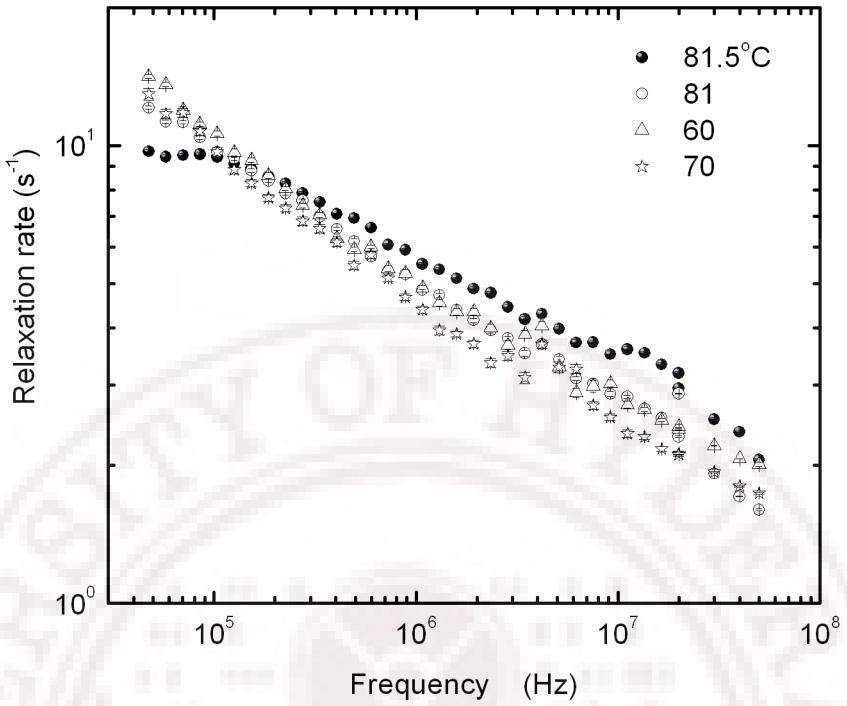

Figure 4.5: PMRD profiles at four temperatures in the nematic phase of 4O.3

4.3.2.1 Experimental Results and Analysis

Spin-lattice relaxation measurements over four decades of frequencies (50 kHz - 50 MHz) were collected at two temperatures in the deep nematic phase (60℃ and 70℃) and two temperatures near the I-N transition (ΔT =1℃and 0.5℃). Fig. 4.5 shows the PMRD profiles at four temperatures. Spin lattice relaxation times as function of temperature (Sailaja 1994) are shown in Fig. 4.6. The temperature dependent data read from the dispersions is plotted in Fig. 4.7. In the low frequency regime below 2 MHz relaxation rates are temperature independent. Strong temperature dependence is seen only at high frequencies. The proton spin relaxation dispersions obtained in nematic phase were analyzed considering three mechanisms mediating the relaxation namely ODF, SD and R according to Eqn. 2.10. i.e.

$$R_{1total} = R_{1ODF} + R_{1SD} + R_{1R} \tag{4.2}$$

where R_{1ODF}, R_{1SD} and R_{1R} are given by equations 2.35, 2.52 and 2.55 respectively. Figs. 4.8 and 4.9 show the fitted dispersions.

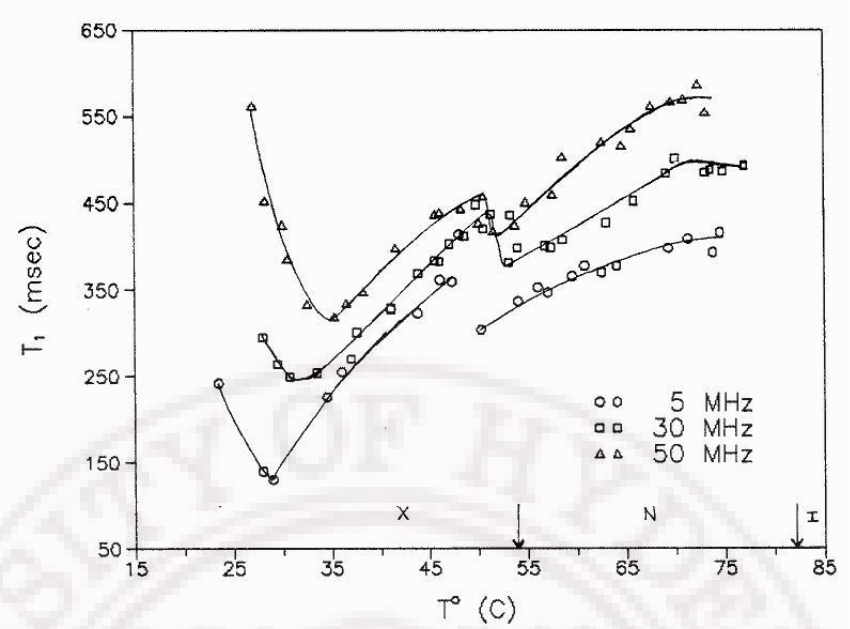

Figure 4.6: Spin lattice relaxation time T_1 as a function of temperature T at three frequencies in 4O.3. Solid lines are drawn as a guide to the eye. The vertical lines denote the transition temperatures.

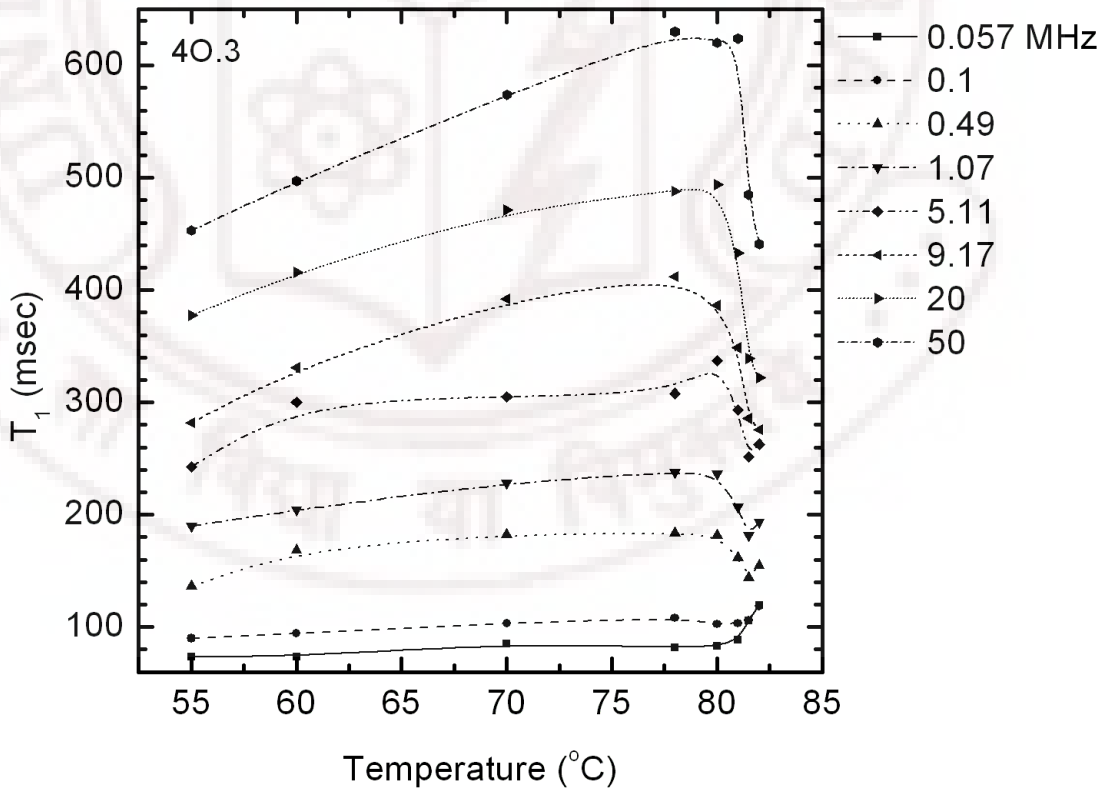

Figure 4.7: Spin lattice relaxation time T_1 as a function of temperature T at different frequencies in 4O.3. The lines joining the points are for eye guide.

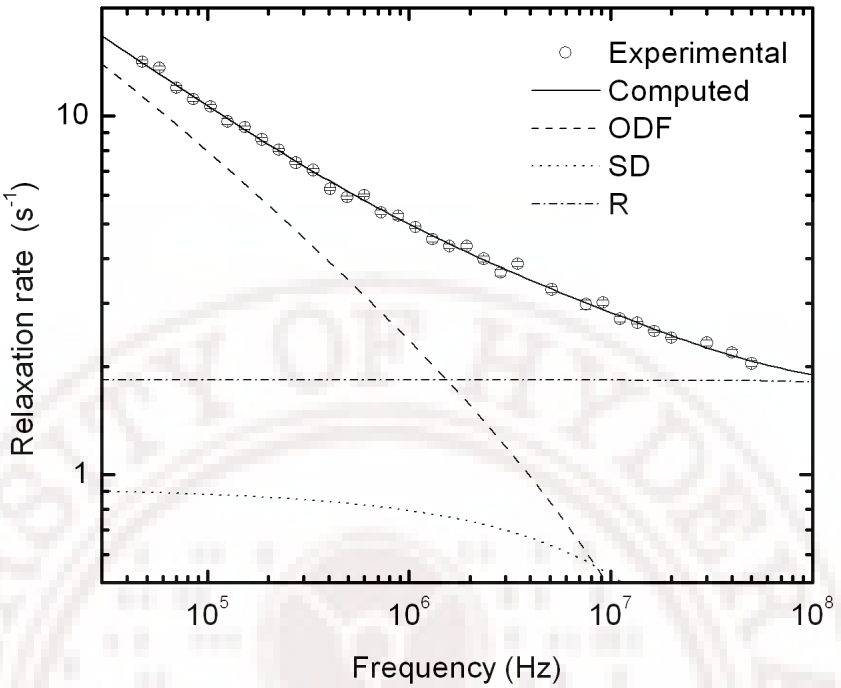

Figure 4.8: PMRD of 4O.3 in the nematic phase at 60°C.

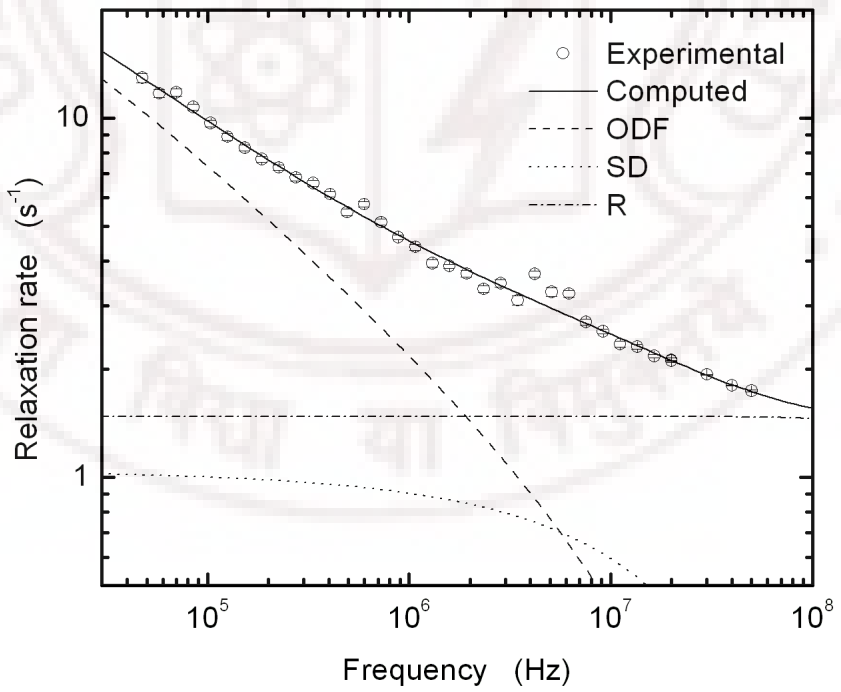

Figure 4.9: PMRD of 4O.3 in the nematic phase at 70°C.

The parameters q_{zch} and q_{pch} are found to be nearly equal at every temperature.

ODF is the dominating mechanism up to 2 MHz. Reorientations start contributing significantly to relaxation rate above 2 MHz frequency. Here SD contribution to the total relaxation seem to be relatively quite small. Motional parameters obtained from this analysis are tabulated in Table 4.1. The correlation time associated with reorientations is much smaller so that its contribution to the dispersion is practically found to be a constant C'. This contriution C' showed weak temperature dependence. The cutoff frequencies and wavelengths of the ODF in this system are tabulated in Table 4.2.

4.3.3 Butyloxy Benzilidene Butylaniline (4O.4)

The third system studied in nO.m series is Butyloxy Benzilidene Butylaniline (4O.4). This has a phase sequence given by *(Flannery and Haas 1970)* as shown below.

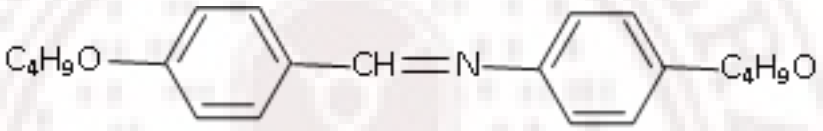

Figure 4.10:

S_X 38.6℃ **S_B** 44.7℃ **S_A** 45.1℃ **N** 74℃ **I**

This system has wide nmeatic phase and a very narrow range of S_A and S_B phases.

4.3.3.1 Experimental results and analysis

Spin-lattice relaxation measurements were carried out as explained for other samples in this series earlier, in the deep nematic phase at 60℃. Dispersion is shown in Fig. 4.11. Fig. 4.12 shows the temperature dependent relaxation data measured earlier at three frequencies (5 MHz, 15 MHz and 39.6 MHz) *(Sailaja 1994)*. Relatively strong temperature dependence of relaxation times can be seen, compare to the other two members of the family discussed above. 4O.4 dispersions were analyzed following similar procedure as it was explained in case of 4O.3, considering three mechanisms mediating the relaxation namely ODF, SD and R (Fig. 4.11). Optimized analysis reveals that ODF is the dominating mechanism up to 1 MHz. Self diffusion dominates in the intermediate frequencies 1 MHz to 10 MHz. Reorientations contribute dominantly to relaxation rates at higher frequencies. The correlation time associated with reorientations is much smaller so that its contribution to the dispersion is taken as a constant C'. Motional parameters obtained from such analysis are tabulated in Table 4.1. The cutoff frequencies and wavelengths calculated are tabulated in Table 4.2

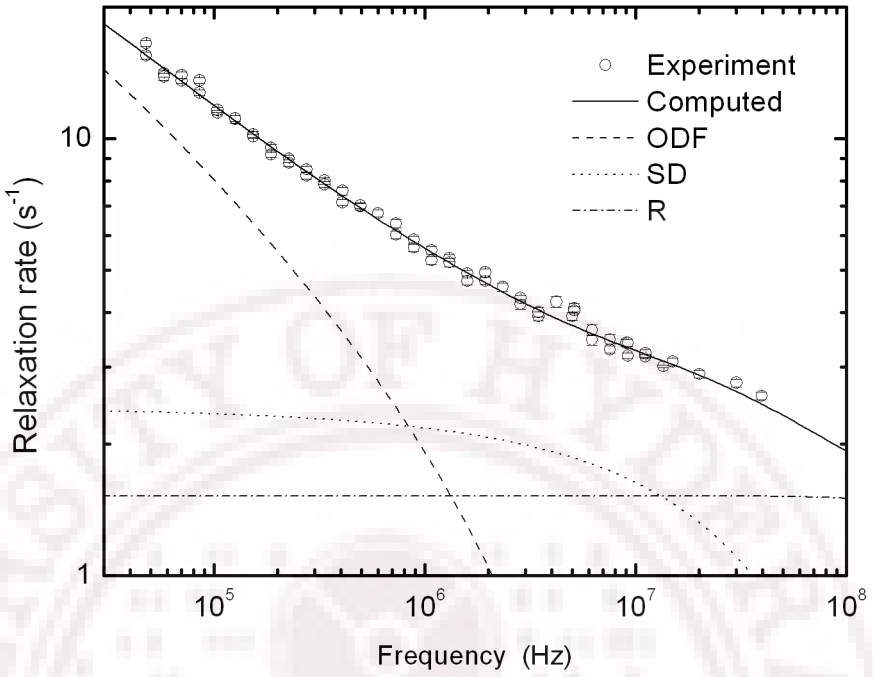

Figure 4.11: PMRD of 4O.4 in the nmeatic phase at 60℃.

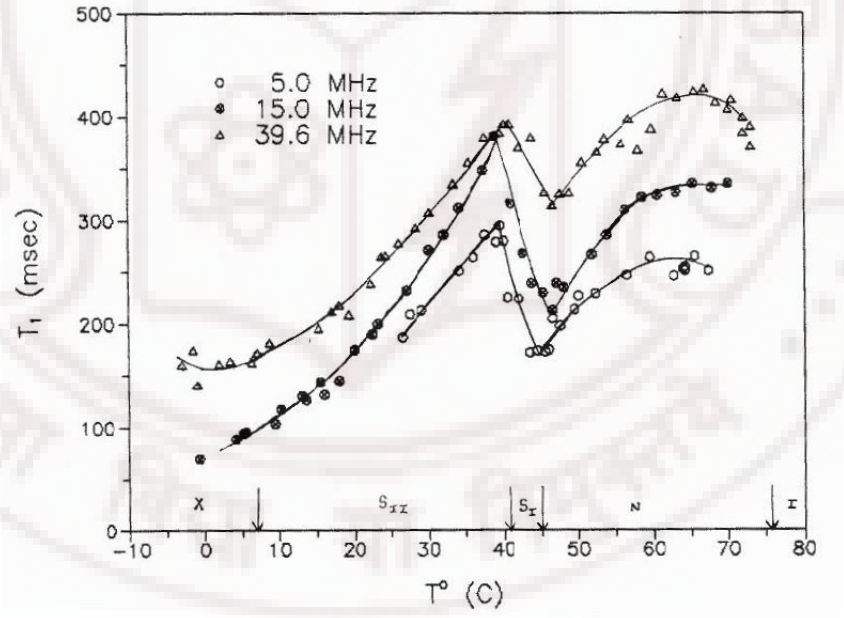

Figure 4.12: Spin lattice relaxation time T_1 as a function of temperature T at different frequencies. The lines joining the points are for eye guide.

4.3.4 Binary Mixture of 4O.2 and 4O.4

The analysis of data in the three 4O.m systems brings out certain contrastig comparision. In 4O.2, there is an underlying S_B phase below the nematic phase. From

Table 4.1, it is seen that there is no dffusion contribution to the relaxation process and the ODF contribution seems to suggest the lower cutoff wavelengths for ODF are comparable to molecular sizes. This inturn indicates the abscence of smectic like organization. In 4O.3, there is a small contribution from SD as well, and analysis of ODF reflects the presence of lower wavelength cutoff values, which indcate the presece of clusters of smectic organizations. However, these clusters have comparable dimensions along & perpendicular to the director (so-called isotropic clusters for simple discription), and their size does not seem to grow with decrease in temperature. It may be noted that this system (4O.3) does not have an underlying smecitc phase.

In 4O.4, the contributions of SD is even more, and the lower cutoff wavelengths of ODF suggest the presence of smectic clusters with unequal sizes in the two directions (so-called anisotropic clusters). Now the case of 4O.3 wherein there are (so-called) isotropic clusters of smectic organizations in the nematic phase and which do not change in their size with temperature is comparable to the earlier observaqtion on 7BCB (4-Cyanophenyl-4´-n-heptylbenzoate). It was concluded that such a dynamic molecular organization in the nematic phase represents a frustrated phase where smectic clusters as seeds, do form, but can not grow in size, to finally condense into a smectic phase, due to sustainable elastic properties of the medium *(Satheesh 2000)*. In the light of these observations on the three homologous members, it is felt that a binary mixture of 4O.2 and 4o.4 might be an interesting system to see if it exhibit this type of dynamic organization.

With this in mind a 1:1 (number of moles) mixture of 4O.2 and 4O.4 is prepared and studied using proton relaxometry. The phase sequence of this mixture is found using polarizing microscope, and is as shown below.

$$\mathbf{S_X} \quad 45.1℃ \quad \mathbf{N} \quad 71.5℃ \quad \mathbf{I}$$

This system has wide nematic phase and an unspecified smectic phase.

4.3.4.1 Experimental Results and Analysis

Spin-lattice relaxation measurements were done as explained earlier, in the nematic phase at three temperatures (55℃, 60℃, and at 65℃). Dispersions are shown in Fig. 4.13. Fig. 4.14 shows the temperature dependent relaxation data at 40 MHz. Relaxtion times as function of temperature in the nematic phase are shown in Fig. 4.15. Strong temperature dependence of relaxation times at high frequencies can be seen here too. As it was guided by the temperature dependence of relaxation rates the conditions used in the analysis of 4O.3 and 4O.4 are implimented in this case too. Figs. 4.16 to 4.18 show the fitted dispersions. Nonlinear least square method

of analysis reveals that ODF is the dominating mechanism up to 1 MHz. Self diffusion dominates in the intermediate frequencies 1 MHz to 10 MHz. Reorientations contribute dominantly to relaxation rates at higher frequencies. The data, however, show there is no frequency dependence to the relaxation contribution from reorientations,as has been in the case in 4O.3 and 4O.4, indicating that indicating that this situation corresponds to $\omega\tau_c \ll 1$ limit in the experimental frequency range. Therefore the relaxation contribution due to reorientations is taken as a constant (C'). Motional parameters obtained from such analysis are shown in Table 4.1. From the table it can be seen that the fits require inequality of the three elastic constants reflecting the elastic properties in this system. The cutoff frequencies and wavelengths calculated are provided in Table 4.2.

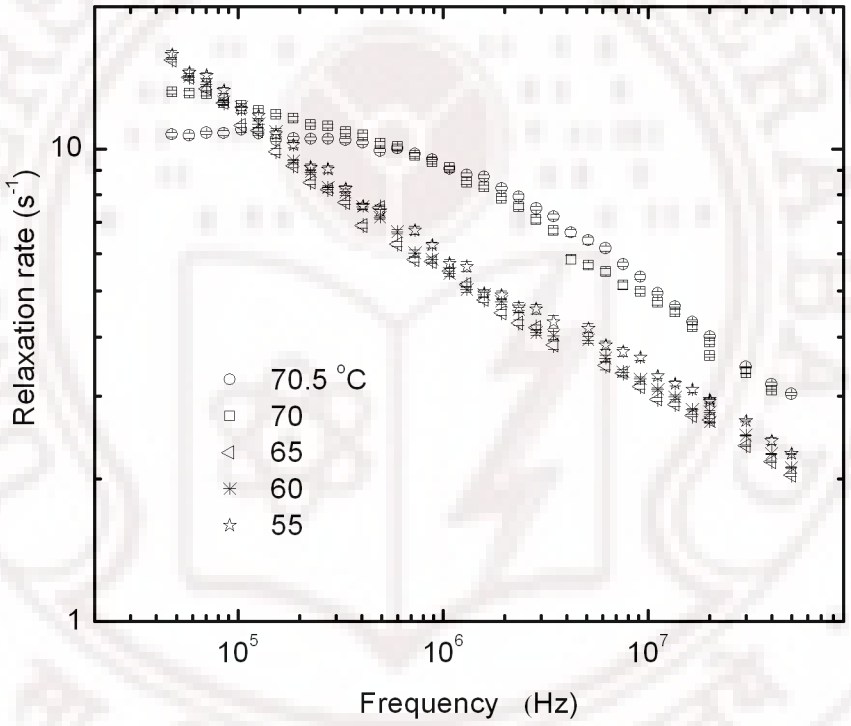

Figure 4.13: PMRD profiles in the nematic phase in 1:1 mixture of 4O.2 and 4O.4.

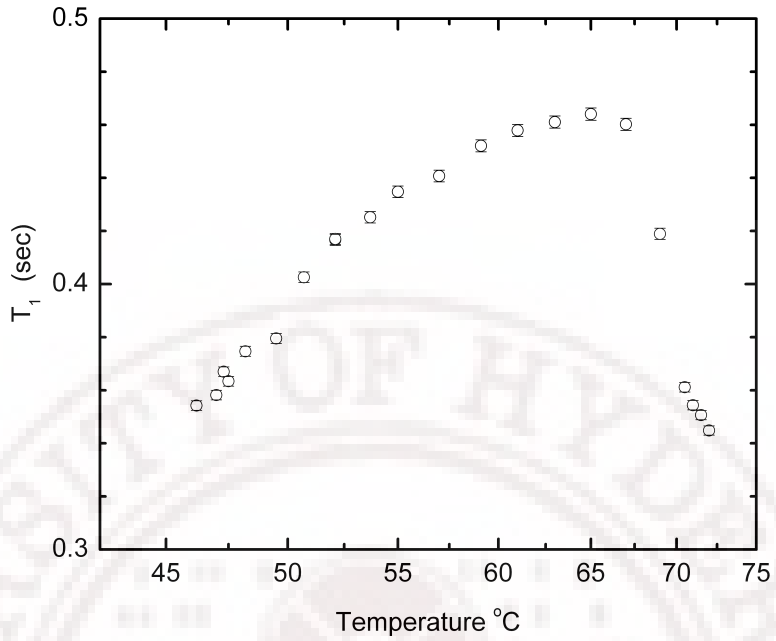

Figure 4.14: Spin lattice relaxation time T_1 as a function of temperature T at 40 MHz.

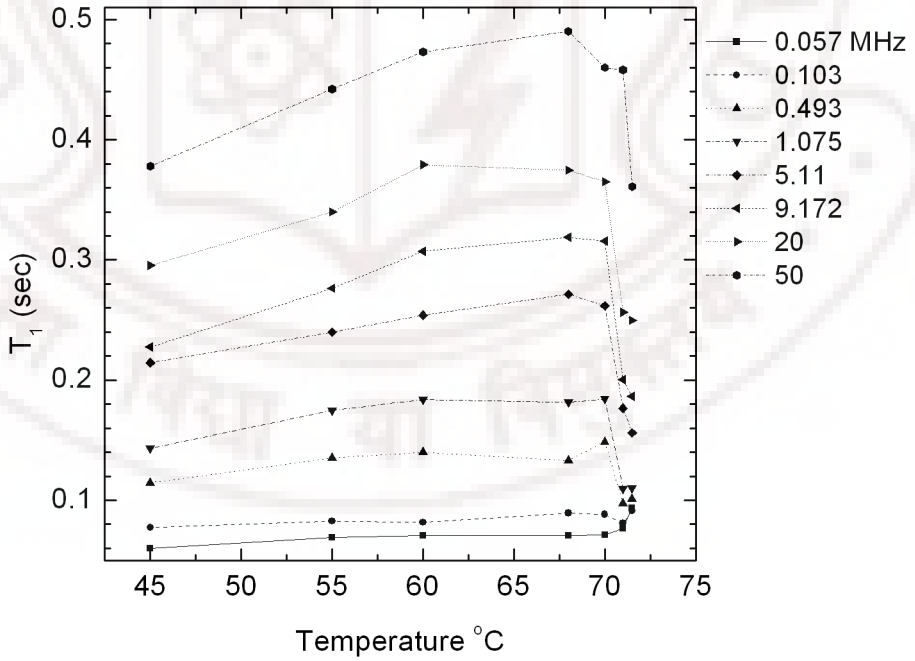

Figure 4.15: Spin lattice relaxation time T_1 as a function of temperature T at different frequencies in the mixture of 4O.2 and 4O.4. The lines joining the points are for eye guide.

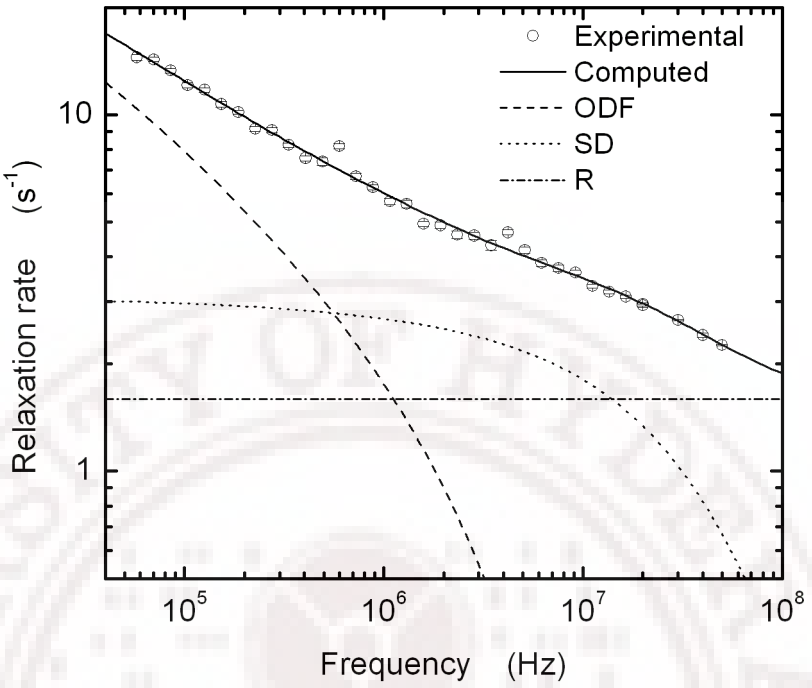

Figure 4.16: PMRD profile of 4O.2 and 4O.4 mixture in the nmeatic phase at 55℃.

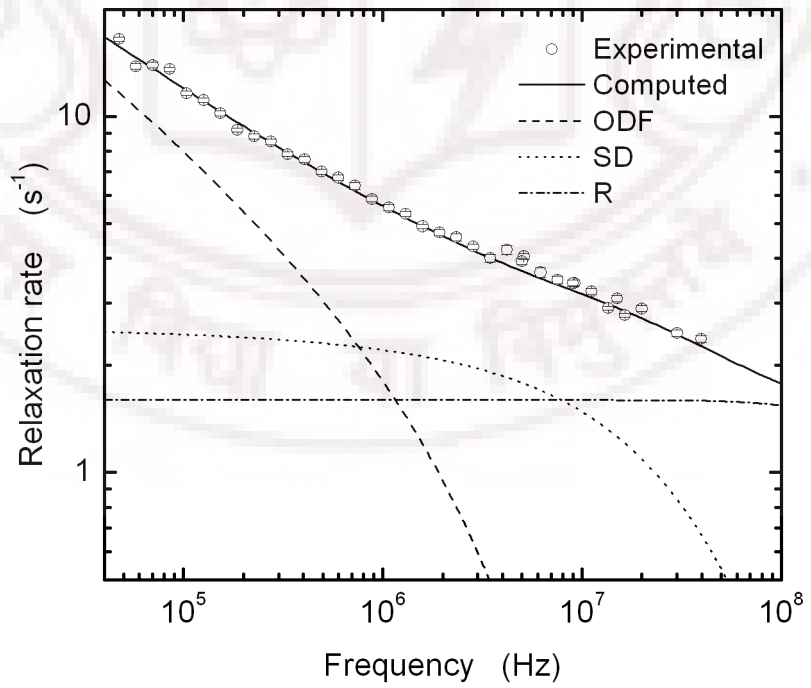

Figure 4.17: PMRD profile of 4O.2 and 4O.4 mixture in the nematic phase at 60℃.

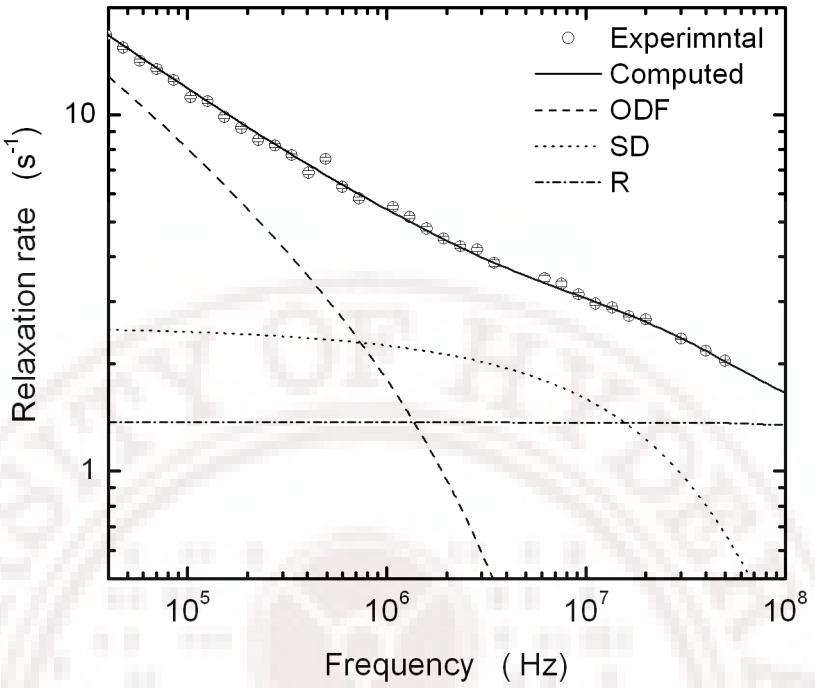

Figure 4.18: PMRD profile of 4O.2 and 4O.4 mixture in the nematic phase at 65℃.

nO.m	T ℃	K_3 $10^{-6}dynes$	q_{zch} 10^8cm^{-1}	q_{pch} 10^8cm^{-1}	A_{ODF} $10^{-6}s^{-2}$	B 10^8s^{-2}	D $10^{-12}m^2s^{-1}$	C 10^9s^{-2}	τ_R $10^{-9}s$
4O.2	60	1.09	0.32	0.3	3.43			2.08	1.12
		(0.19)	(0.02)	(0.013)	(0.29)			(0.1)	(0.02)
4O.3	60	1.02	0.107	0.107	2.293	1.101	15.02	1.8*	
		(0.02)	(0.04)	(0.04)	(0.025)	(0.4)	(2.7)	(0.46)	
	70	1.001	0.105	0.105	2.0954	1.271	15.5	1.47*	
		(0.03)	(0.042)	(0.042)	(0.034)	(0.89)	(1.7)	(0.11)	
4O.4	60	1.54	0.028	0.048	3.15	4.87	25.7	1.52*	
		(0.02)	(0.002)	(0.003)	(0.023)	(0.2)	(1.23)	(1.52)	
	55	1.38	0.062	0.027	2.98	3.097	12.78	1.75*	
4O.2		(0.03)	(0.002)	(0.001)	(0.02)	(0.03)	(0.5)	(0.05)	
+	60	1.17	0.071	0.036	2.72	3.22	16.69	1.56*	
4O.4		(0.02)	(0.01)	(0.001)	(0.02)	(0.03)	(0.5)	(0.05)	
	65	1.03	0.048	0.039	2.47	3.78	19.95	1.37*	
		(0.037)	(0.005)	(0.003)	(0.016)	(0.04)	(0.78)	(0.07)	

* in the limit $\omega\tau_r \ll 1$ it is taken as $C\tau_r = C'$

Table 4.1: Parameters extracted from the fits of proton spin-lattice relaxation rate dispersions in the nematic phase of 4O.2, 4O.3, 4O.4 and the mixture of 4O.2 and 4O.4. Data were fitted to equation 2.10 considering the contributions from ODF, SD, and R. Uncertainities in the parameters are enclosed in the parathesis

nO.m	T ℃	ν_{zch} MHz	ν_{pch} MHz	λ_{zcl} A	λ_{pcl} A
4O.3	60	37.3	36.6	58.58	58.58
	70	34.8	34.8	60.1	60.1
4O.4	60	6	5.6	180	157
4O.2	55	4.1	2.1	193	246
+	60	5.9	4.8	157	161
4O.4	65	7.1	6.47	125	133

Table 4.2: Cutoff frequencies and wavelenghts calculated from the parameters extracted.

4.3.5 Discussion

The results show that ODF and R mechanisms essentially mediate the proton relaxation in the entire frequency range in 4O.2 (Fig. 4.2). The computed cutoff frequencies of director fluctuations are well outside the experimental frequency range. The upper cutoff frequency is thus greater than 50MHz and hence lower cutoff wavelength should be less than 50Å, indicating that the lower cut off wavelength of ODF modes is in the range of molecular size. It is known that typically the average size of the smectic clusters normally determine this lower cutoff waveleths in the nematic phase, and such low values in 4O.2 (reaching molecular size) are indication of abscence of smectic clusters in the medium *(Venu and Sastry 1998, Venu and Sastry 1999)*. Similar trend was observed earlier in a few other liquid crystals, with only a nematic phase without underlying S_A. (Venu and Sastry 1999, Phanikumar 2003). 4O.2 however has an underlying smectic phase S_B, which is almost like crystalline organization. It is interesting that it seems to make a difference in the dynamic orgaqnization of the nematic medium, depending upon whether the underlying layered phase is S_A or S_B. The near temperature independence of relaxation data over the frequency range (Fig. 4.3) shows that ODF contribution as expected *(Vold and Vold 1989)* as well as R cotributions are essentially independent of temperature. This strongly suggest very low activation energy hindering the reorientational motions. Earlier studies *(Rebeirio 1987, Satheesh 2000, Phanikumar 2003)* also lead to similar conclusions. It appears that whenever the director fluctuations dominate NMR relaxation up to few tens of MHz, meaning that the director modes have wavelengths as shorts as molecular size (i.e. clean nematic phases with no smectic clusters), the reorientations experience very low hindrance. This seems to be consistent with the fact that the reorientations about short axis (which are the main type of reorientations contributing to the relaxation in nematic phases) are asymptotically compared to the ODF modes having length scales of the order of molecular size *(Satheesh 2000)*. This compound also exhibits isotropic elastic properties (all the Frank elastic constants as

estimated from the fit of the experimental data being approximately the same).

4O.4 provides a contrasting situation. The self diffusion of the molecules (SD) is a dominating mechanism in the intermediate frequency range (Fig. 4.11) and director modes get cutoff around a few MHz (Table 4.2). Further the lower cutoff wavelengths of the director modes are anisotropic in the sense that they have different values in the directions parallel and perpendicular to the director. As per the above discussion, these lower wavelength cutoff values are assigned to corresponding average smectic cluster size in the medium *(Satheesh 2000)*, then the present results indicate the presence of anisotropic smectic clusters in the nematic phase. The existance of the underlying S_A phase makes the detection of such clusters in the nematic phase plausible. Further this compound exhibits anisotropic elastic properties ($K_3 > K_1$ and K_2) (Table 4.1).

The results of 4O.3 can now be compared with those of both the neighbors in the homologous series (4O.2 and 4O.4). Like in 4O.4, SD contributes to the relaxation in 4O.3 in the intermediate frequency range. Similarly the ODF modes in 4O.3 exhibt lower cutoff wavelengths, though smaller compared to 4O.4, of the order of 60Å both along the transverse and longitudinal directions (Table 4.2). That means 4O.3 exhibits isotropic smectic-like clusters comprising of a few molecules unlike in 4O.4. The results also indicate that the sizes of these clusters remain the same on lowering the temperature by 10°C (Table 4.2). Further, the elastic constants seem to be of equal magnitude in this compound (as in 4O.2). Concluding the observations on 4O.2 and 4O.4, it appears that an underlying S_A phase and not S_B leaves a signature in the high temperature nematic phase. There appear to be smectic organizations with anisotrpic sizes and the elastic cofficiets are found to be unequal. Though 4O.3 shows smectic clusters, they don't grow in sizes as the system is cooled. It is interesting to mention this observation in the context of the fact that a S_A phase is not found at low temperatures in this compund. Similar behavior was observed earlier *(Satheesh 2000)* and such nematic phases were called frustrated nematic phaseses. These frustrated nematic phases are different from pure nematic phases (as in 4O.2), as well as nematic phases with underlying smectic phases (as in 4O.4). These studies further strengthen the earlier conclusions found between the nature and size of smectic organizations in nematic phase, and stability of low temperature smectic phases.

It is interesting to observe how a mixture of two compounds, 4O.2+4O.4 behave. Such a system with 1:1 molar ratio has shown anisotropic elastic properties (Table 4.1) as well as anisotropic and relatively (to 4O.3) larger smectic clusters (Table 4.2). Further these clusters grow in size as the sample is cooled. These results are

consistent with the fact that this mixture was found to have an underlying smectic phase. Thus, 50% mixture of 4O.2 and 4O.4 is not exactly like 4O.3.

4.4 PMRD Investigations of 4O.m Liquid Crystals Just Below T_{IN}

4.4.1 Experimental Results and Analysis

Just below T_{IN} PMRD data at two different temperatures 81℃ and 81.5℃ for 4O.3 and 70℃ and 70.5℃ for the binary mixture of 4O.2 and 4O.4 are collected. ΔT_{IN} is 1℃ and 1.5℃ respectively in both the cases. Data were analyzed with a suitable model *(Dong 1994)*, considering order parameter fluctuations (OPF), molecular self diffusion (SD) and molecular reorientations (R). The analysis was carried out using non-linear least square method based on Levenberg-Marquardt algorithm. Parameters extracted are tabulated in Table 4.3. Results of analysis of these data at each temperature are as follows.

4.4.1.1 4O.3

At ΔT_{IN} = 1℃: Here the major contribution to relaxation is arising from nematic order parameter fluctuations (OPF) showing $\omega^{-0.5}$ dependence above 0.6 MHz. A plateau is observed below this frequency. The relaxation contribution due to translational diffusion (SD) is showing dispersion above 3 MHz. and is dominant up to 50 MHz. The contribution of R which is due to molecular reorientations around short axis is small and fast in the experimental frequency range of study. Here its contribution is constant over the frequency range of study (Fig. 4.19).

At ΔT_{NI} = 1.5℃: Here the major contribution to the relaxation is again from OPF. Fruther the analysis show that the $\omega^{-0.5}$ region due to OPF relaxation modes is extending to lower frequencies. SD is seen to be important at higher frequencies above 5 MHz. Here SD contribution to total relaxation rate is less (13%) compared to ΔT_{NI} = 1℃ (25%). Here also molecular reorientations are fast in the experimental range of study (Fig. 4.19).

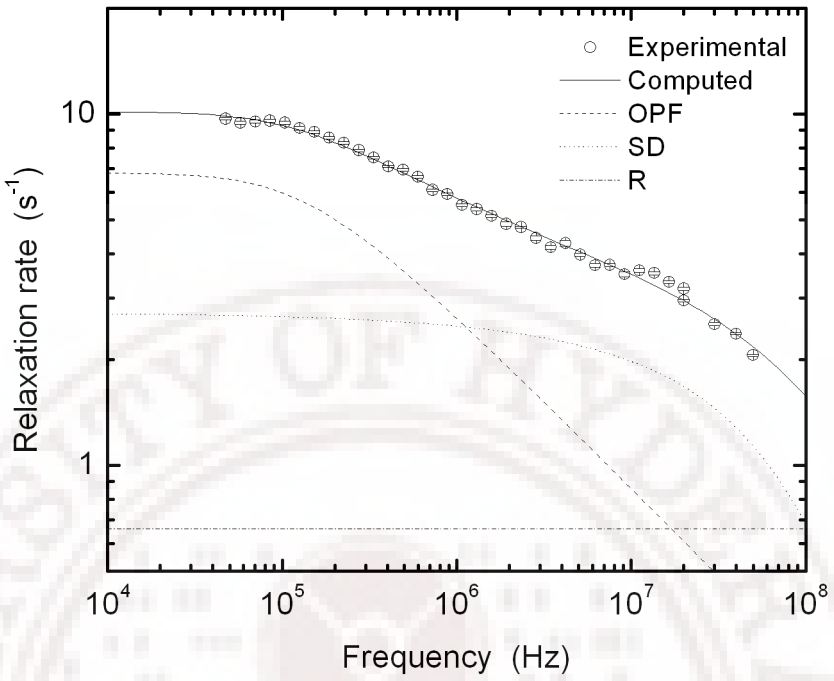

Figure 4.19: PMRD of 4O.3 1℃ below T_{NI}.

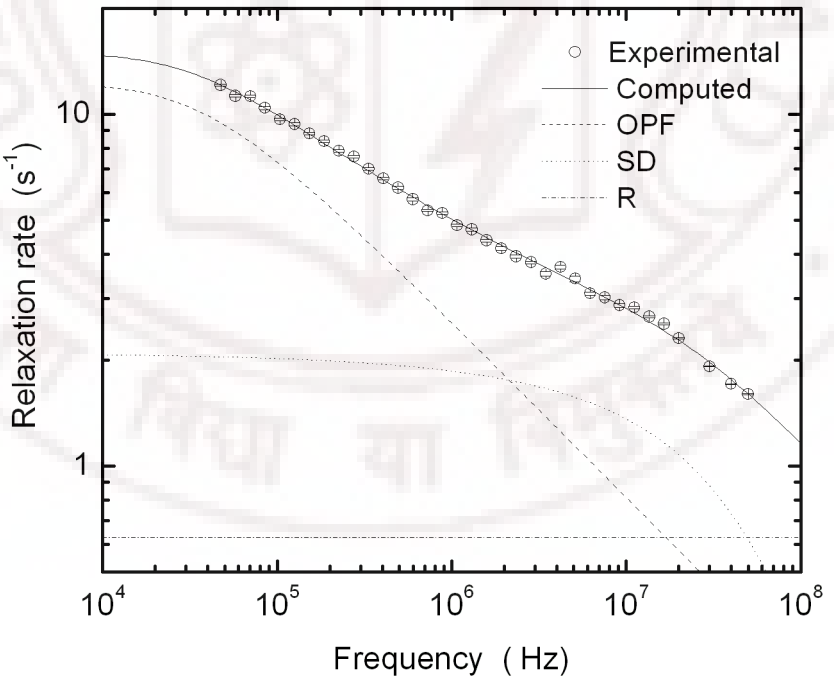

Figure 4.20: PMRD of 4O.3 1.5℃ below T_{NI} .

4.4.1.2 Mixture (4O.2 + 4O.4)

At ΔT_{IN} = 1℃: Here the major contribution to relaxation is arising from nematic order parameter fluctuations (OPF) showing $\omega^{-0.5}$ dependence above 1 MHz. A plateau is observed below this frequency. The relaxation contribution due to translational diffusion (SD) is showing dispersion above 2 MHz. Its dominance is not seen throughout the frequency range of study up to 50 MHz. The contribution of R which is due to molecular reorientations around short axis is small and fast in the experimental frequency range of study. Here R is constant (C') over the frequency range of study (Fig. 4.21).

At ΔT_{IN} = 1.5℃: Here the major contribution to the relaxation is arising from OPF. However the results of the analysis show that the $\omega^{-0.5}$ region due to OPF relaxation modes extending to low frequencies. SD is seen at intermediate frequencies 1 - 20 MHz and reorientations dominate up to 50 MHz. Here SD contribution to total relaxation rate (40%) is comparable to ΔT_{IN} = 1℃ (44%). Here also molecular reorientations are fast in the experimental range of study (Fig. 4.22)

Just below the isotropic-nematic transition, the relaxation due to nematic order parameter fluctuation (OPF) is caused by the fluctuation in the magnitude of the long-range orientational order. This long-range orientational order is the order parameter of the isotropic-nmeatic transition, which is of weakly first order nature. From the Table 4.3 it is clear that the correlation times (τ_o) associated with the OPF are sharply increasing for a change of 0.5℃ in temperature. The constant A_o has also shown strong temperature variation. The increase in correlation time or equivalently the corresponding correlation length as the temperature decreases, in turn indicates the progressive onset of nematic order parameter. This slowing down of the correlation time as the nematic phase stabilizes, was observed earlier in other systems 4PCH *(Pusiol and Chavez 1999)* and in 8OCB *(Phanikumar 2003)*. The smaller correlation time associated with nematic order parameter fluctuation near to T_{IN} is attributed to the thermal effects, which randomize nematic order. The relaxation mechanism due to OPF modes is similar to that of short-range nematic clusters that exist just above T_{IN} *(Dong 1994)*.

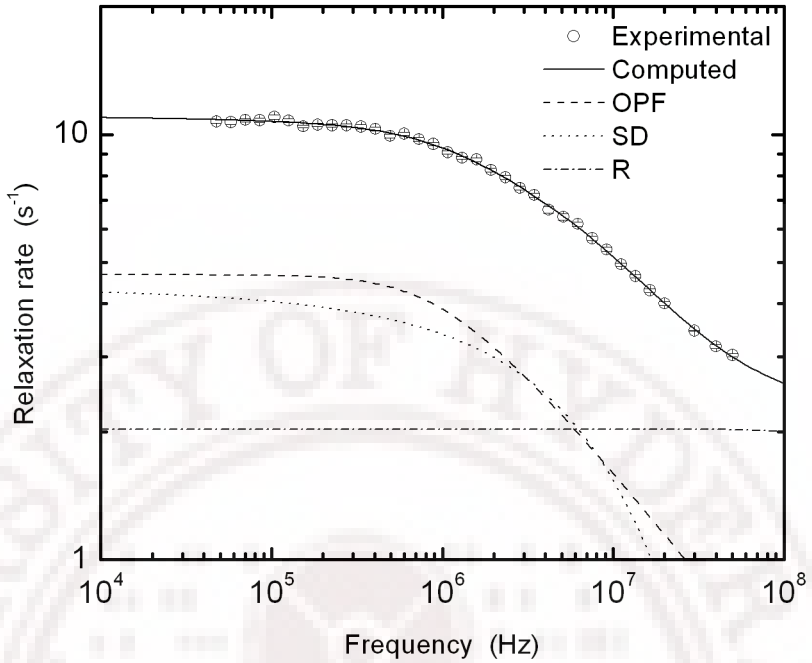

Figure 4.21: PMRD proile of 4O.2 and 4O.4 mixture at ΔT = 1℃

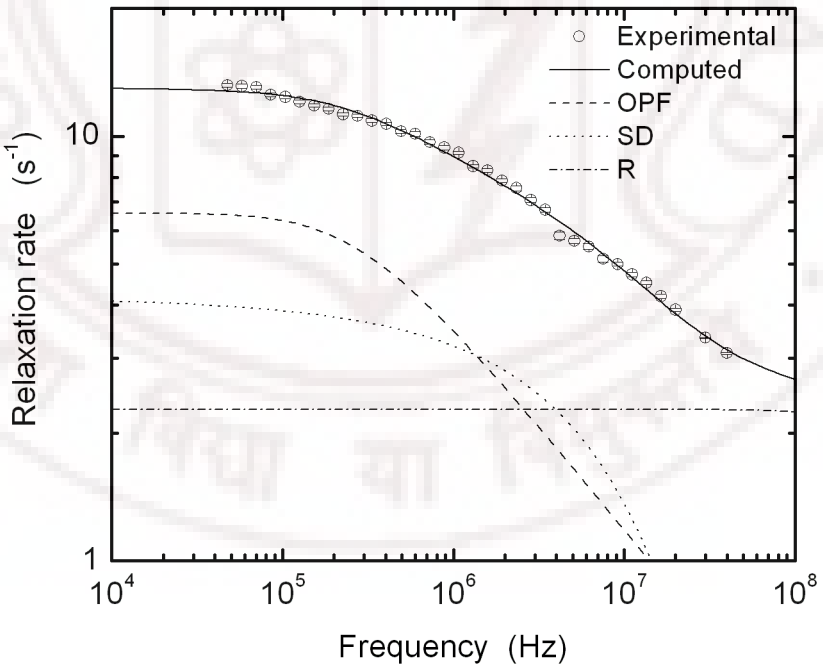

Figure 4.22: PMRD proile of 4O.2 and 4O.4 mixture at ΔT = 1.5℃

nO.m	T	A_o	τ_o	B	D	C'
	℃	$10^2 s^{\frac{-3}{2}}$	10^{-8}s	$10^8 s^{-2}$	$10^{-12} m^2 s^{-1}$	
4o.3	81	62.39	8211	3.31	18.98	0.63
		(0.89)	(649)	(0.31)	(1.59)	(0.3)
	81.5	66.5	2058	7.75	34.16	0.6
		(1.13)	(80)	(0.13)	(0.98)	
4O.2	70	69.72	1316	1.979	4.8	2.34
+		(5.43)	(117)	(0.07)	(0.27)	(0.05)
4O.4	70.5	113.53	255.3	2.01	5.2	2.17
		(17.5)	(18.5)	(0.16)	(0.32)	(0.1)

Table 4.3: Parameters extracted from the fits of proton spin-lattice relaxation dispersions at just below T_{IN} in 4O.3 and the mixture of 4O.2 and 4O.4. Data were fitted to equation 2.10 considering relaxation rate contributions from OPF, SD and R. Uncertainities in the parameters are enclosed in the parathesis.

4.5 Conclusions

These studies show that PMRD study in nematic liquid crystals, together with temperature dependence studies provides an insight into the molecular motions in liquid crystas. Present investigations show that in 4O.2 and 4O.3 contributions from director fluctuations spread to considerably high frequencies which, in support of earlier results, seems to be a common feature of liquid crystals of low viscous, or nematics without underlying smectic phases. On the other hand simlar effects from 4O.4 and the mixture are limited to low frequencies consistent with the results on high viscous liquid crystals. It is observed that translational self-diffusion contribution is increasing as the end chain length increases. In low viscous liquid crystals self-diffusion process is fast and hence their contribution to the relaxation is small within the experimental frequency range. The binary mixture of 4O.2 and 4O.4 in appropriate ratio could be expected to behave like 4O.3 as the result of odd-even effects. But the dynamics observed in 1:1 mixture are more similar to 4O.4. One could perhaps further study this mixture to verify this conjunction by varying the ratio of the composition. Just below T_{NI} the nematic order parameter fluctuations are the dominant relaxation mechanism. The time scales of nematic order fluctuations and their slowing down are observed. Present PMRD studies in an unique way give an insight into how the molecular processes evolve with change in the end chain length in 4O.m homologous series. It also provides an opportunity to compare these results with earlier studies on high and low viscous samples.

Chapter 5

^{19}F and ^{1}H spin-lattice relaxation dispersion study of singly fluorinated isothiocyanato-tolanes: Detection of slow motions in the isotropic phase of liquid crystals

5.1 Introduction

Nuclear magnetic relaxation dispersion studies have been hitherto mostly employing protons as the probing nuclei to examine molecular processes in liquid crystals. Spin relaxations in such systems are mediated by dipolar interactions, which in turn depend on the time correlation functions of the orientation of the molecules *(Abragam 1961)*. Molecular models to describe experimental data in different mesophases based on the underlying molecular reorientational dynamic processes are well documented *(Dong 1994)*. In this context, use of nuclear probes that could have qualitatively different relaxation path seems to be an interesting prospect to investigate the molecular processes. With this objective we consider two liquid crystals with their molecules containing a lone fluorine on the aromatic core: the lone fluorine can essentially relax only via spin-rotation interaction under the circumstances, in a typical NMR experiment. This is further facilitated by the fact that it has a larger spin-rotation constant making this mechanism effective (unlike protons) *(Green and Powles 1965)*. Its (inter-molecular) homo-nuclear dipolar interactions are negligible in practical terms, and it turns out that the (intra-molecular) hetero-nuclear interaction (with core protons) is also insignificant in comparison to the pathways provided by the spin-rotation mechanism, unless the lines of proton and fluorine overlap at low enough fields, as it happens in a field-cycling NMR experiment. This then results, of course in a cross-relaxation process aiding flourine spin-lattice mechanism further. This paper reports

on the contrasting relaxation dispersion results in the isotropic phase of these liquid crystals, employing both proton and fluorine nuclei.

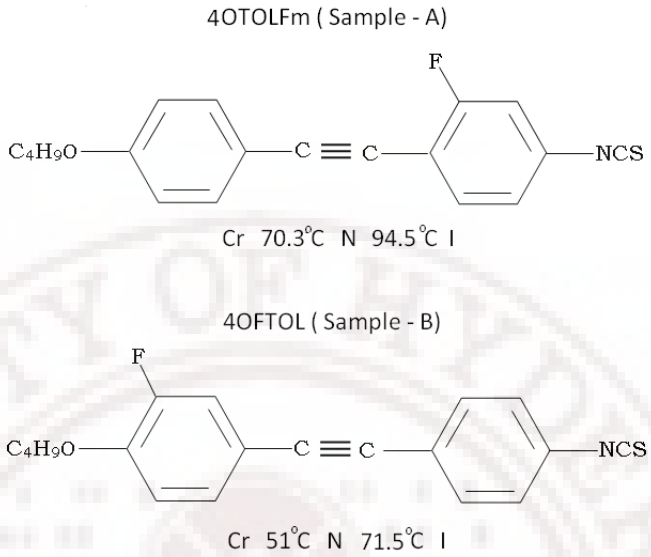

Figure 5.1: Molecular structures and phase sequences of the two fluorinated liquid crystals Sample-A and Sample-B

Studies on isothiocyanato-tolane derivatives with fluorine atoms at various lateral positions have been attracting recently considerable attention. These liquid crystals are first reported by Greenfield in 1993 *(Greenfield et al. 1993)*. Since then several such compunds were designed, synthesized and physical propertis using calorimetry, NMR, UV and infrared spectroscopy were reported. *(Gauza et al. 2003a, Gauza et al. 2003b, Gauza et al. 2004a, Gauza et al. 2007c, Gauza et al. 2005b, Catanescu et al. 2004a, Wu 2002, Wen et al. 2003, Hsu et al. 2006, Gauza et al. 2008a)*. The importance of these laterally fluorinated tolanes originates in their enhanced physical properties, important for display applications; these have high birefringence and low viscosity, with exceptionally high values for figure-of-merit, both at room temperatures and at elevated temperatures. *(Wu 1997, Wu 1998, Wu 2001, Gauza et al. 2007b, Wen et al. 2005, Gauza et al. 2004b, Catanescu et al. 2004b, Gauza et al. 2005b, Gauza et al. 2008b)*. Mixtures of these compounds showing enhanced desirable properties also designed *(Gauza et al. 2003b, Gauza et al. 2003c, Dabrowski et al. 2007)*. These liquid crystals found wide applications in laser beam stearing, polymer dispersed liquid crystals (PDLC) optical swiching,telecommunication industry and polarization independent light swiching *(Wu 2001, Lu et al. 2004, Ren et al. 2004, Gauza et al. 2007b, Wen et al. 2005, Gauza et al. 2008b)*. The lateral substitution of fluorine mainly reduces the melting point, eleminates the underlying smectic nature widens the nematic range and reduces the viscosity.Detailed dielectric measurements

in a series of such systems *(Czub et al. 2005)* provide useful data on the time scales of rotational relaxation of molecules and their anisotropy in different mesophases. These were discussed in terms of the molecular structure, with particular reference to the location of the fluorine on the ring. In the present study two such systems (shown in Fig. 5.1), abbreviated as 4OTOLFm and 4OFTOL, are chosen. Nuclear spin-lattice relaxation time (T_1) dispersions of ^{1}H and ^{19}F in the isotropic phase of these systems are measured as a function of temperature, and the data are interpreted based on mechanisms that could effectively relax the two different nuclear spins.

5.2 Experimental methods

Frequency dispersions of the two nuclei are measured in 4OTOLFm and 4OFTOL, over the frequency range nearly 100 kHz to 40 MHz using a field-cycling commercial relaxometer (Stelar, Italy), supplemented by a home-built variable-field pulsed NMR spectrometer to cover higher frequencies. Experimental setup and various pulse sequences used to measure T_1 are explained in Chapter 3. Temperature was regulated by passing dry air over the sample controlled at the desired temperature. The T_1 measurements of proton have estimated errors within 2%, while those of fluorine are prone to higher errors (estimated to be within 5%) arising from inherent weak signal strength due to the lone fluorine. The stability in temperature is estimated to be within 0.1℃. The samples, obtained from the laboratories in Warsaw, are sealed after removing the dissolved oxygen through freeze-pump-thaw cycles. In 4OTOLFm (sample-A), frequency dispersion profiles of T_1 are collected for both the nuclei at three temperatures T, differing from the clearing temperature (T_{IN}) by $\Delta T = (T - T_{IN}) = 1$, 3.5, and 11.5℃. The T_1 relaxation rates are also measured as a function of temperature at chosen resonance frequencies ν_L ($\omega = 2\pi\nu_L$). In the second system 4OFTOL (sample-B) dispersion profiles of both nuclei are collected: ^{1}H data are collected at four temperatures ($\Delta T = 0.5$, 1.5, 2.5, and 4℃) while ^{19}F data are collected at one temperature ($\Delta T = 1.5$℃). The results are shown in Figs. 5.2-5.7. Proton data of sample-A may be seen in Figs. 5.2 (dispersion of T_1 rate at different temperatures) and 5.3 (temperature dependence of T_1 rate at different resonance frequencies). Figs. 5.4 and 5.5 present similar data on the fluorine nucleus in the same sample. Dispersions of T_1 rates of proton and fluorine nuclei in sample-B are shown in Figs. 5.6 and 5.7, respectively.

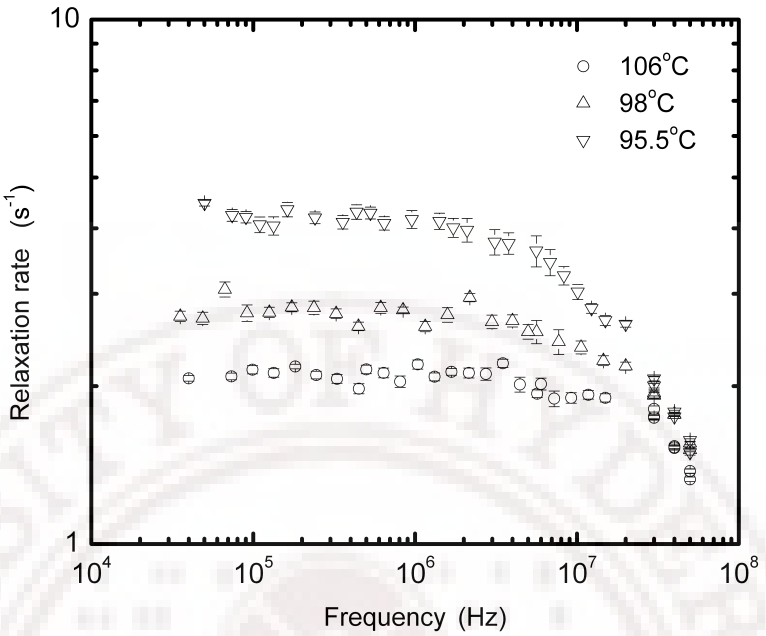

Figure 5.2: Proton spin-lattice relaxation rates in sample-A plotted against Larmor frequency at different temperatures in the isotropic phase

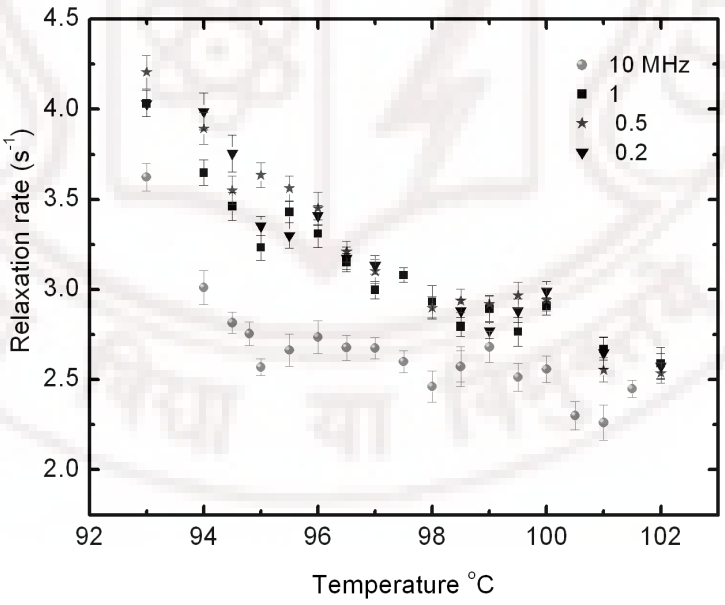

Figure 5.3: Proton spin-lattice relaxation rates in sample-A plotted against temperature at different Larmor frequencies

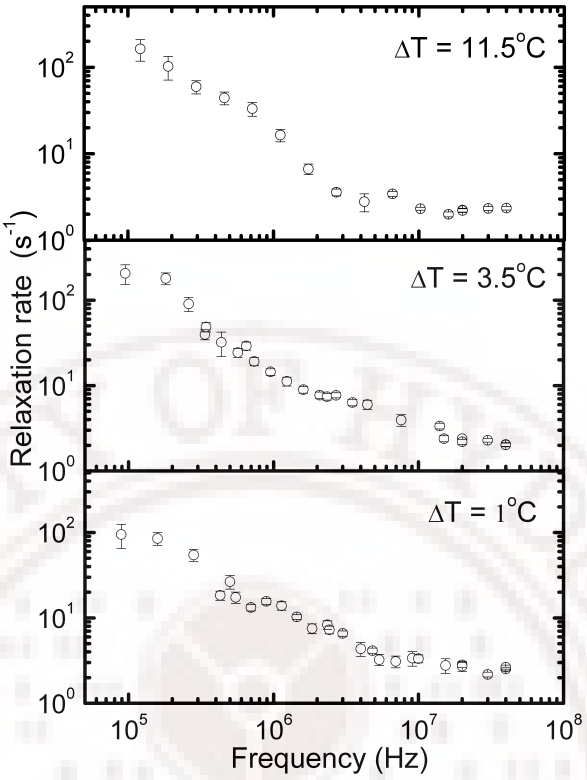

Figure 5.4: Fluorine spin-lattice relaxation rates in sample-A plotted against Larmor frequency at different temperatures in the isotropic phase

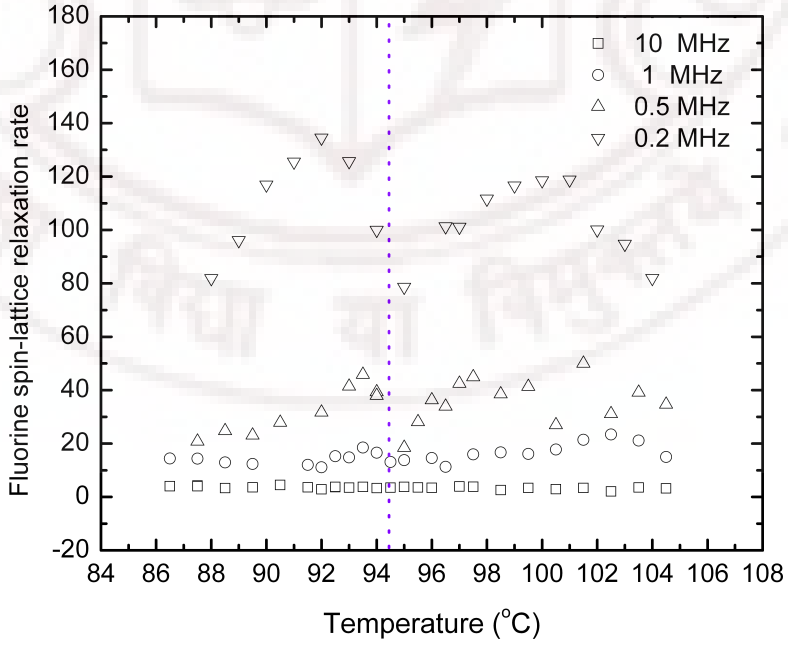

Figure 5.5: Fluorine spin-lattice relaxation rates in sample-A plotted against temperature at different Larmor frequencies

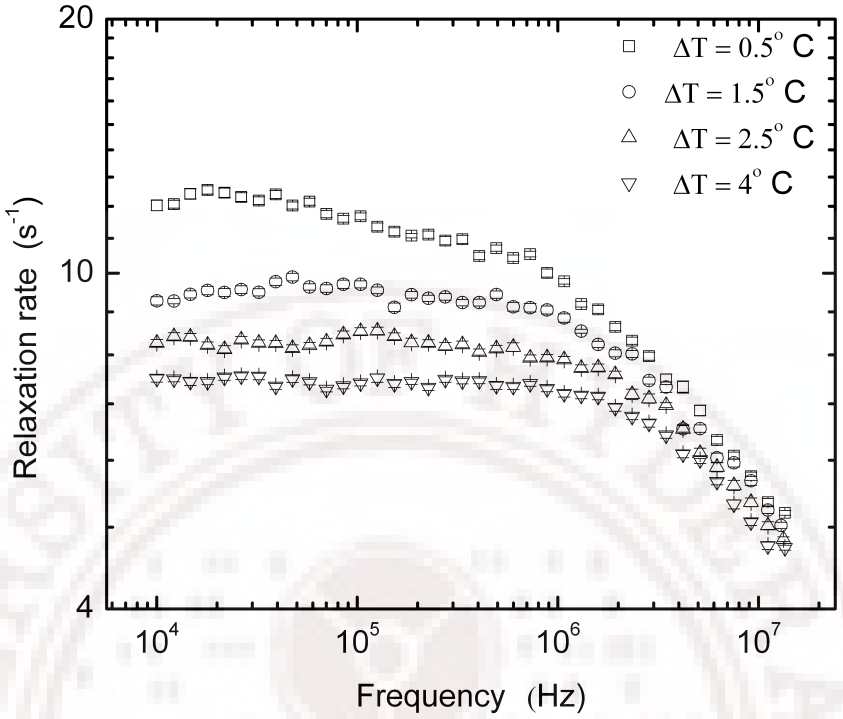

Figure 5.6: Proton spin-lattice relaxation rates in sample-B plotted against Larmor frequency at different temperatures in the isotropic phase

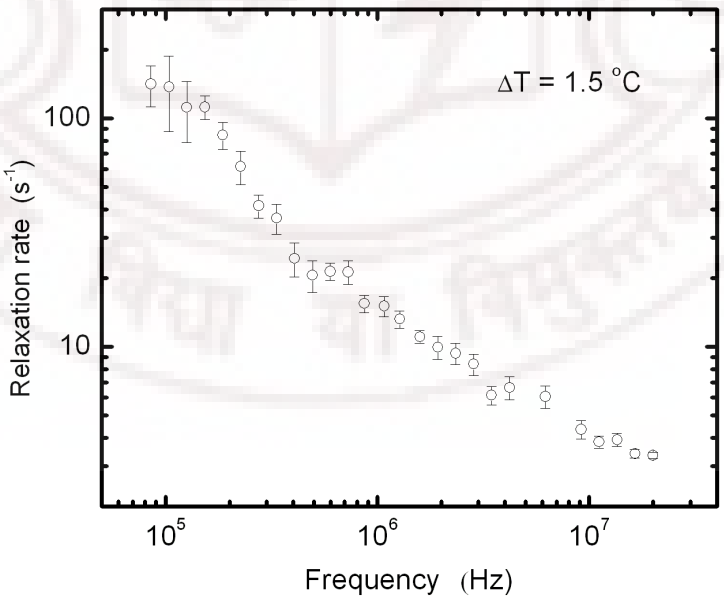

Figure 5.7: Fluorine spin-lattice relaxation rates in sample-B plotted against Larmor frequency at 73℃ in the isotropic phase

Proton T_1 rates in the isotropic phase of both the samples (Figs. 5.2 and 5.6) are essentially frequency independent in the sub-MHz region at all the temperatures, and show discernible dispersion only at higher frequencies (∼10 MHz) as the samples are cooled towards their clearing points. Temperature variation of the proton relaxation rate in sample-A shown in Fig.5.3, indicates the pre-transitional behaviour at lower frequencies, consistent with the onset of short-range nematic order fluctuations. In contrast, fluorine relaxation dispersions in both the samples are qualitatively different (Figs. 5.4 and 5.7). They all exhibit significant dispersion starting from relatively lower frequencies, extending over the rest of the high frequency region. Temperature dependence studies on these two nuclei in sample-A covering a reasonably wide range in the isotropic phase (∼12℃ above the clearing point) provide a contrasting scenario (Fig. 5.3 for proton data and Fig. 5.5 for fluorine data). These results are discussed below, looking for a plausible interpretation of the experimental data reported by the fluorine probe.

5.3 Models for relaxation

5.3.1 Proton relaxation

Proton spin relaxation in these systems is primarily mediated by the time-modulation of proton-proton dipolar coupling, and in the isotropic phase is effectively aided by both inter- and intra-molecular dipolar interactions arising from individual dynamic processes. These typically occur in the ns region thereby inducing a frequency dispersion of the relaxation above 10 MHz. However, at temperatures nearer to T_{IN}, short-range nematic order develops on time scales which progressively slow down as clearing point is reached, and the correlation times of these nematic clusters critically increase, matching with the higher end of the dispersion profile progressively. In the present case, it is found that the dispersions can be accounted for by individual reorientations of molecules and the critical contributions near T_{IN}. As a consequence, the total proton spin-lattice relaxation rate $R_1 = T_1^{-1}$ is expressed as

$$R_{1P} = R_{10} + R_{1R} + R_{1CF}. \tag{5.1}$$

The first term on the right hand side represents (constant) background contribution to the observed relaxation rate, not accounted for by the other terms. The second term is due to the molecular reorientations characterized by the correlation time τ_R

and is explained in Chapter 2 (Eqn. 2.51) *(Bloembergen et al. 1948)* as.

$$R_{1R} = A_{1R} \sum_{p=1}^{2} \frac{p^2 \tau_R}{1 + (p\omega\tau_R)^2}$$

In the limit of fast reorientations, $\omega\tau_R \ll 1$, the above contribution becomes frequency independent and is constant at a given temperature. In 4OTOLFm for example, correlation times for reorientations parallel and perpendicular to the molecular axis were estimated from detailed dielectric measurements to be 0.18 ns for reorientations about the long axis and 2.55 ns about the short axes *(Czub et al. 2005)*. Consequently the frequency dispersion in the frequency range studied is primarily influenced by dynamics about the short axes, represented by R. The third term in Eqn. (5.1) originates from the time-modulation of dipolar interactions due to the short range nematic order fluctuations *(Dong 1994, Chavez et al. 2000, de Gennes 1969)*. Spinlattice relaxation due to short range nematic order fluctuations is explained in seciton 2.5 of Chapter 2. (Eqn 2.22.)

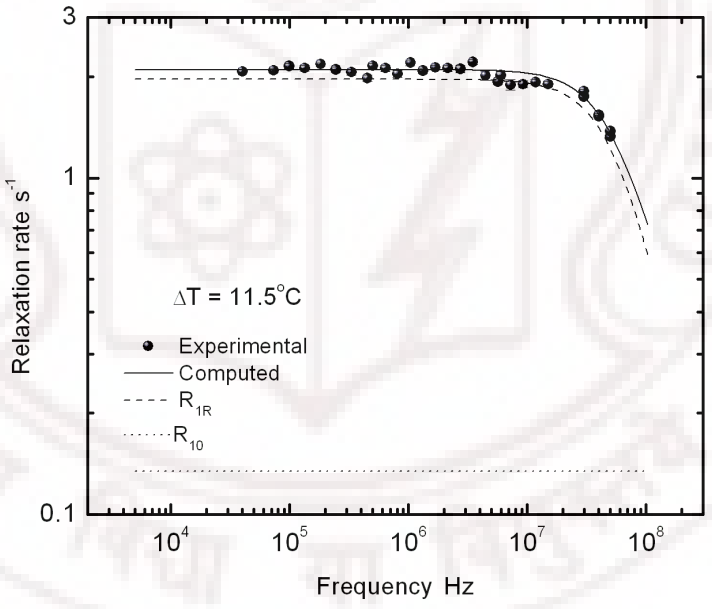

Figure 5.8: Proton spin-lattice relaxation rates in sample-A plotted against Larmor frequency 11.5℃ away from the transition in the isotropic phase (T_{NI} = 94.4℃)

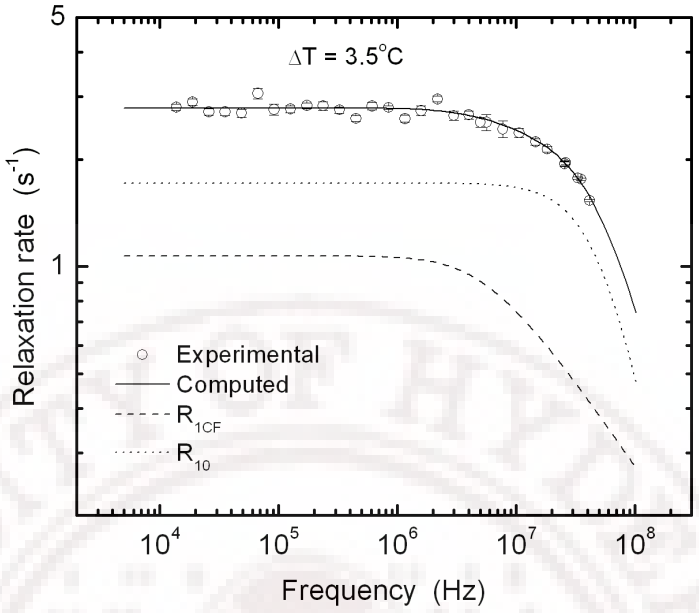

Figure 5.9: Proton spin-lattice relaxation rates in sample-A plotted against Larmor frequency 3.5℃ above N-I transition (T_{NI}=94.4℃).

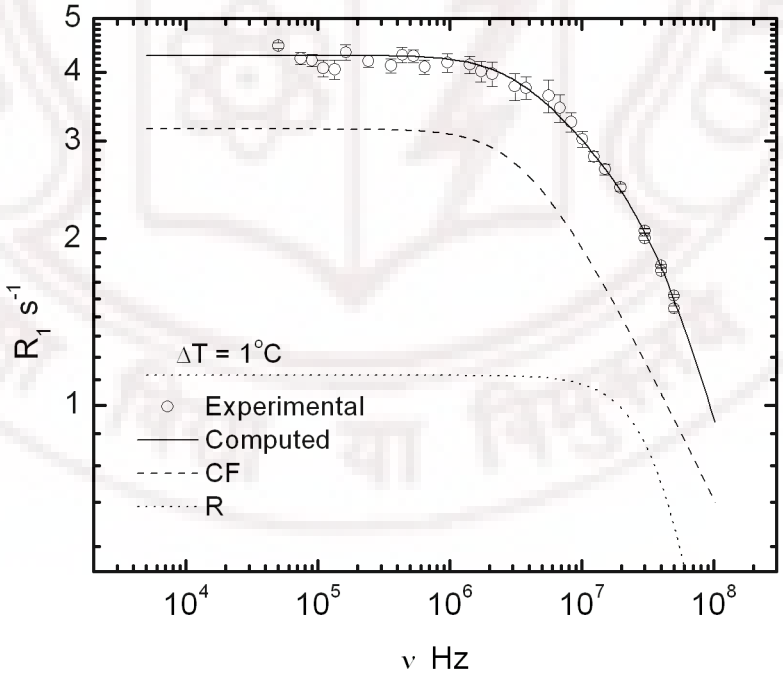

Figure 5.10: Proton spin-lattice relaxation rates in sample-A plotted against Larmor frequency 1℃ above the N-I transition.

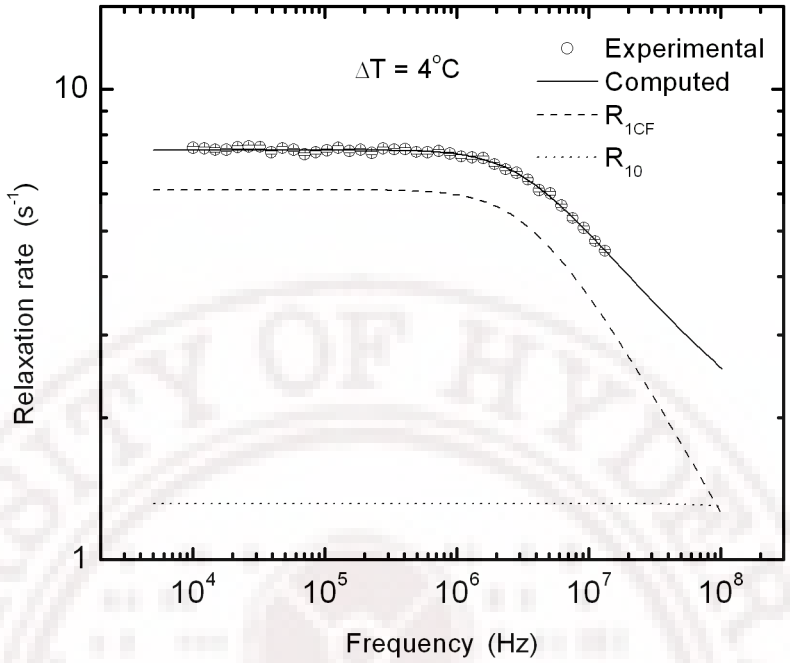

Figure 5.11: Proton spin-lattice relaxation rates in sample-B plotted against Larmor frequency 4℃ above T_{NI}.

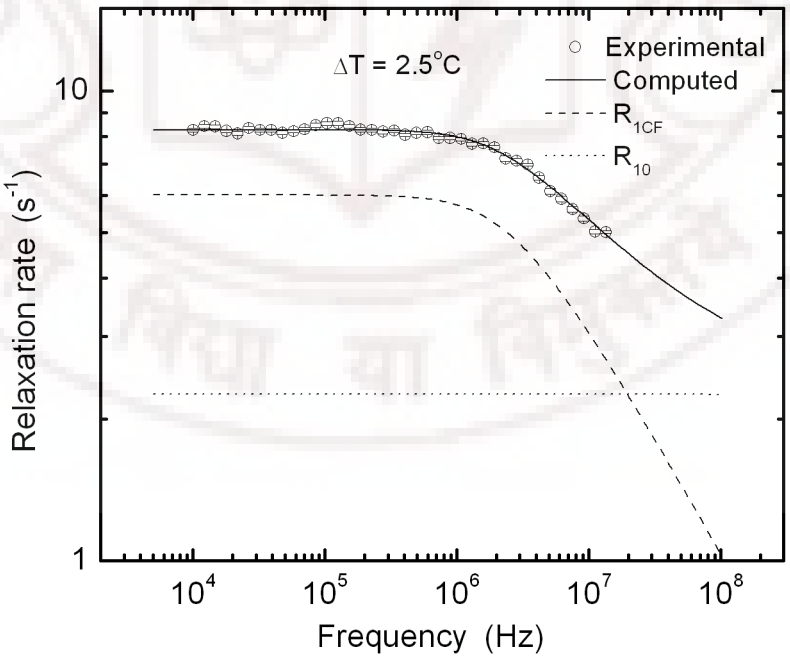

Figure 5.12: Proton spin-lattice relaxation rates in sample-B plotted against Larmor frequency 2.5℃ above T_{NI}.

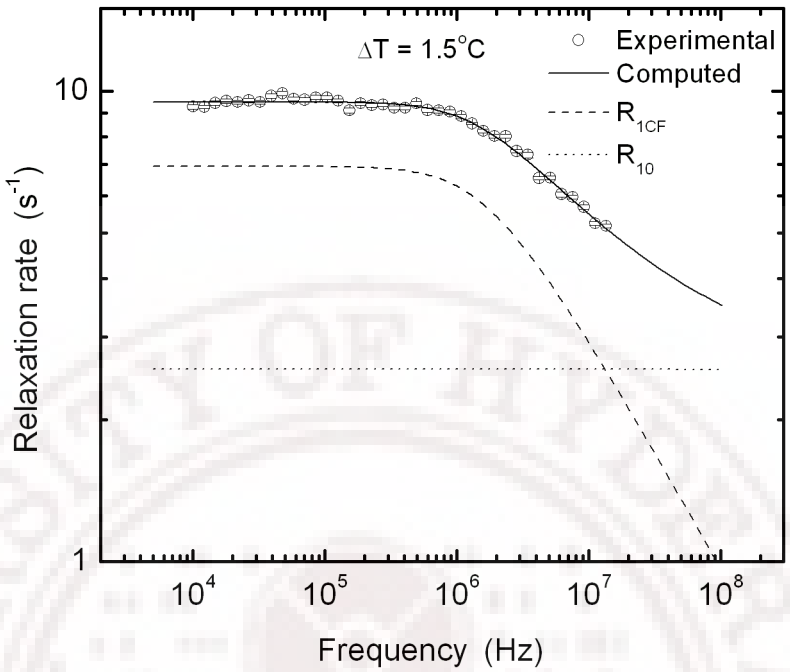

Figure 5.13: Fluorine spin-lattice relaxation rates in sample-B plotted against Larmor frequency 1.5℃ above T_{NI}.

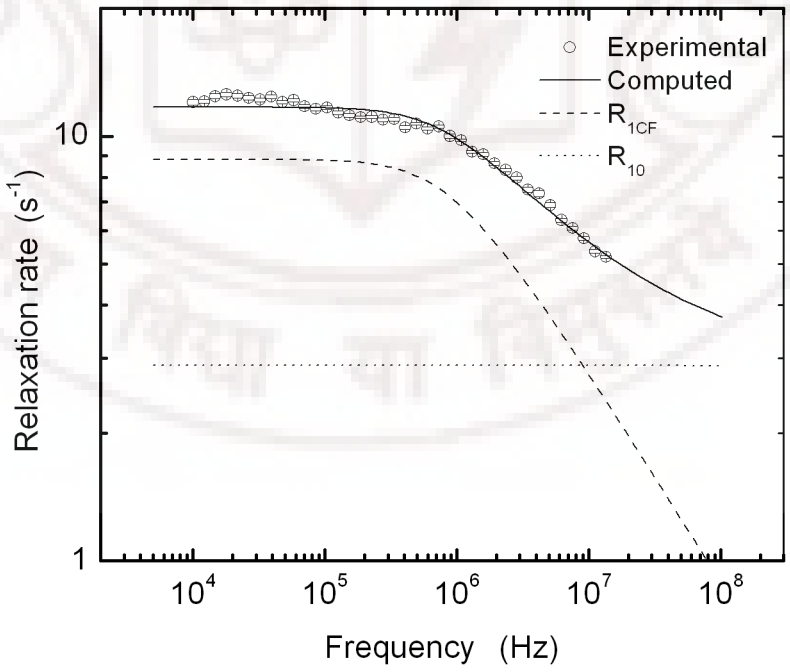

Figure 5.14: Fluorine spin-lattice relaxation rates in sample-B plotted against Larmor frequency 0.5℃ above T_{NI}.

5.3.2 Fluorine relaxation

Presence of lone fluorine on the core of the liquid crystal molecule imparts a qualitatively different mechanism for its spin-lattice relaxation. Intra-molecular dipolar mechanism is not effective since the hetero-nuclear coupling with the ring protons is not feasible unless the individual resonance frequencies of the two nuclear species are within the overlap region of their line-widths. Such is not the case, unless the experiments are performed at very low Larmor frequencies. In this low frequency region, additional mechanisim is provided by cross-relaxation process via fluorine-proton hetero-nuclear dipolar interaction (CR region). The inter-molecular homo-nuclear dipolar interactions involving fluorine are on one hand negligible, and on the other are too fast to contribute to dispersion in the frequency region investigated. Thus the fluorine spin relaxation for most part of the dispersion, excluding CR region, is expected to be aided primarily by those mechanisms which can generate fluctuating magnetic fields at its site, without reference to magnetic interactions with the other nuclei within the molecule. It is known that such is the case with spin-rotation interaction, and is particularly effective in the case of fluorine due to its relatively large coupling constant. It may be noted that it is relatively ineffective in the case of protons due to their weak coupling to rotations, and is thus considered unimportant compared to the other pathways available to them in liquid crystal systems.

Spin-rotation interaction arises from the time-dependent magnetic fields generated at the nucleus from (random) changes in angular momentum components associated with the molecule, and its contribution to the spin-lattice relaxation is related to time correlations among them, under certain approximations *(Chavez et al. 2000, Brown et al. 1963, Hubbard 1963)*. The effect of this interaction on relaxation process is qualitatively different from that of dipolar coupling: the relaxation rate now depends on the angular momentum correlation times (τ_J), rather than on the reorientational correlation times (τ_R) (under the valid approximation of well separated τ_J and τ_R). It has also been well recognized that the details of the underlying molecular processes (eg. transient rotation model involving sharp jumps between different orientations *versus* Brownian rotational dynamics coarse-grained suitably to include the angular momentum variables) are unimportant since their effect is only indirectly accessed on a much coarser time scale of the spin relaxation *(Chavez et al. 2000)*. This interaction is explained and expression are given in the section 2.4.2 of Chapter 2. (Eqn. 2.20) For typical molecules constituting simple liquids, τ_{SR} is the correlation time associated with the angular momentum fluctuations of the molecule, and is in the range of 10^{-12} to 10^{-13} s. The present experiments are thus not expected to yield frequency dispersion under the influence of such dynamic processes ($\omega\tau_{SR} \ll 1$).

The experimental observations presented in this respect, summarized in Figs. 5.4 and 5.7, however indicate unmistakable dispersion of spin-lattice relaxation in the low frequency region (∼1 MHz) reported by a spin probe whose only mechanism of relaxation in this frequency region seems to be the spin-rotation interaction. An explanation for this observation perhaps lies in examining the concept connected with the model: the torques experienced by the molecule due to its interactions with its neighbours are on the time scale of molecular interactions (like, e.g. molecular collisions), and hence are fluctuating rapidly as is normally concluded. This however does not take into account the possibility that there could be slow collective modes in the system which can in principle produce torques on a very different (slow) time scale, and a well designed probe could sense such an environment, and hence report on the underlying collective molecular processes.

In this context, conclusions of earlier molecular dynamic studies in liquid crystals using electron spin resonance (ESR) techniques, in their mesophases in general and in their isotropic phase in particular, may be recalled. Extensive investigations on the line shapes of ESR spectra of different nitroxide radicals dissolved in liquid crystals indicated that simulation of spectral shapes based on simple rotational dynamical models was not adequate in accounting for the observed data *(Green and Powles 1965, Freed 1977)*. Subsequent time domain studies using 2-d ESR methods confirmed that such probing nitroxide molecules were subjected to influences of local ordering. The effect of time fluctuations of this ordering is two fold: on one hand it produces a potential arising out of the mean torques and the angular momentum components of the probe tend to relax on a faster time scale in the presence of this torque; and on the other the potential of the mean torque itself in addition undergoes a slow rotational diffusion as a result of the possibility that the locally ordered structure, termed as the *cage*, itself tumbles on much slower time scale, in effect representing the collective modes in the system. And the larger the probe molecule is, the more sensitive is its own dynamics to these modes, and hence the more discernible will be the details of these processes to the probing spins residing on the molecule. The question of dealing with a wide spectrum of torques influencing the random rotational dynamics of a probing molecule is normally approximated to the assumption of existence of two distinct regions relative to the time scale of the experiment: those which are very fast and provide the usual mechanism for the angular momentum relaxation on a very fast time scale; and those which persist on a much longer scale competing with the time scales of the spin dynamics. These are accounted for, formally, by extending the space of stochastic variables to include the *cage* dynamics as well along with measurable spin variables. The random process as described in this composite space is then presumed to be Markovian, and is

dealt with suitably by generalizing the relevant stochastic Liouvelle equation (SLE). The method of dealing with slow modes to account for observations in magnetic resonance spectroscopy through this augmented SLE was developed by Freed and his coworkers *(Freed 1994, and references therein)* and extensive 2-dimensional ESR work on probes of different sizes to elucidate this mechanism was reported *(Sastry et al. 1996a, Sastry et al. 1996b)*. The idea was to include these slow modes through the model of a slowly relaxing local structure (SRLS) influencing the dynamics of the probe, besides the other local processes. Modeling the dynamics of this local structure is a matter of choice, and for simplicity an isotropic rotational Brownian motion of the *cage* on a well separated time scale (correlation time τ_c) could be chosen to represent the effect of these slow collective modes. Detailed work on the ESR probes in liquid crystals established the presence of SRLS mechanism *(Freed 1994, and references therein)*, and the correlation times of such cages in the isotropic phases are estimated to be in the range of several tens of ns, and the inferred value depends on the size and symmetry of the reporting probe-the effect being increasingly significant on more anisotropic and larger ESR probes as a rule. Important message from these interesting investigations, relevant to our present work, is the fact that even in the isotropic phase of liquid crystals a given molecule could experience very slow torques which is a result of short range cooperative behavior of the anisotropic molecules of the medium.

The above scenario needs to be discussed in the present context, with two important differences: here the probe molecule is one of the liquid crystal molecules itself and hence the effect of these slow processes is expected to be most effectively experienced and reported; and secondly, unlike the case of the ESR relaxation processes mentioned (which are sensitive to correlations among different molecular orientations and hence experience the effect of the fluctuating torques rather indirectly via coarse-grained angular variables), the relaxation mechanism of fluorine (under the specific experimental situation stated) is primarily governed by the relaxation processes of the (liquid crystal) molecular angular momentum components themselves, thus leading to a direct observation of these slow processes. The field-cycling NMR techniques focussing exclusively on the slow time scales, seems to make this attempt viable and valuable.

These ideas can now be readily adopted to the nuclear spin relaxation phenomena. Fluorine nuclei in the present case are, for all practical purposes, exclusively relaxed *via* the spin-rotation interaction (excludig the CR region) and hence *via* the angular momentum fluctuations. These in turn are sensitive to the local torques experienced in the medium, and following the arguments advanced in the earlier ESR work one can

divide them into two time-scales: the faster time scales aiding (time scales ($\sim 10^{-12}$ to 10^{-13}) in the usual angular momentum relaxation processes encountered in simple unstructured liquids; and the slower time scales of the *cage* dynamics corresponding to slower angular component fluctuations. The fluorine spin-lattice relaxation in these liquid crystals thus could expected to be frequency dependent from such slow processes, and its frequency dependence can be modeled in simple terms as *(Brown et al. 1963, Freed 1977)*:

$$R_{1C} = A_C \frac{\tau_C}{1 + \omega^2 \tau_C^2}. \tag{5.2}$$

Here A_C is a temperature dependent constant. The slow dynamics discussed could not effectively be reported by protons present in the molecule due to their smaller spin-rotation constant; the efficacy of this relaxation mechanism for protons could be upto two orders of magnitude smaller relative to fluorine. The absence of neighbouring fluorines in this liquid crystal molecule brings the spin-rotation interaction into a sharper focus, and the results can be interpreted in simpler terms without interference from homo-nuclear intra-molecular dipolar interactions among fluorines. The corresponding inter-molecular interactions are expected to have negligible dispersion in the frequency region under consideration, and cannot be contributing in the frequency window of our experiments.

The critical fluctuations of short-range orientational order reported by the protons, and which are found to be within the range of experimental time scales, could also be sources of fluctuating torques on similar time scales. Therefore they are expected to further augment the fluorine spin-lattice relaxation through the spin-rotation coupling. Thus we model the spin-lattice relaxation process of fluorine in this system, including the background contribution arising from fast fluctuating torques which are not accounted for by the above models, as:

$$R_{1F} = R_{10} + R_{1C} + R_{1CF}. \tag{5.3}$$

The first term on the right hand side accounts for the fast relaxing angular momentum components and provides a frequency independent and characteristically temperature dependent contribution. The second term (given by Eqn. 2.20) corresponds to spin-rotation contributions, time-modulated by the slow torques induced by the SRLS. The last term (Eqn. 2.22) takes care of the pre-transitional slowing down. We propose that the observed dispersion in fluorine relaxation, outside the CR region, is due to the second and third terms, and proceed with the evaluation of the relevant time scales.

At very low fields, the resonance frequencies of these two nuclei can be made close enough so that their NMR lines overlap; this leads to the gradual onset of an extra relaxation mechanism as the Larmor frequency is decreased due to the hetero-nuclear dipole interaction between the two nuclei. The cross-relaxation arising from this couplig *(Abragam 1961)* will lead to a more effective spin-lattice relaxation of the fluorine nuclei, reflected as additional contribution not accounted for by the dynamic processes included in Eqn. 5. As the NMR lines of the two nuclei to broaden as one approaches T_{IN}, the onset of these effects due to this cross-relaxation is expected to be occuring at relatively higher frequencies as the clearing point is reached from above. The experimental data indeed indicate that such is the case, and is further discussed in the next section.

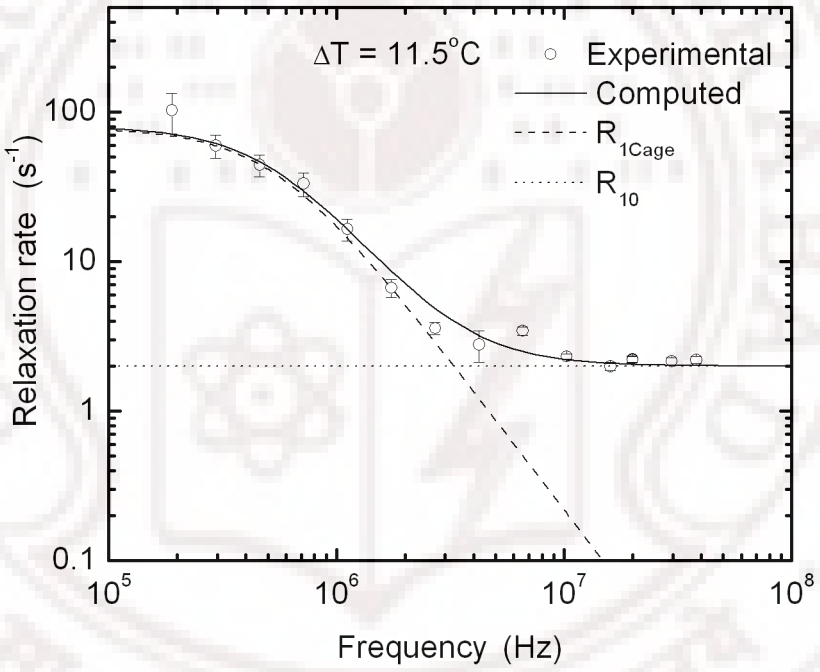

Figure 5.15: Fluorine spin-lattice relaxation rates in sample-B plotted against Larmor frequency very near the transition in the isotropic phase.

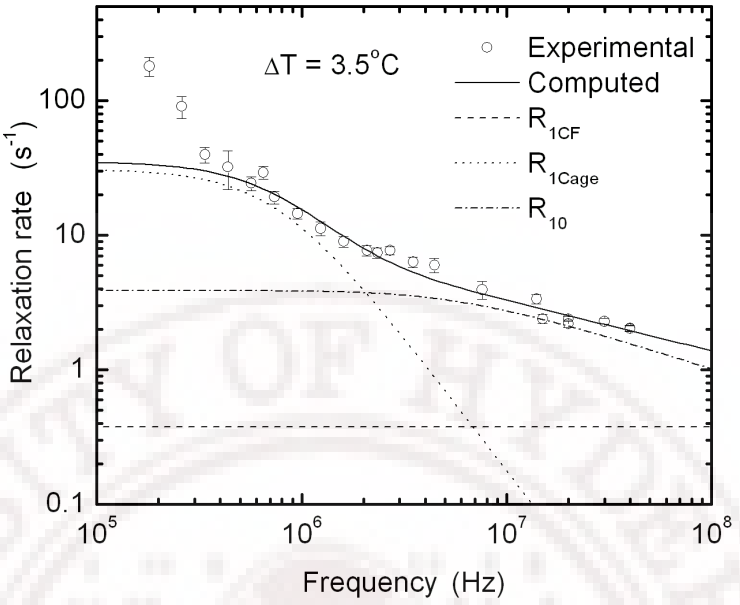

Figure 5.16: Fluorine spin-lattice relaxation rates in sample-B plotted against Larmor frequency very near the transition in the isotropic phase.

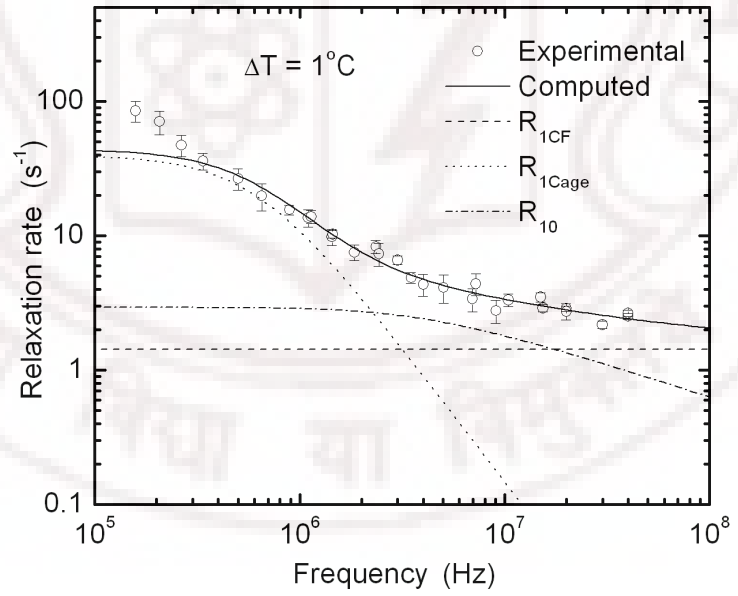

Figure 5.17: Fluorine spin-lattice relaxation rates in sample-B plotted against Larmor frequency very near the transition in the isotropic phase.

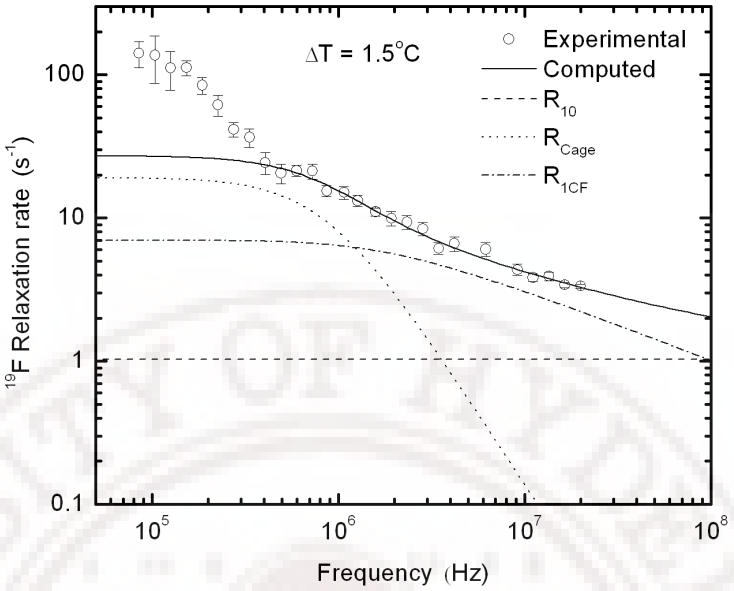

Figure 5.18: Fluorine spin-lattice relaxation rates in sample-B plotted against Larmor frequency very near the transition in the isotropic phase.

5.4 Analysis and discussion

The proton dispersion data of sample-A are fitted to Eqn. 5.1 at the three investigated temperatures, and the fits are shown in Figs. 5.8 - 5.10. Each dispersion is decomposed into a frequency-independent contribution (from molecular reorientations about the long-axis and translational diffusion), dispersive component from the reorientations about the short-axes, and critical contribution to dispersion as expressed in Eqn. 2.22. The model parameters are determined by fitting the experimental data using non-linear least squares procedure, and the results are summarized in Table 5.1. The analysis shows that at the two temperatures nearer to the clearing point (i.e. ΔT = 1 and 3.5°C), there are two dynamic processes contributing to the relaxation rate, apart from a constant background. The contribution from the critical fluctuations is considerable near the transition, and τ_{CF} is 68 ns. This value decreases rapidly to about 47 ns by heating the sample by about 2.5°C. At the highest temperature studied (i.e. ΔT = 11.5°C) there is no evidence of this contribution. The (short-axes) molecular reorientations in this sample are found to be occurring with a τ_R varying in the range 1.67 to 1.39 ns as the sample is heated above clearing point by about 11.5°C. Similar analysis of proton data of sample-B was performed (Figs. 5.11 - 5.14; Table 5.1). Data in this sample were collected nearer to the clearing point (ΔT = 0.5, 1.5, 2.5, and 4°C). The dispersions differ

qualitatively from those of the sample-A. Firstly, the data could be accounted for entirely by the critical dispersion from short-range nematic order fluctuations, apart from a constant background. Apparently in this system the reorientations of the molecule even about its short-axes seem to be taking place on a much faster time scale, compared to sample-A. Secondly, the critical dispersions extend to much lower frequencies in this system for comparable temperature differences from the clearing point yielding a significantly higher value for the τ_{CF}, (varying from about 336 to 81 ns over this range). It may be noted that these two samples differ only in the placement of the fluorine atom on the core (see Fig. 5.1). The magnitude of τ_{CF} in these compounds is comparable with that observed in another related liquid crystal, 6CHBT (4-trans-4'n-hexyl-cyclohexyl-isothiocyanatobenzene) with this technique *(Phanikumar et al. 1998)*. The τ_R value of 6CHBT was about 2.46 ns very near the clearing point while τ_{CF} was about 150 ns. Referring to Fig. 5.3, the proton relaxation rates (collected at four chosen frequencies) progressively increase with decrease in temperature in the isotropic phase, with clear evidence of increasing critical contribution at lower frequencies as the transition temperature is reached.

For analysis of the fluorine results based on Eqn. 5.3 , data in the frequency region where the cross-relaxation contributes significantly were excluded. This was identified in the experimental data as the low frequency range where there is a sudden jump in the relaxation rates, as seen in Figs. 5.15 to 5.18. It may be observed from Figs. 5.15 to 5.18 that this onset of CR region occurs progressively at higher frequencies as the sample temperature is lowered towards T_{IN}. For example, in both sample-A and sample-B, at about ΔT=1°C, this point occurs at approximeately 500 kHz. This corresponds to nearly 130G of Zeeman field, and the two nuclei differ in their resonance frequencies, at this field, by about 50 kHz. This typically is the order of the sum of the line-widths expected in broad-line NMR spectrum near the isotropic nematic phase transition. Figs. 5.15 to 5.17 shows that this overlap is reduced by about 50% by heating the sample by nearly 10°C. Analysis of the fluorine data excluding the above CR contribution, was carried out (Eqn. 5.3), taking into account modulation of spin-rotation interaction by the short range nematic order fluctuations (τ_{CF}) and the slower dynamics of the *cage* (τ_C), apart from a frequency independent contribution from fast angular momentum fluctuations. The characteristic times indicative of critical contributions at various temperatures were inferred from the analysis of the proton data, and are used as inputs for the fluorine model. The results are presented in Table 5.2.

Fluorine dispersions indicate clearly the presence of another, slower molecular processes corresponding to the cooperative modes (SRLS) in the system. This process,

modeled simply as a Lorentzian contribution to the spin-lattice relaxation rates mediated by spin-rotation dynamics, is characterized by characteristc time of the order of 260-290 ns in sample-A and about 190 ns in sample-B. In sample-A this dynamics is distinctly time-separated from critical fluctuations (see Figs. 5.15) to 5.17, while these two time scales are comparable in sample-B (see Fig. 5.18). Interestingly, the relaxation mechanism of proton does not seem to be susceptible to this process, as is avident from all the proton investigatons reported so far; these are no discernible low frequency dispersion in the isotropic phase, the slowest process reported being the critical fluctuations near the phase transition. One is thus led to the conclusion that the lone fluorine on the core is uniquely placed to report on this slower dynamics, though a different relaxation pathway. Relaxometric studies on such systems offer a novel experimental tool to pursue these processes rather directly. In contrast, critical fluctuations of the short range nematic fluctuations appear to be mediating spin relaxation of both nuclei (though through different mechanisms), and temperature dependence of the corresponding relaxation dispersion profiles confirm their contribution.

Sample	T°C(ΔT)	$R_{10}s^{-1}$	$A_{CF}s^{\frac{-3}{2}}$	$\tau_{CF}ns$	$A_R\ 10^8s^{-2}$	τ_R ns
4OTOLFm	106(11.5)	0.135±0.1	–	–	2.83±0.26	1.39±0.06
	98(3.5)	–	69.9±12.2	46.9±6.9	2.3±0.1	1.50±0.03
	95.5(1)	–	171±7.8	67.9±3.2	1.35±0.1	1.67±0.06
4OFTOL	75.5(4)	1.85±0.3	276.8±11.5	81.2±3.3	–	–
	74(2.5)	2.3±0.2	260.1±9.8	106±4	–	–
	73(1.5)	2.56±0.2	243.1±6.3	162.4±5	–	–
	72(0.5)	2.9±0.1	209.4±3.4	336.1±8.2	–	–

Table 5.1: Parameters extracted by fitting the ^{1}H dispersions to Eqn. 1.

Sample	T°C(ΔT)	A s^{-1}	$A_C\ 10^8\ s^{-2}$	$\tau_C$ns	$A_{CF}\ 10^2s^{\frac{-3}{2}}$	τ_{CF} ns
4OTOLFm	106(11.5)	2.15±0.02	2.55±0.01	289.7±1.8	–	–
	98 (3.5)	0.377	1.47±0.09	209.4±28.3	258.6±3.2	47
	95.5 (1)	1.43±0.25	1.52±0.11	260.6±34	160.1±32.7	75
4OFTOL	73 (1.5)	1.04±0.53	1.01±0.14	188.3±42.3	254.1±55.9	160

Table 5.2: Parameters extracted by fitting the ^{19}F dispersions to Eqn. 5. τ_{CF} values are fixed near to the values determined by proton relaxation

Fig. 5.5 shows the observed temperature variation of fluorine relaxation rate at four frequencies (0.2, 0.5, 1.0 and 10 MHz) between 86 and 105°C, covering nematic and isotropic phases. We focus only on the isotropic side of this data. The features of this variation are qualitatively different compared to the temperature variation of proton data (Fig. 5.3). The relaxation rates at 10 MHz are practically independent of temperature. At lower frequencies these show a tendency to increase as the sample

is heated from its clearing point, reach a maximum, and then start decreasing. The relative increase in the rates before they reach their respective maxima is higher at lower frequencies. The formation of relaxation rate maxima with increase of temperature is in principle a signature of the spin-rotation interaction, since the relevant correlation time (of angular momentum components) increases with increase of temperature. For an appropriately placed NMR time-window, this has the potential to lead to an initial increase in the relaxation rate. However interpretation of the temperature dependent data of fluorine, particularly at the low frequencies encompassing CR region, is not straight forward. Here, the observable relaxation rates (with temperature) are a combination of temperature dependent changes in the spin-rotation interaction contribution appropriate to the frequency of observation on one hand, and, on the other, changing contribution from cross-relaxation as the line-widths of the two lines decrease on moving away from the transition point. What is observed in the experiment is the cumulative effect, as one probes the frequency region dominated by leading temperature dependent cross-relaxation mechanism. The observation of a very similar behaviour on the low temperature side (Fig. 5.5) lends support to this interpretation, due to very similar underlying physical reasons on the nematic side also.

5.5 Conclusions

This experimental study presents perhaps the first observation of fluorine spin-lattice dispersion in a liquid crystal. The system is chosen such that its only effective relaxation mechanism is due to the spin-rotation interaction over a wide frequency range. The dispersion profiles at different temperatures in the isotropic phase show a prominent low frequency dispersion, followed by long tails at higher frequencies. An explanation of the low frequency behaviour is traced to the presence of slow dynamic process arising from slowly relaxing local structure (*cage* dynamics), which was earlier postulated to explain ESR data in isotropic phases of liquid crystals. However the time scales reported by the present study for the *cage* differ from those inferred from the ESR studies by an order of magnitude. Of course, the nature of the probes and their experimental time scales in the two experiments are also considerably different. Based on the *cage* model, the present experiments are explained as reflecting the sensitivity of the fluorine probe, exclusively interacting with fluctuating torques and reporting on their correlations. This is in contrast to the results obtained from proton spin-lattice relaxation study. Interestingly, both the probes are sensitive to the critical fluctuations of the short-range nematic order in the isotropic phase, and yield consistent observable data at different temperatures with comparable time scales

of this process. This difference in the sensitivity of the probes to the two different cooperative phenomena deserves further investigations.

The two nuclei have comparable gyromagnetic ratios, and hence they can be dipolar-coupled at low enough Larmor frequencies. Field-cycling relaxometry permits such an experiment, and as a result we see the effect of cross-relaxation in the relaxation dispersion profile in the frequency region where such dipolar contacts are prominent. This observation also provides an opportunity to infer atleast qualitatively about the changes in spectral line-widths near the phase transition. The temperature dependent studies of the relaxation rates further lend support to the models proposed in connection with the dispersion behaviour of the respective nuclei. In conclusion, singly fluorinated molecules in such complex fluids are seen to be exclusively sensitive to angular momentum time-correlations directly, and seem to offer a unique opportunity to probe very slow molecular processes, arising out of other cooperative modes in the system.

Chapter 6

Proton Magnetic Relaxation Dispersion Studies of Protein-Denaturant Interactions

6.1 Introduction

Current understanding of the protein folding and stability is largely based on a structural classification into native, molten globule and denatured conformational states. Experimental studies till now showed that proteins in the presence of strong chemical denaturants approach a random coil configuration implying that polypeptide chain is exposed to the bulk solvent. On the other hand evidences are also mounting for stable conformations of proteins in the presence of controlled amounts of denaturants. *(Denisov et al. 1999, Dobson 1992, Shortle 1993, Bhuyan 2002, Kumar and Bhuyan 2004, Kovrigin and Potekhin 1999).* Considering the widely acknowledged importance of protein-solvent interactions for stability and folding, non-native protein hydration is very little understood despite many efforts. Both stoichiometric binding theory for direct protein-denaturant interactions and denaturant-mediated alteration in protein-solvent interactions afford interpretations of unfolding transitions *(Schellman 1978, Schellman 1987).* Recent reports indicate that sub-denaturing concentrations of GdnHCl can stabilize proteins by committing $GdnH^+$ and Cl^- ions to screen charge-charge interactions in the native state of the protein *(Pace et al. 2000, Mayr and Schmid 1993, Morjana et al. 1993, Monera et al. 1994, Makhatadze et al. 1998, Ibarra-Molero et al. 1999a, Ibarra-Molero et al. 1999b, Bhuyan 2002, Kumar and Bhuyan 2004).* A more recent demonstration shows that even urea, when used in sub-denaturing concentrations, stabilizes proteins, implying that protein-denaturant interactions also lower the conformational entropy of the protein (Bhuyan 2002). X-ray structures of protein crystals soaked in low molarity solutions of chemical denaturants show that both $GdnH^+$ and urea interact with different groups of the protein through non-covalent bonding, producing non-specific networks of intramolecular in-

teractions *(Dunbar et al. 1997, Pike and Acharya 1994, Hibbard and Tulisky 1978).*

These observations underscore the complexity of the mechanism by which denaturants achieve their protein-unfolding action. In an earlier study GdnHCl, urea, and salt were used to establish that the GdnHCl stabilization originates from both entropic effect due to intra-molecular protein cross-linking action of $GdnH^+$ and electrostatic effect due to the interaction of Cl^-, and also possibly of $GdnH^+$, with charged groups of ferrocytochrome c *(Bhuyan 2002).* It was, however, not clear whether the stabilization adds on to the global stability of the protein or is manifested at sub-global level. With this rationale, we wish to investigate protein structure in the presence of sub-denaturing or moderate concentrations of GdnHCl, with focus on the possibility of stiffening and entropically stabilizing proteins.

Nuclear magnetic relaxation dispersion (NMRD) technique can be used to investigate protein-interior dynamics of water and protein folding *(Denisov and Halle 1996, Halle et al. 1999).* The advent of field-cycling (FCNMR) technique *(Noack 1986, Kimmich and Anardo 2004)* in particular amplified its applications especially in the study of protein dynamics. The magnetic relaxation dispersion method has been used to study urea and GdnHCl induced protein unfolding *(Halle et al. 1999, Denisov et al. 1999, Modig et al. 2003)*, although the specific effect of protein stabilization at sub-denaturing concentrations of the denaturants has not been investigated. In this context, present work reports on the influence of GdnHCl on hydration dynamics of lysozyme and bovine serum albumin (BSA), by use of proton magnetic relaxation dispersion (PMRD). The two proteins chosen for the study here are paradigms for structural, functional, and folding studies *(Evans et al. 1991, Morozova et al. 1995, Knubovets et al. 1999, Tanford et al. 1973, Kuwajima et al. 1985, Radford et al. 1992, Wildegger and Kiefahber 1997, Elkadi et al. 2006, Ahmad et al. 2004, Efimova et al. 2007, and the references therein)* and are extensively used in biochemistry. Both lysozyme and BSA were studied earlier with PMRD measurements *(Denisov and Halle 1996, Kiihne and Bryant. 2000, Halle et al. 1999).*

6.2 Experiments

A commercial preparation of hen egg white lysozyme obtained from Calbiochem was used without further purification. BSA was obtained from Sigma and chromatographed using sefedex G75 column in 50 mM sodium phosphate buffer at pH 7 and the monomeric fraction obtained was dialyzed against deionized water (Fig. 6.1). GdnHCl was obtained from United States Biochemical (USB, Cleveland, Ohio). Lysozyme and BSA samples were prepared in aqueous solutions of GdnHCl. The pH

was adjusted to 4.4 (electrode reading) by adding trace amounts of dilute HCl/NaOH. Protein concentrations are determined using UV absorption spectra. Concentration of GdnHCl was determined by refractive index measurements by the use of an Abbe-type refractometer. The pH was found to stay constant in the entire duration of PMRD measurements. No attempt was made to remove dissolved oxygen as the interest in the present studies was on the relative variation in the PMRD profiles as a function of denaturant concentration.

6.2.1 PMRD Measurements

For ^{1}H relaxation dispersion measurements 6 mM lysozyme and 0.2 mM BSA samples were used. Measurements were performed using a commercial fast field-cycling NMR (FFCNMR) relaxometer (Stelar, Italy) covering the frequency range of 10 kHz to 10 MHz, and a home built pulsed NMR spectrometer tunable in the 5-50 MHz frequency range to cover higher frequencies. Conventional inversion recovery sequences were employed for measuring the longitudinal relaxation times on the pulsed NMR spectrometer while non-polarization and pre-polarization sequences *(Anoardo et al. 2001)*, were used (as was explained in sections 3.2 and 3.3 of Chapter 3) for measurements on the FFCNMR relaxometer (for the frequencies above and below 4 MHz, respectively). The temperature of the sample in the pulsed NMR spectrometer was regulated at 27±0.2°C using a home-built gas-flow type cryostat and a PID temperature controller. The FFCNMR spectrometer employs VTC90 unit (Stelar, Italy) for this purpose, and the estimated stability in this case was within 0.2°C.

6.2.2 Equilibrium unfolding measurements

Protein samples were prepared in the 0-6 M range of GdnHCl in 50 mM phosphate at pH 6.5 (BSA) or in water at pH 4.4 (lysozyme). Final protein concentrations were 5 M for BSA and 2.2 M for lysozyme. Samples were equilibrated at 27^{o}C for at least 8 hours before recording fluorescence spectra. Emission spectra (excited at 280 nm, slit width: 0.75 nm) were taken in the 320-370 nm range, setting the slit width to 1.25 nm. These measurements employed a photon counting instrument (FluoroMax-3, Jobin-Yvon, Horiba). The cell temperature was regulated at 27±0.5^{o}C by the use of a home-built external water circulation system.

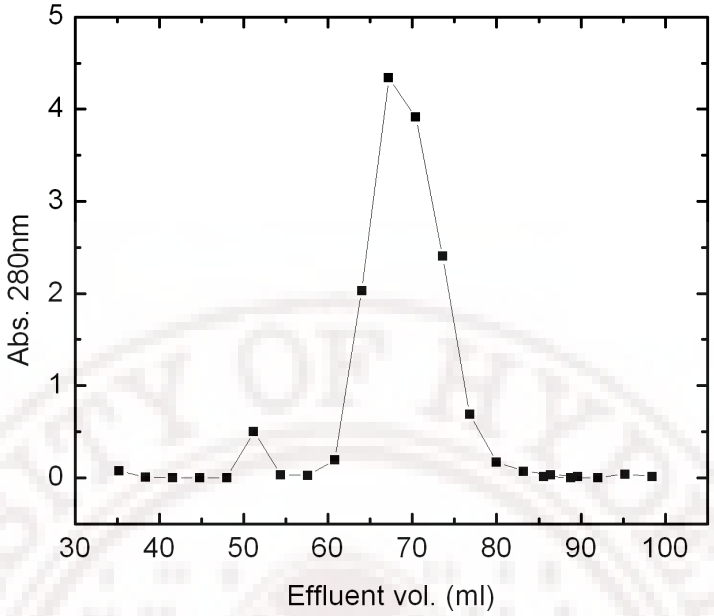

Figure 6.1: BSA monomer extraction. Near 50 ml of Effluent volume aggregated protein, and after that BSA monomer was observed.

6.3 Results and Analysis

To study the effect of GdnHCl on protein hydration dynamics we recorded ^{1}H relaxation dispersion profiles of protein solutions containing different concentrations of the denaturant in the 0-5 M range for lysozyme and 0-2.15 M for BSA. Fig. 6.2 and 6.3 show three representative profiles for spin-lattice relaxation rate, R_1, as a function of resonance frequency, for lysozyme and BSA respectively.

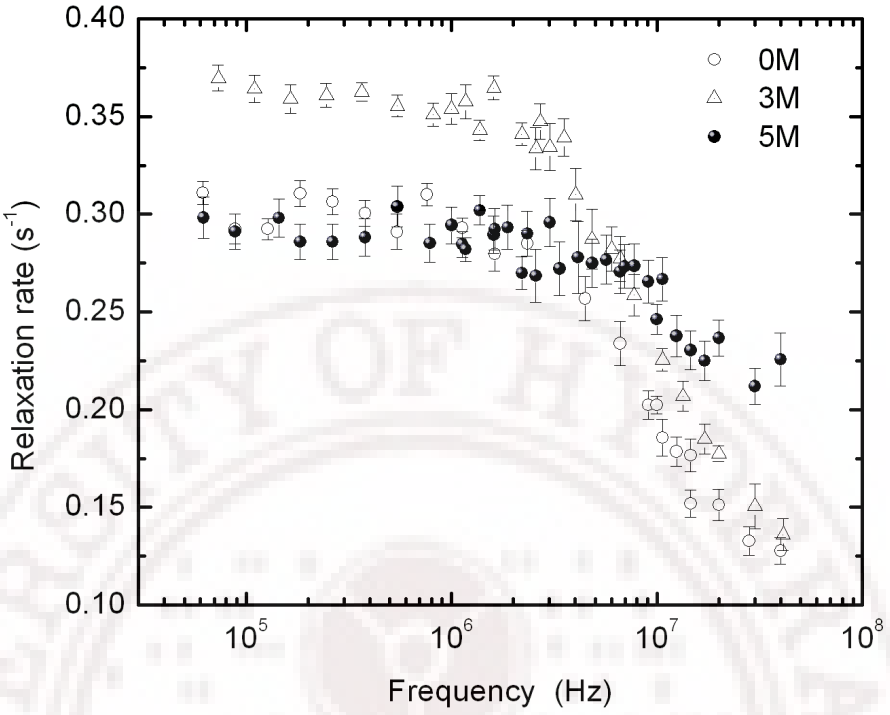

Figure 6.2: PMRD of lysozyme at 0 M, 3 M and 5 M concentrations of GdnHCl

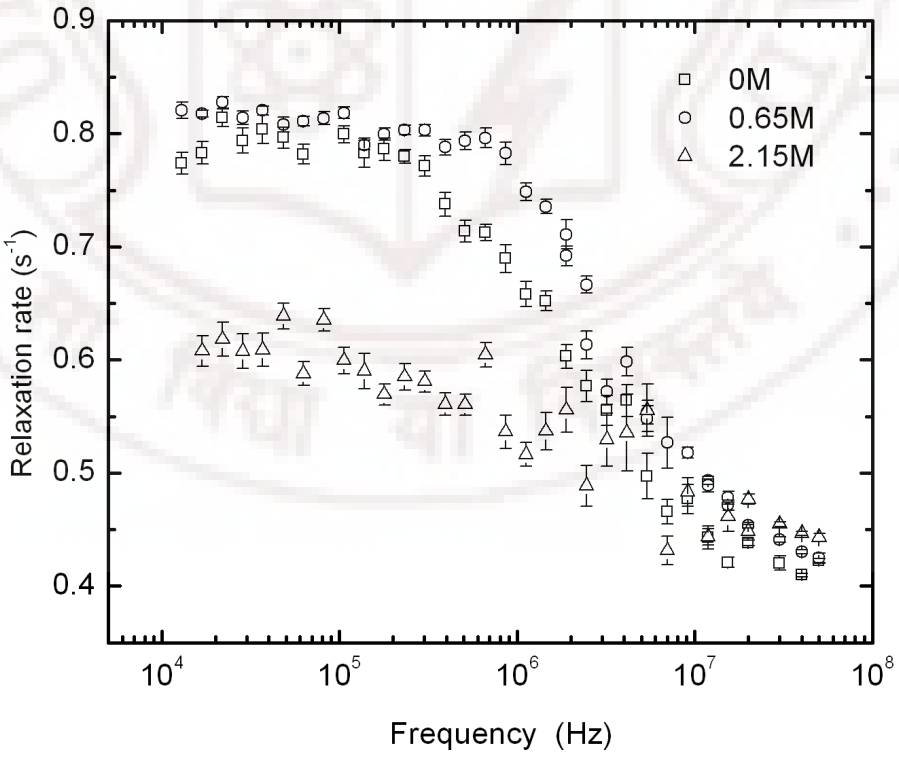

Figure 6.3: PMRD of BSA at 0M, 0.65 M and 2.15 M concentrations of GdnHCl

6.3.1 Results on Lysozyme:

With initial increments of GdnHCl the dispersion step in T_1^{-1} increases relative to that for the native lysozyme solution. The dispersion, however, rapidly weakens for increments beyond 3 M GdnHCl as seen from the rather shallow dispersion step for the samples containing 5 M GdnHCl (Fig. 6.2). This qualitative assessment of dispersion plots indicates nonlinear effect of GdnHCl concentration on lysozyme hydration dynamics. The relaxation dispersion initially increases and then decreases displaying an inflection centered around 3 M of GdnHCl. Considering the dispersions to be due to long-lived internal waters and labile hydrogens of the protein backbone *(Halle et al. 1999, Halle and Denisov 2001, Venu et al. 1997)* the frequency dependence of the relaxation rate was analyzed using a model described by

$$T_1^{-1} = R_b + \alpha + \beta\tau_c \left[\frac{0.2}{1 + (\omega\tau_c)^2} + \frac{0.8}{1 + (2\omega\tau_c)^2} \right]. \tag{6.1}$$

Here R_b represents the contribution to the relaxation from the bulk water molecules. α represents contribution from the water molecules that are loosely bound to the protein surface. The third term on the right hand side represents contributions from the integral water molecules buried inside the protein and the labile protons exchanging with the bulk water protons at a rate slow compared to the global correlation time of the protein, τ_c, but fast compared to the inherent relaxation rate (R_I). Since the dominant spin-spin interaction for protons in the type of systems under consideration is the dipolar (Abragam 1961), the parameter β includes the dipolar coupling constant (ω_D), the fraction of protons in integral water molecules and the labile protons in the total water molecules (f_I), and orientational order parameter (S_I), which is included to take into consideration the averaging of the spin interaction by fast internal motions of the water molecules and labile protons. Thus, β is described by

$$\beta = \sum_{\mu} f_{I\mu}\omega_{D\mu}^2 S_{I\mu}^2. \tag{6.2}$$

Here the summation is over different species of protons (integral waters and labile protons, for example) contributing to the relaxation dispersion. To obtain the parameters $R_{1b} + \alpha$, β and τ_c, the relaxation dispersion data for each concentration of GdnHCl were fitted to Eqn. 6.1 using nonlinear least squares procedure based on Levenberg-Marquardt algorithm. These fits are shown in Figs.6.4-6.11. The denaturant dependence of R_{1b} at 40MHz is shown in Fig.6.12.

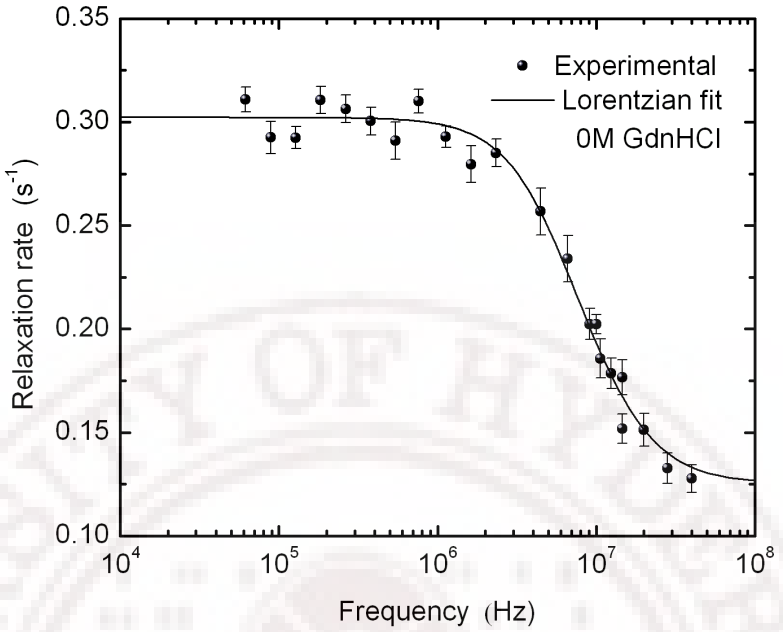

Figure 6.4: PMRD of lysozyme at 0 M concentration of GdnHCl

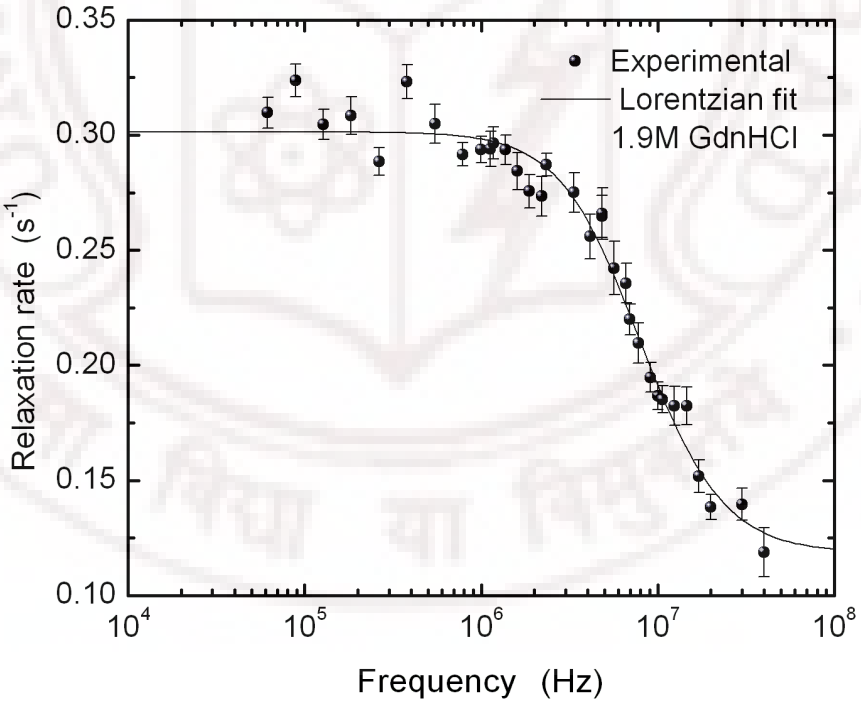

Figure 6.5: PMRD of lysozyme at 1.9 M concentration of GdnHCl.

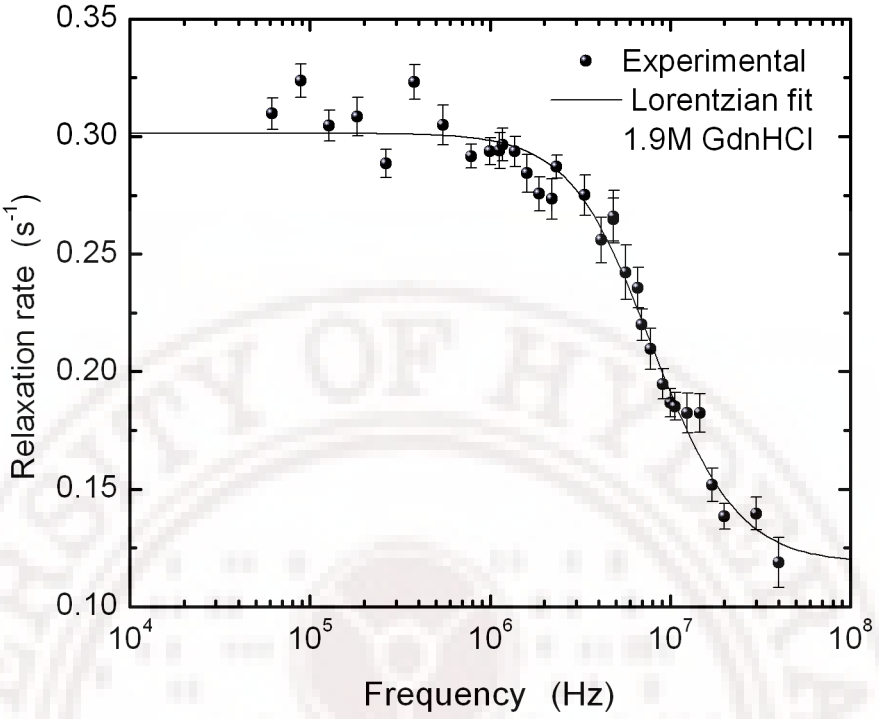

Figure 6.6: PMRD of lysozyme at 2.5 M concentration of GdnHCl.

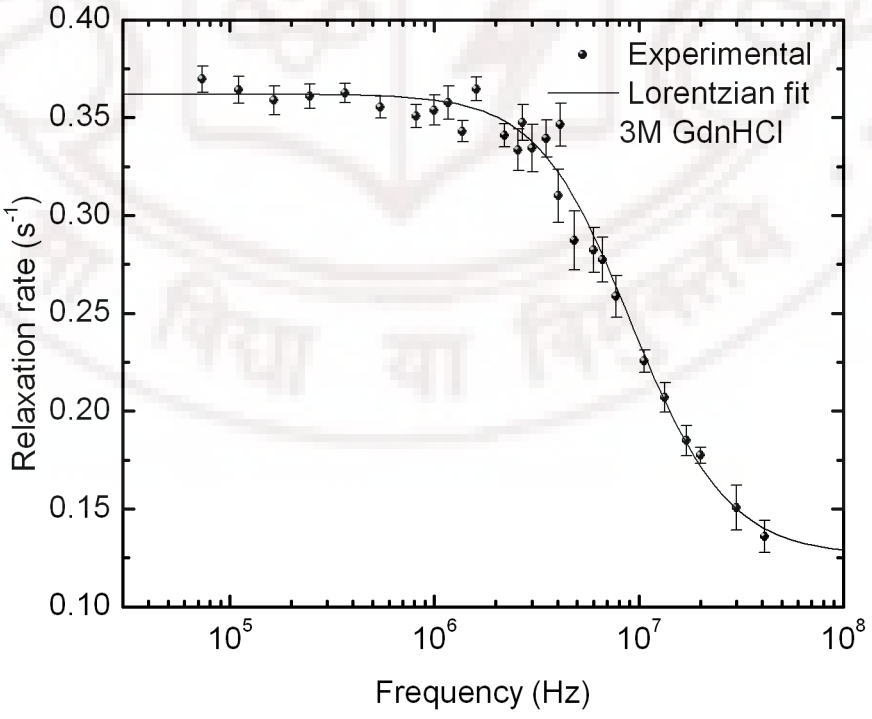

Figure 6.7: PMRD of lysozyme at 3 M concentration of GdnHCl.

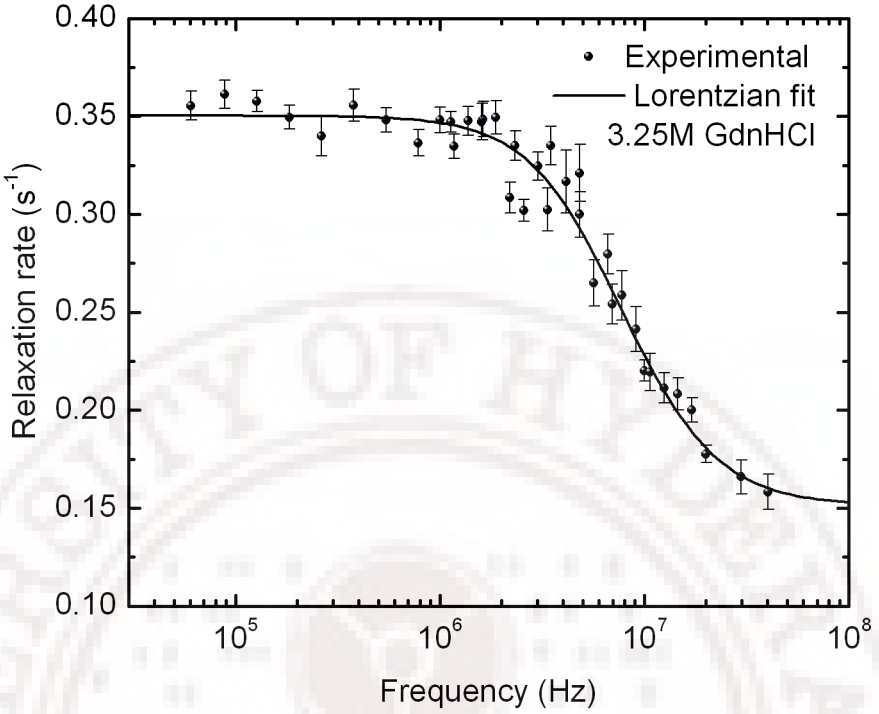

Figure 6.8: PMRD of lysozyme at 3.25 M concentration of GdnHCl.

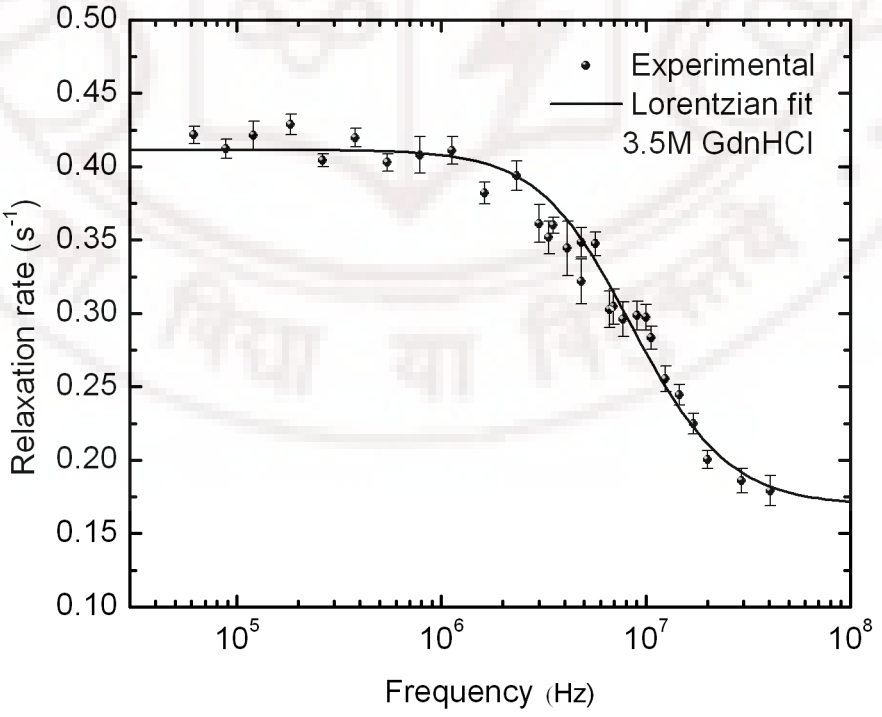

Figure 6.9: PMRD of lysozyme at 3.5 M concentration of GdnHCl.

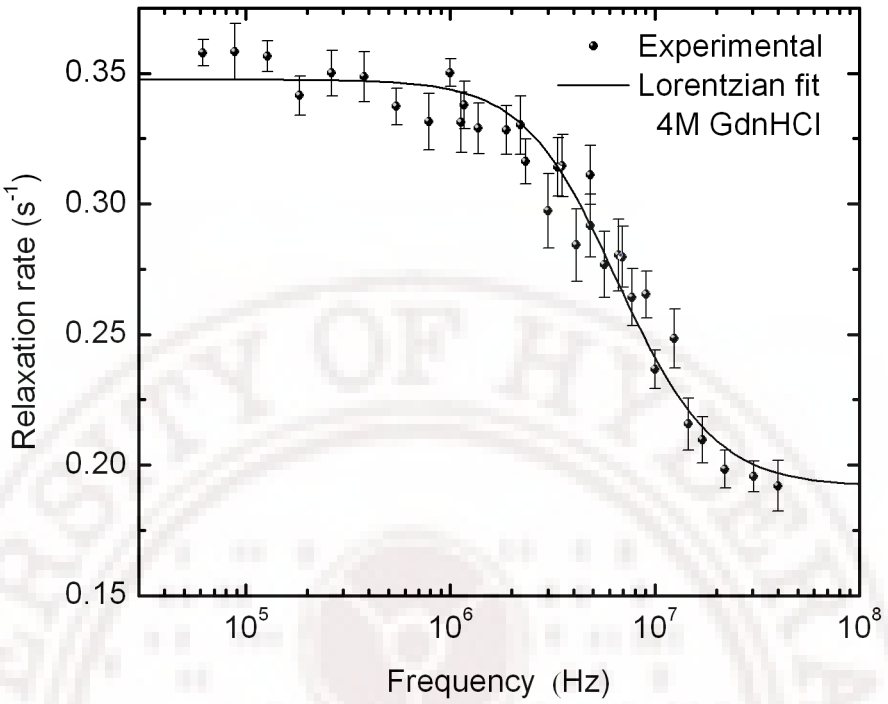

Figure 6.10: PMRD of lysozyme at 4 M concentration of GdnHCl.

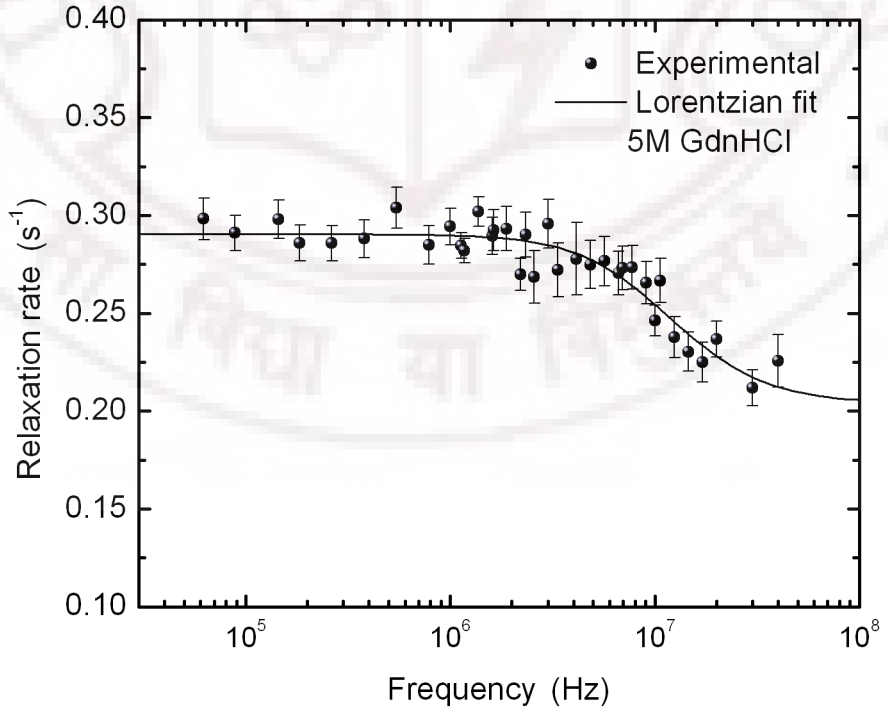

Figure 6.11: PMRD of lysozyme at 5 M concentration of GdnHCl.

The correlation times associated with the dynamics of bulk water and the surface waters (τ_{cb} and τ_{cs}, respectively) are very short resulting in extreme narrowing condition *(Abragam 1961)* for the Larmor frequencies used here (i.e. $\omega\tau_{cb}$ and $\omega\tau_{cs} \ll 1$). Consequently, the corresponding contributions (R_{1b} and α) are proportional to the respective correlation times. The relaxation rates of bulk water in the presence of GdnHCl (Fig.6.12) is subtracted from experimentally determined $R_{1b} + \alpha$. Variation of α with denaturant concentration is plotted in Fig.6.13. Fig.6.13 also shows the variation of α due to change in the viscosity of the solvent with denaturant concentration *(Cantor and Schimmel 1980)*. It is computed assuming that the variation in α is mainly due to the variation in the corresponding correlation time, which in turn is proportional to viscosity. The experimental and calculated distributions are not closely comparable. The experimentally observed α varies initially slower than the expected.

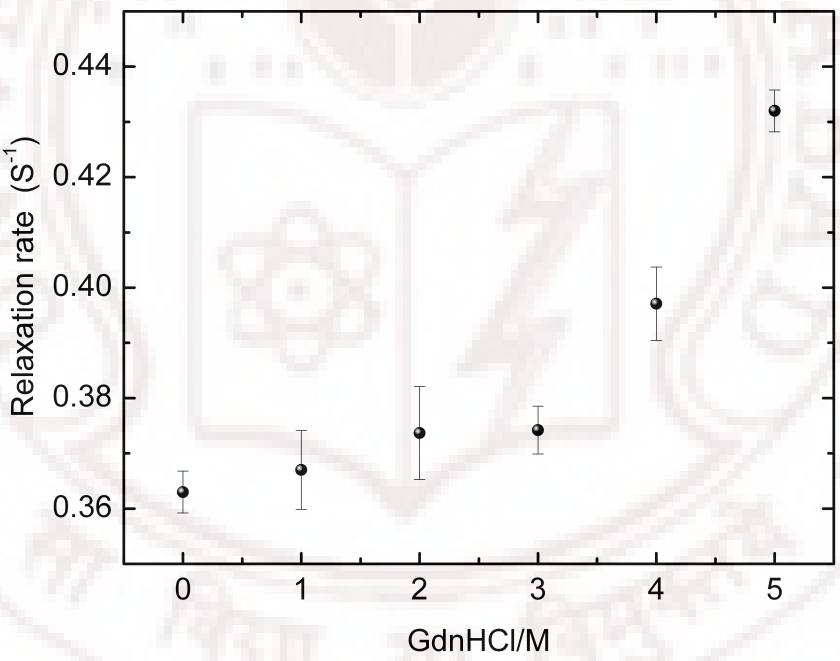

Figure 6.12: Effect of GdnHCl on the ^{1}H longitudinal relaxation rate constant for bulk water (R_b) measured at 40 MHz, 27°C

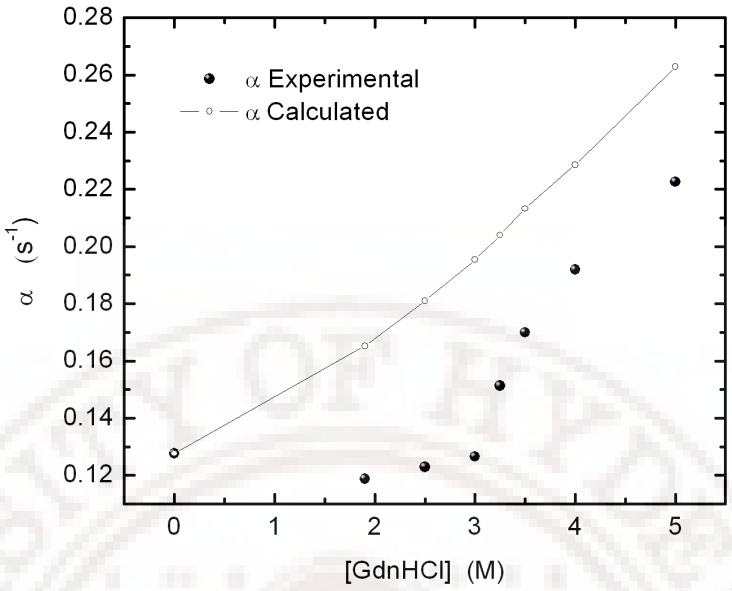

Figure 6.13: GdnHCl dependence of α that represents the contribution of the protein surface waters to the observed relaxation rate constant for the lysozyme-H_2O system

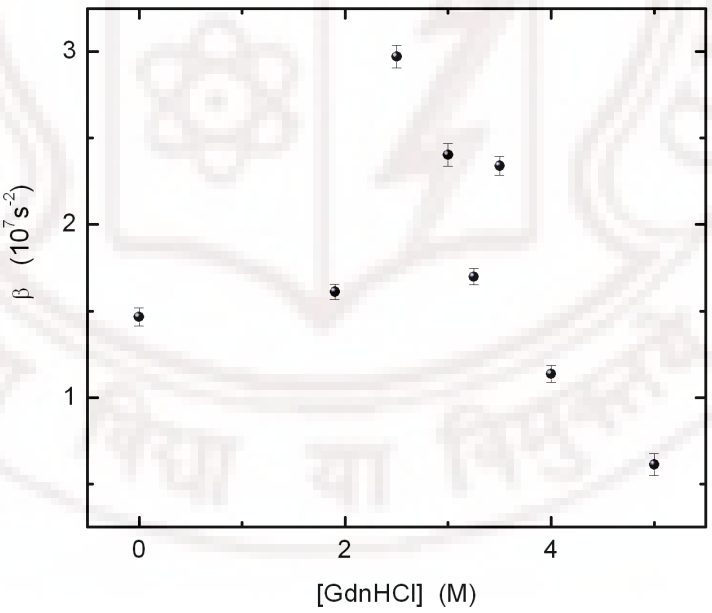

Figure 6.14: Variation of β with increments of GdnHCl concentration in lysozyme

GdnHCl(M)	$R_b+\alpha$ (s^{-1})	β ($10^7 s^{-2}$)	τ_c 10^{-9}s
0	0.4922	1.466 (0.051)	1.1914 (0.044)
1.9	0.4887	1.612 (0.043)	1.1326 (0.034)
2.5	0.4965	2.971 (0.066)	0.832 (0.02)
3	0.5055	2.403 (0.066)	0.98 (0.029)
3.25	0.5328	1.698 (0.047)	1.169 (0.036)
3.5	0.5545	2.34 (0.054)	1.052 (0.028)
4	0.5892	1.136 (0.05)	1.37 (0.066)
5	0.6579	0.612 (0.064)	1.0738 (0.125)

Table 6.1: Parameters extracted by model free analysis of lysozyme dispersions. Dispersion are fit to equation 6.1 using Levenberg Marquart algorithm. Uncertainties in the parameters are enclosed in the parenthesis

Fig. 6.14 shows the variation of β as a function of GdnHCl. The observed trend is little influenced by τ_c because the global correlation time does not change significantly within the concentration range of GdnHCl employed in this study. Interestingly, with increments of the denaturant concentration, β initially increases and then decreases displaying a broad region of inflection centered around 3 M of GdnHCl. The accentuated decrease in the value of β above 3 M denaturant is due to the unfolding effect of the denaturant. Unfolding of the tertiary structure leads to a reduction in the number of long-lived internal waters and hence a gradual loss in the dispersion amplitude *(Modig et al. 2003)*. But the initial rise in the value β in the sub-denaturing to denaturing region is certainly not due to an increase in the number of internal waters. As no major structural changes are expected to occur in the protein at such low concentrations of GdnHCl, neither the f_I's nor ω_D's are expected to vary. Therefore we attribute the observed variation in β to the variation in S_I, implying that S_I increases in the presence of sub-denaturing to denaturing concentrations of the denaturant.

6.3.2 Results on BSA

PMRD data were collected on a series of dilute solutions of BSA. Fig. 6.3 shows three representative profiles for spin-lattice relaxation rate, R_1, as a function of resonance frequency. These dispersions show that with initial increments of GdnHCl the dispersion step increases relative to that observed in the native BSA solution. The dispersion rapidly weakens for increments beyond 0.6 M GdnHCl as it is obvious from rather shallow dispersion step for the sample containing 2.15 M GdnHCl (Fig. 6.3). This qualitative observation is similar to lysozyme and indicates nonlinear effect of GdnHCl concentration on BSA hydration dynamics too. Unlike the case of lysozyme, BSA dispersions however extend over two decades of Larmor frequencies. These dispersions are too large to be considered as simple Lorentzian (Fig. 6.15) spectral density functions, expected from the buried water molecules perturbed by rotational diffusion of nearly spherical non-interacting proteins, while exchanging with the bulk *(Halle et al. 1999)*. Earlier PMRD studies on BSA *(Suzanne and Bryant 2000, Koenig and Brown 1992, Grosch and Noack 1976)* also showed signatures of non-Loretzian dispersions. These stretched dispersions are subject to interpretations with based on an assumed distribution of correlation times *(Halle et al. 1998)*. The plausible causes include: structural heterogeneity induced complex reorientational dynamics, a distribution of proton exchange rates for buried water molecules and labile protein protons, or a distribution of inter-molecular dipole couplings. The structural complexity of protein thus makes the analysis non-trivial.

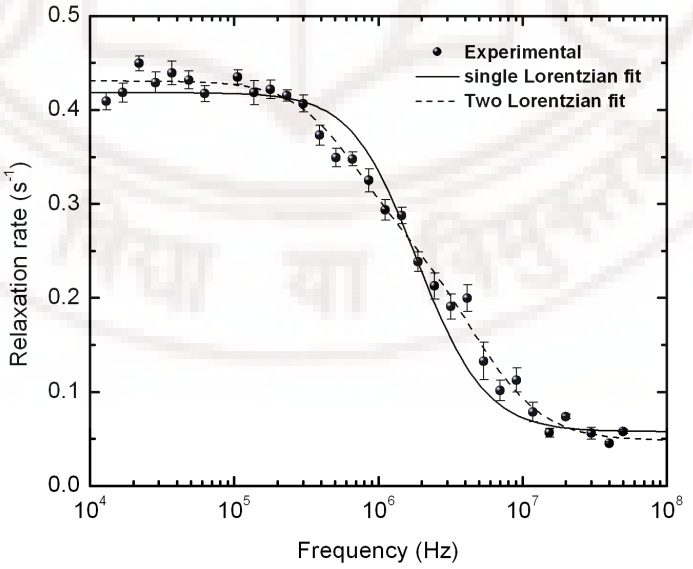

Figure 6.15: Comparision of single and multi Lorentizian fits of BSA ^{1}H dispersions at 0 M concentration GdnHCl

However it was emphasized that model-free approach for analyzing such stretched dispersion profiles could yield parameters with well-defined physical significance *(Halle et al. 1998)*. This technique was then demonstrated to analyze stretched dispersions of BPTI to explain the salt effect. Based on these arguments we analyzed the data using a model-free approach method. BSA dispersions were fitted to a multi Lorentzian equation, which is further explained below.

$$T_1^{-1} = R_b + \alpha + \sum_N \beta_N \tau_{cN} \left[\frac{0.2}{1 + (\omega\tau_{cN})^2} + \frac{0.8}{1 + (2\omega\tau_{cN})^2} \right]. \tag{6.3}$$

Here R_b, α, and β have meanings as described earlier in the analysis of lysozyme data (Eqn. 6.1). N stands for the number of Lorentzians considered. The number of Lorentzians to be included can be objectively determined by means of the F-test *(Press et al. 1992)*. Starting with N =1 and successively adding terms until the probability P(N+1)<P_0, (probability cutoff P_0 is taken as 0.8), a well defined N-Lorentzian representation of the experimental data can be achieved. To obtain the parameters $R_{1b} + \alpha$, β_N and τ_{cN} the relaxation data for each concentration of GdnHCl were fitted to equation 6.3 using nonlinear least squares procedure based on Levenberg-Marquardt algorithm *(Press et al. 1992)*. Table 6.2 shows the robustness of the analysis, and the fits through the dispersion data are shown in Fig. 6.16-6.24. Parameters obtained are shown in Table 6.3.

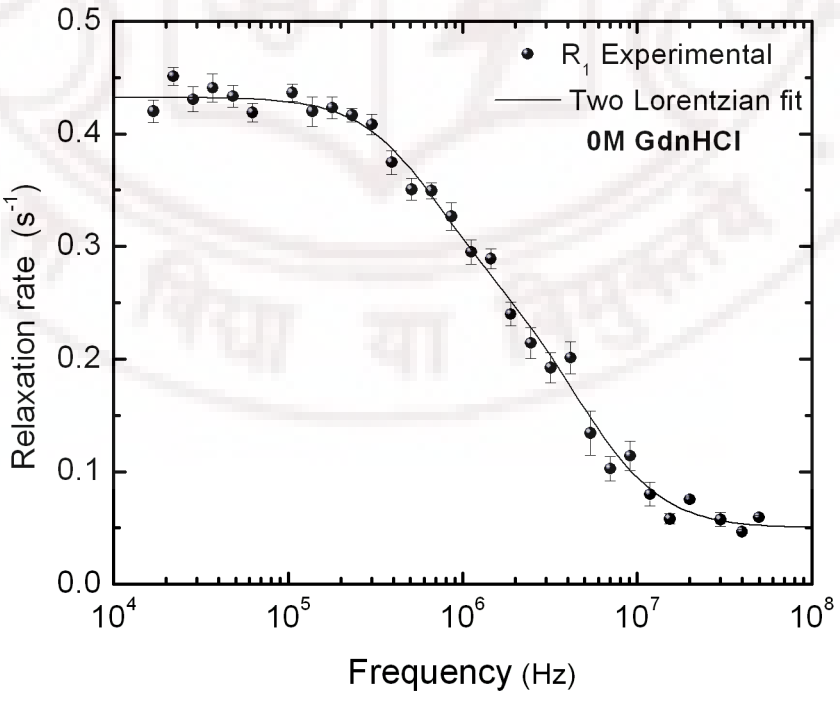

Figure 6.16: PMRD of BSA at 0 M concentration of GdnHCl

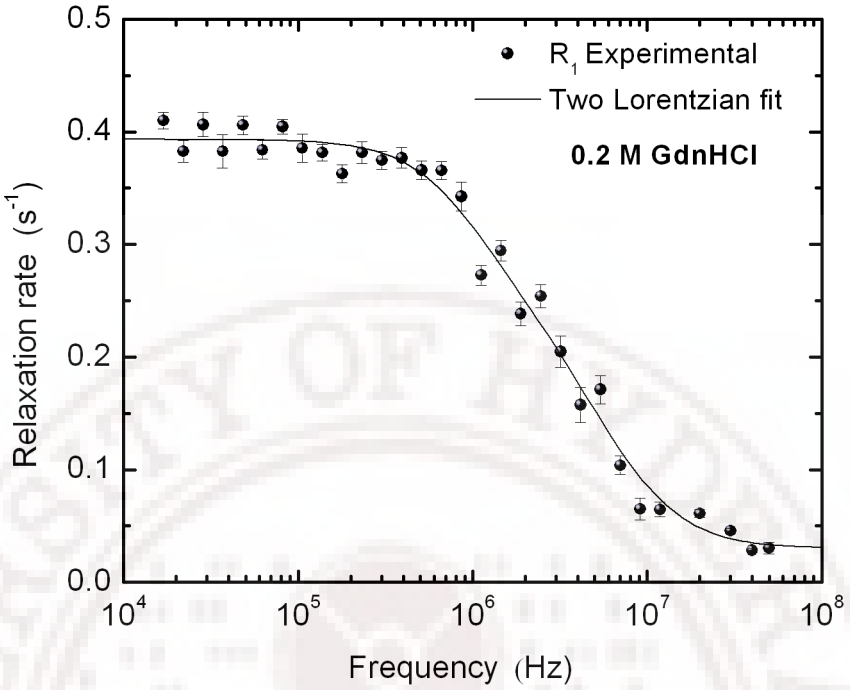

Figure 6.17: PMRD of BSA at 0.2 M concentration of GdnHCl.

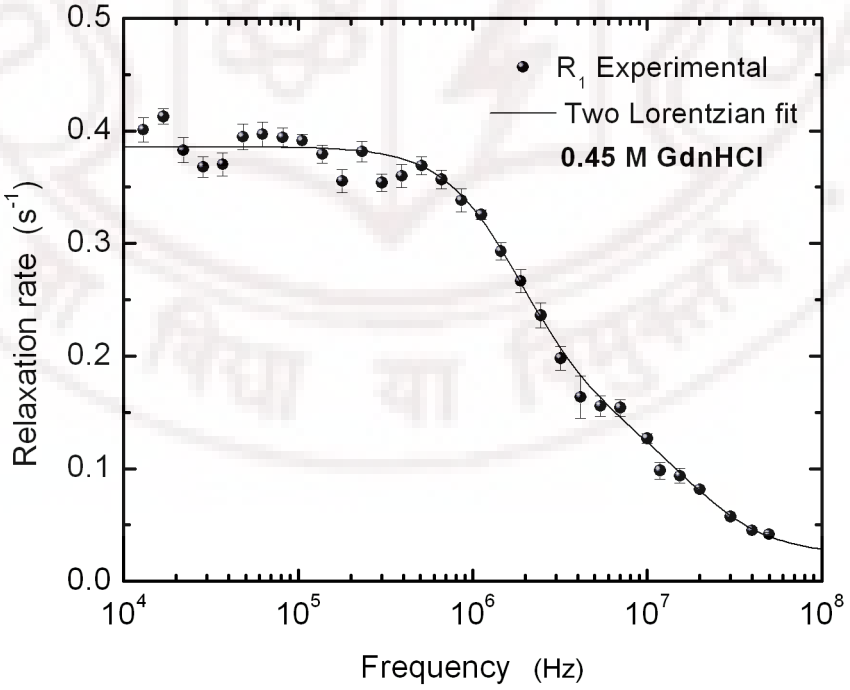

Figure 6.18: PMRD of BSA at 0.45 M concentration of GdnHCl.

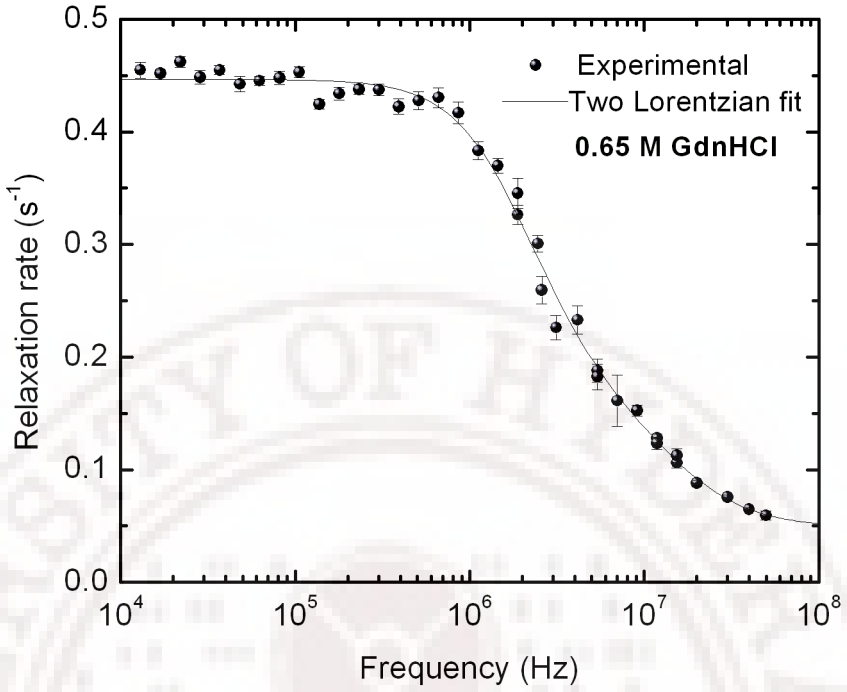

Figure 6.19: PMRD of BSA at 0.65 M concentration of GdnHCl.

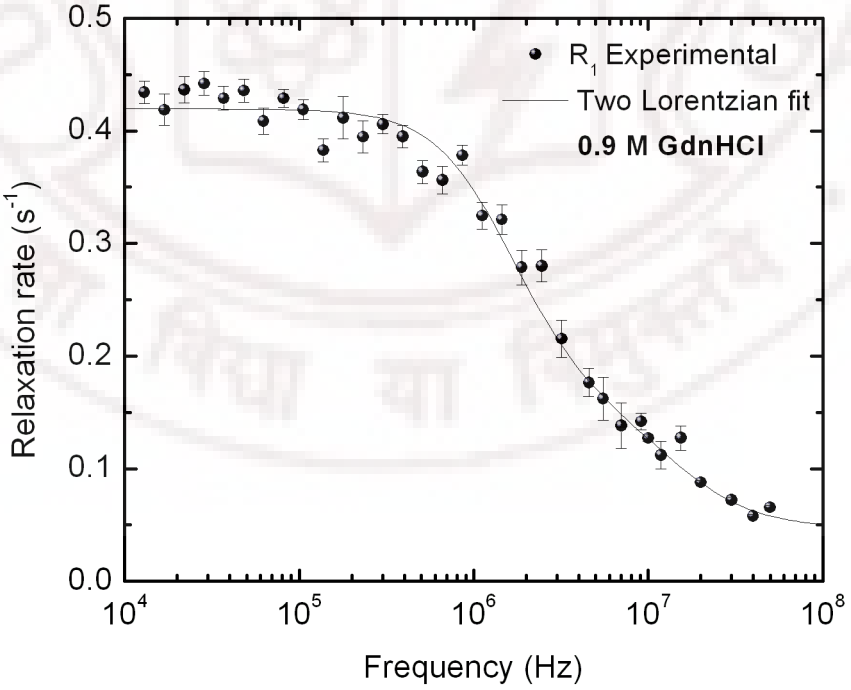

Figure 6.20: PMRD of BSA at 0.9 M concentration of GdnHCl.

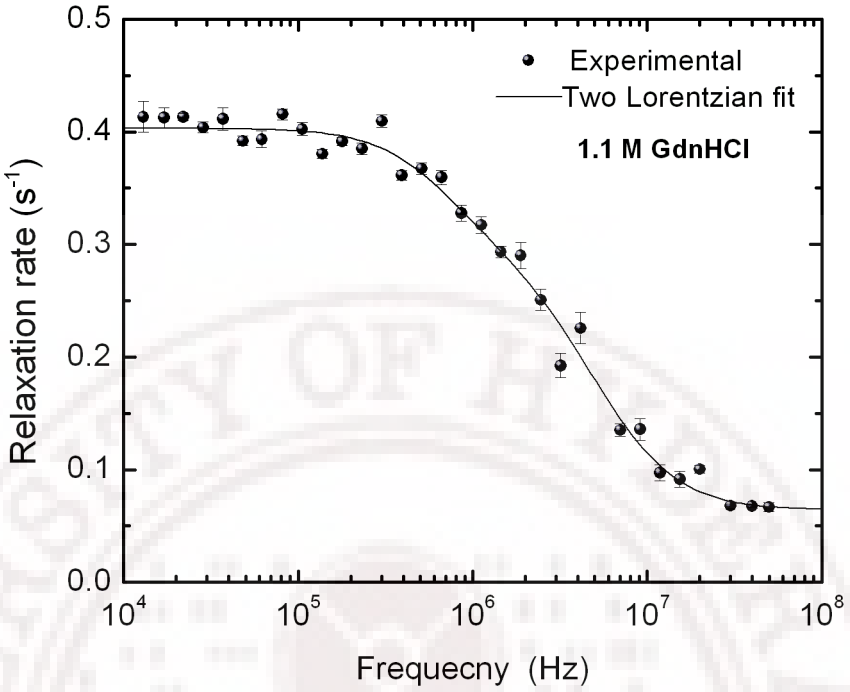

Figure 6.21: PMRD of BSA at 1.1 M concentration of GdnHCl.

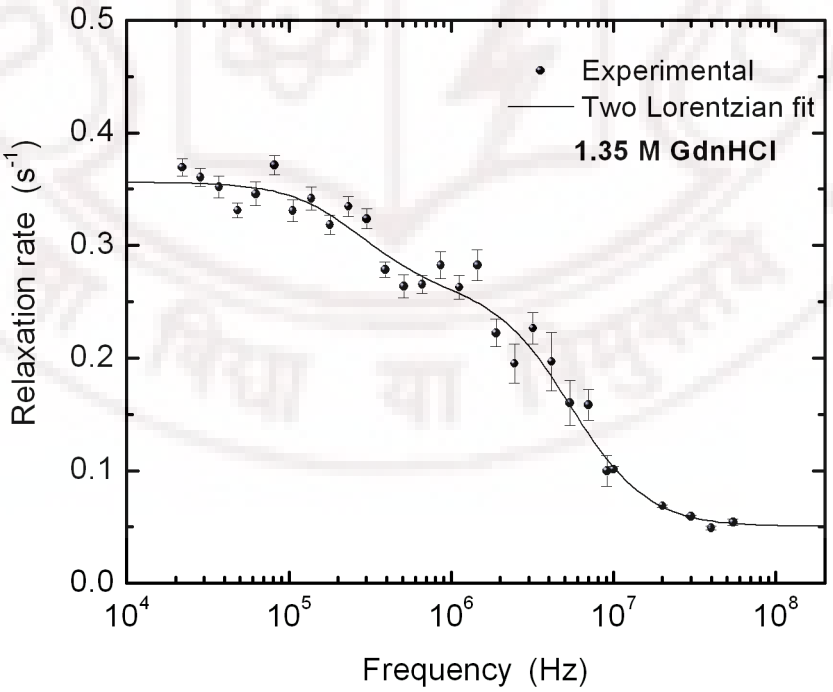

Figure 6.22: PMRD of BSA at 1.35 M concentration of GdnHCl.

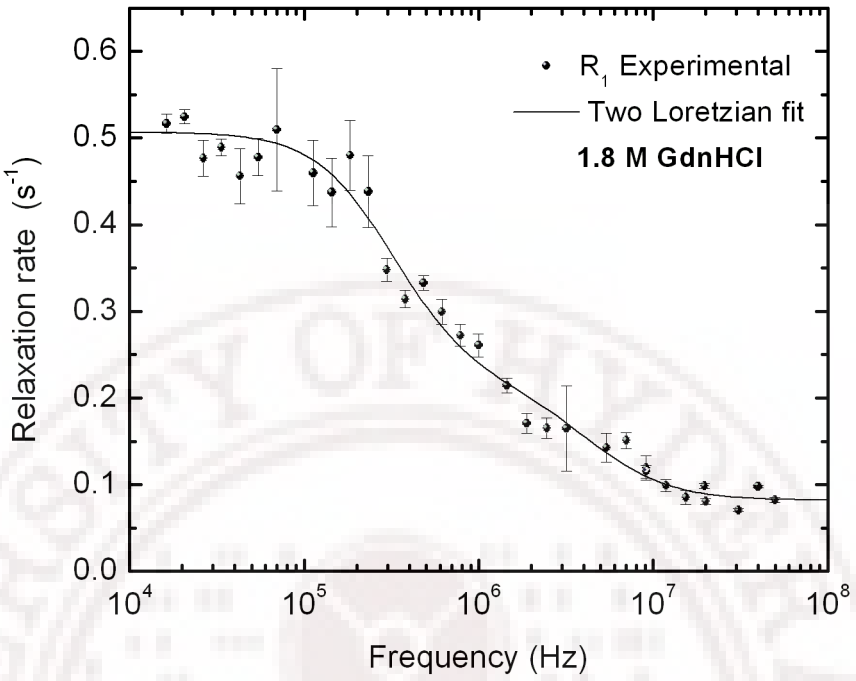

Figure 6.23: PMRD of BSA at 1.8 M concentration of GdnHCl.

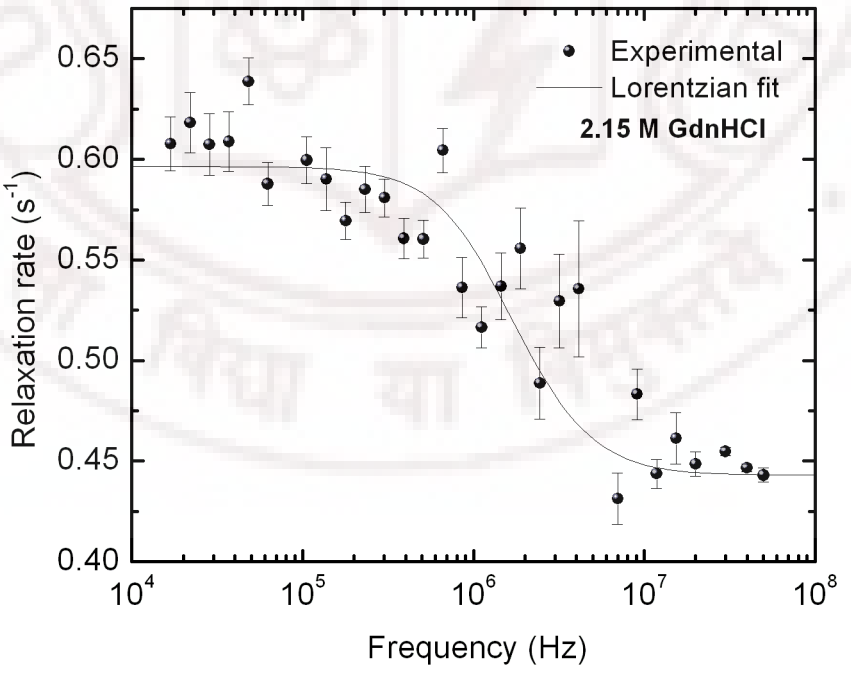

Figure 6.24: PMRD of BSA at 2.15 M concentration of GdnHCl.

Using the parameters obtained from multi-Lorentzian fit the dispersion amplitude

β and the average correlation time $< \tau_c >$ are calculated using

$$\beta = \sum_N \beta_N \qquad \text{and} \qquad \langle \tau_c \rangle = \frac{\sum\limits_N \beta_N \tau_N}{\sum\limits_N \beta_N} \tag{6.4}$$

GdnHCl\M	N	F	P
0	2	2.0954	0.9577
	3	0.9957	0.4557
0.2	2	1.5376	0.8111
	3	1.1265	0.5749
0.45	2	6.3472	1.0
	3	0.9426	0.3637
0.65	2	2.8302	0.9968
	3	0.9641	0.3886
0.9	2	2.6497	0.9909
	3	0.9380	0.3593
1.1	2	1.6733	0.8689
	3	1.0689	0.4847
1.35	2	3.0832	0.9940
	3	0.9692	0.3872
1.8	2	1.3999	0.7542
	3	0.9615	0.4212
2.15	2	1.1626	0.5804

Table 6.2: Robustness of analysis (F-test to fix the number of lorentzian terms to fit BSA proton spin-lattice relaxation dispersions)

From the (R_{1b}+α) values extracted by the nonlinear curve fitting process R_{1b}, the contribution coming form bulk water in the presence of denaturnat is subtracted, as it was done in case of lysozyme, and α values are thus extracted. Fig. 6.25 shows variation of α with denaturant concentration. α decreases initially up to 0.45 M GdnHCl concentrations. Since α depends on the fraction of surface waters (f_s), a possible explanation for this slower variation in α could be the reduction in the number of surface water molecules as the protein is taken through incrementally sub-denaturing conditions. This implies that at such lower concentrations, GdnHCl binding leads to the displacement of some surface waters, suggesting that the initial binding sites for the denaturant are the hydrophilic regions of the protein surface. As strongly denaturing conditions are approached in the presence of higher concentrations of GdnHCl (>3 M) the value of α increases as expected.

GdnHCl M	α s^{-1}	β_1 $10^7 s^{-2}$	β_2 $10^7 s^{-2}$	τ_{c1} $10^{-9} s$	τ_{c2} $10^{-9} s$	β $10^7 s^{-2}$	τ_c $10^{-9} s$
0	0.4129 (0.002)	0.14 (0.03)	1.12 (0.07)	128.8 (15.6)	18.3 (1.9)	1.26 (0.1)	30.38 (2.54)
0.2	0.395 (0.002)	0.21 (0.07)	1.27 (0.08)	79.03 (13.6)	15.67 (2.14)	1.48 (0.15)	24.55 (1.56)
0.45	0.389 (0.003)	0.52 (0.04)	2.36 (0.18)	46.84 (2.47)	4.997 (0.53)	2.88 (0.22)	12.57 (0.77)
0.65	0.415 (0.004)	0.75 (0.08)	1.72 (0.16)	39.25 (2.22)	6.033 (1.08)	2.47 (0.24)	16.11 (0.76)
0.9	0.414 (0.003)	0.75 (0.05)	1.68 (0.12)	53.1 (3.842)	6.1 (0.84)	2.18 (0.17)	17.02 (0.703)
1.1	.4308 (0.002)	0.11 (0.02)	1.25 (0.06)	114.9 (13.8)	17.34 (1.406)	1.35 (0.08)	25.05 (3.3)
1.35	0.418 (0.001)	0.03 (0.01)	1.28 (0.05)	318.75 (49.42)	16.31 (0.76)	1.31 (0.06)	23.32 (0.84)
1.8	0.4515 (0.001)	0.11 (0.01)	0.64 (0.06)	271.97 (20.3)	20.61 (2.78)	0.75 (0.07)	56.944 (12.6)
2.15	0.454 (0.001)	0.218 (0.02)	—	67.98 (6.67)	—	0.2 (0.02)	67.98 (6.67)

Table 6.3: Parameters extracted by model free analysis of BSA dispersions. Dispersion are fitted to Eqn. 6.3 using Levenberg Marquart algorithm. Uncertainties in the parameters are enclosed in the parathesis

Fig. 6.26 shows the variation of β as a function of GdnHCl concentration. Interestingly, with increments of the denaturant concentration β initially increases and then decreases above 0.45 M GdnHCl. The decrease in the value of β above 0.45 M GdnHCl is due to the unfolding effect of the denaturant. These features are quite similar to the observations made in the case of lysozyme. In the light of these observations, we believe that this result is perhaps general, and applicable to globular proteins. These results suggest that in such proteins, initial increments in denaturant concentrations lead to initial increase in the ordering of the internal water, and hence a relatively more stable tertiary structure. Therefore we generalize this variation of β to all globular proteins in which S_I increases in presence of sub-denaturing concentrations of the denaturant resulting in increase of β.

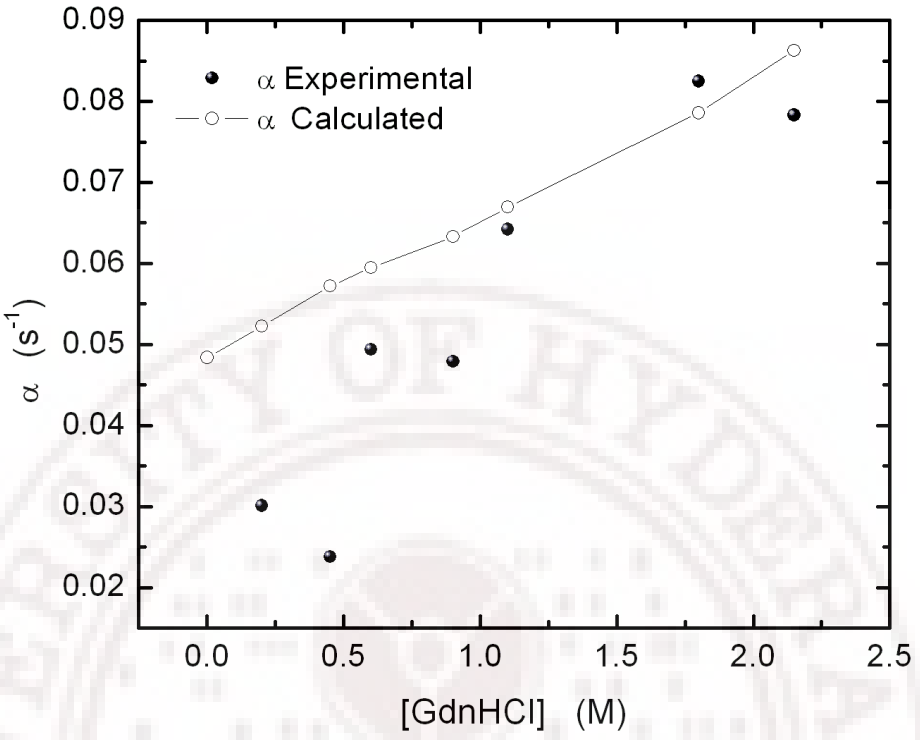

Figure 6.25: Variation of $R_b + \alpha$ with increments of GdnHCl for BSA

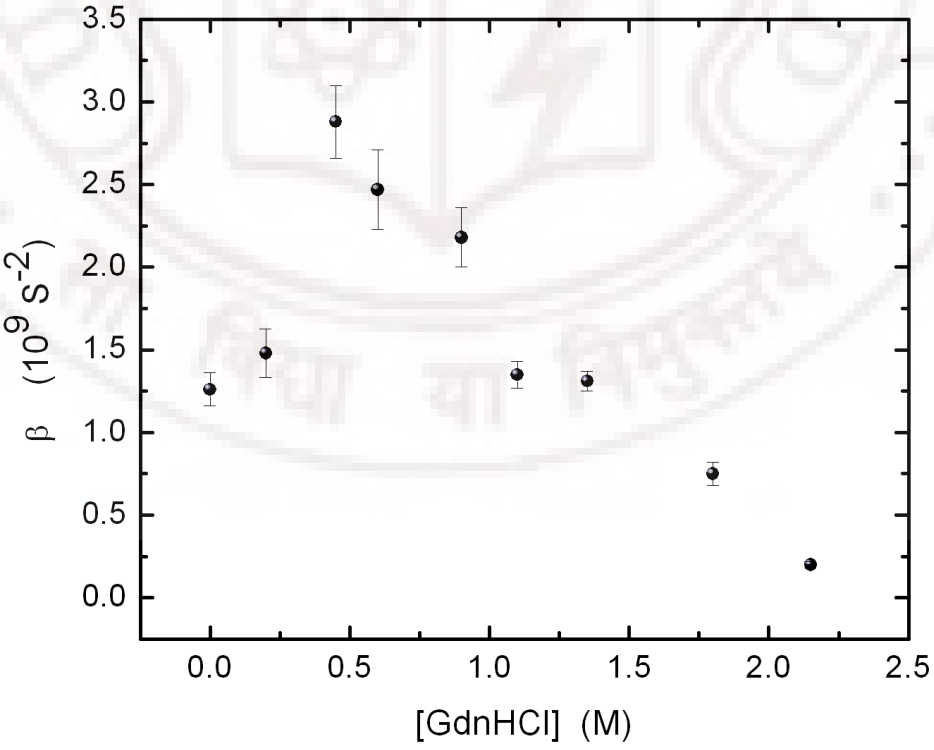

Figure 6.26: Variation of β with increments of GdnHCl for BSA

The two correlation times τ_{c1} and τ_{c2} (Table 6.3) obtained from multi-Lorentzian fits seem to indicate, as the aggregation is not expected at such low concentrations of the protein, that there are two dynamically distinguishable classes of water molecules associated with the protein molecule, giving the stretched dispersion. Obviously one class of water is the well-known buried internal water molecules whose residence times (τ_w) are much longer than the protein rotational correlation time (τ_r). These waters are perturbed by the tumbling motion of protein while exchanging with bulk water. The resultant correlation time τ_c is nearly the same as τ_r as $\tau_r \ll \tau_w$ *(Halle et al. 1999)*. If the other class of water, that is carrying the type of dispersion observed, exists, then it should be sufficiently long lived to give a dispersion but with resident times smaller than τ_r, probably trapped at the surface pockets or large binding cavities *(Modig et al. 2003)* of the protein. The resulting correlation time from these waters is less than the protein rotational correlation times. We could expect this to be the mechanism for the observed second correlation time, $\tau_{c2} < \tau_{c1}$ (Table 6.3). However, inadequate details of complex surface structure and protein-protein interactions leave the problem somewhat in ambiguity. So we considered the average correlation time calculated using model-free method of analysis to explain the observed PMRD dispersions.

Fig. 6.27 shows the variation of $\langle\tau_c\rangle$ with the denaturant concentration. As the GdnHCl concentration increases $\langle\tau_c\rangle$ initially decreases up to 0.45 M and increases abruptly with the increase in the denaturant concentration. Since rotational correlation time of the protein τ_r is generally much shorter than the residence times of the internal water molecules that contribute to the dispersion, the effective correlation time τ_c can be compared with τ_R, and is given by Stokes-Einstein relation as (Halle et al. 1999)

$$\tau_c \approx \tau_R = \frac{\eta V}{k_B T} \tag{6.5}$$

where η is viscosity of the solvent; V is hydrodynamic volume of the protein. k_B is Boltzman's constant and T is the absolute temperature. Viscosity of solvent increases with the denaturant concentration, which in turn slows down the protein tumbling motion. So $\langle\tau_c\rangle$ is expected to increase as GdnHCl concentration is incremented. It is clear from the data that the variations of $\langle\tau_c\rangle$ is in the sub-denaturing conditions is contrary to these expectations based on viscosity considerations. One plausible reason for this could be the shrinkage in the volume of the protein molecule in this concentration regime.

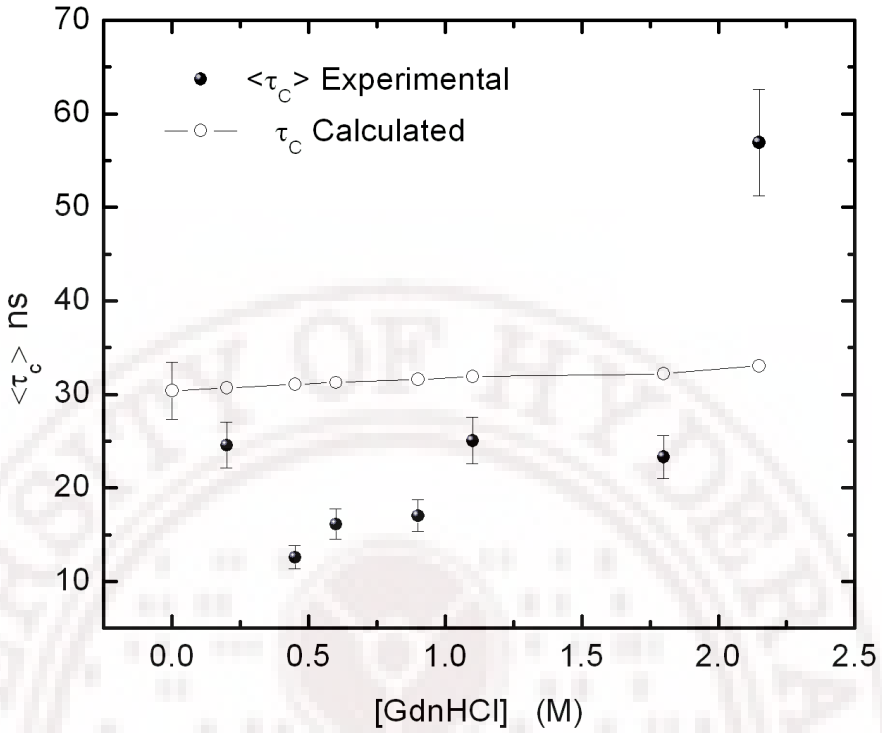

Figure 6.27: Variation of $R_b + \alpha$ with increments of GdnHCl for BSA

6.4 Equilibrium Unfolding of Lysozyme and BSA

To relate the observed variation in the value of β and τ_c to the structure and dynamics of the proteins, we measured their GdnHCl-induced equilibrium unfolding transitions by fluorescence. Fig. 6.28 and 6.29 show the unfolding transitions in both the proteins, respectively. In the primary data, the pretransition region for both proteins is marked by some positive slope. To compare transitions observed from equilibrium unfolding data with PMRD results, β is scaled appropriately in the figures shown. The feature observed here for BSA is consistent with the reported data earlier *(Elkadi et al. 2006)*.

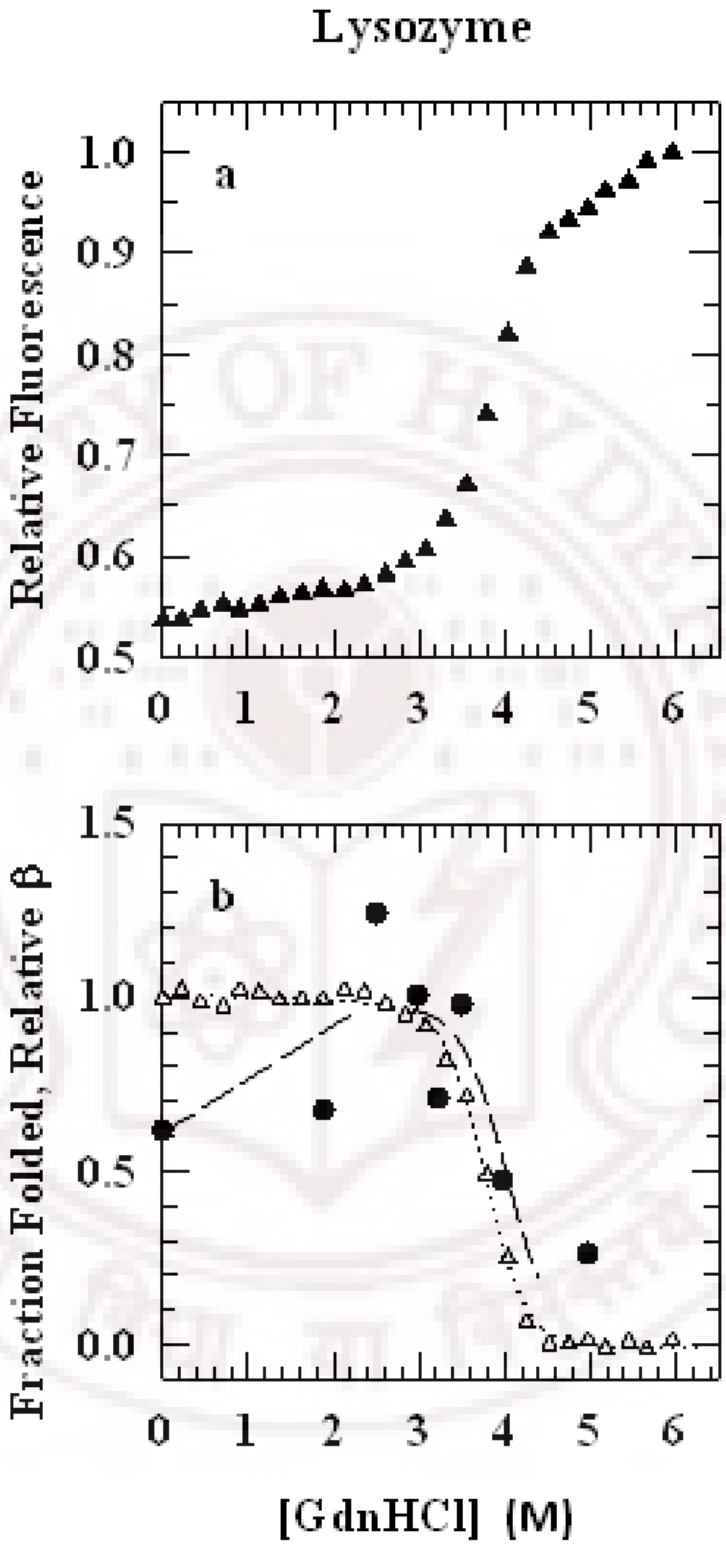

Figure 6.28: GdnHCl-induced equilibrium unfolding of lysozyme. The unfolding data normalized as fraction folded is compared with the variation of β. The continuous lines through the data represent least-squares fits using a two-state model according to equation 6.6

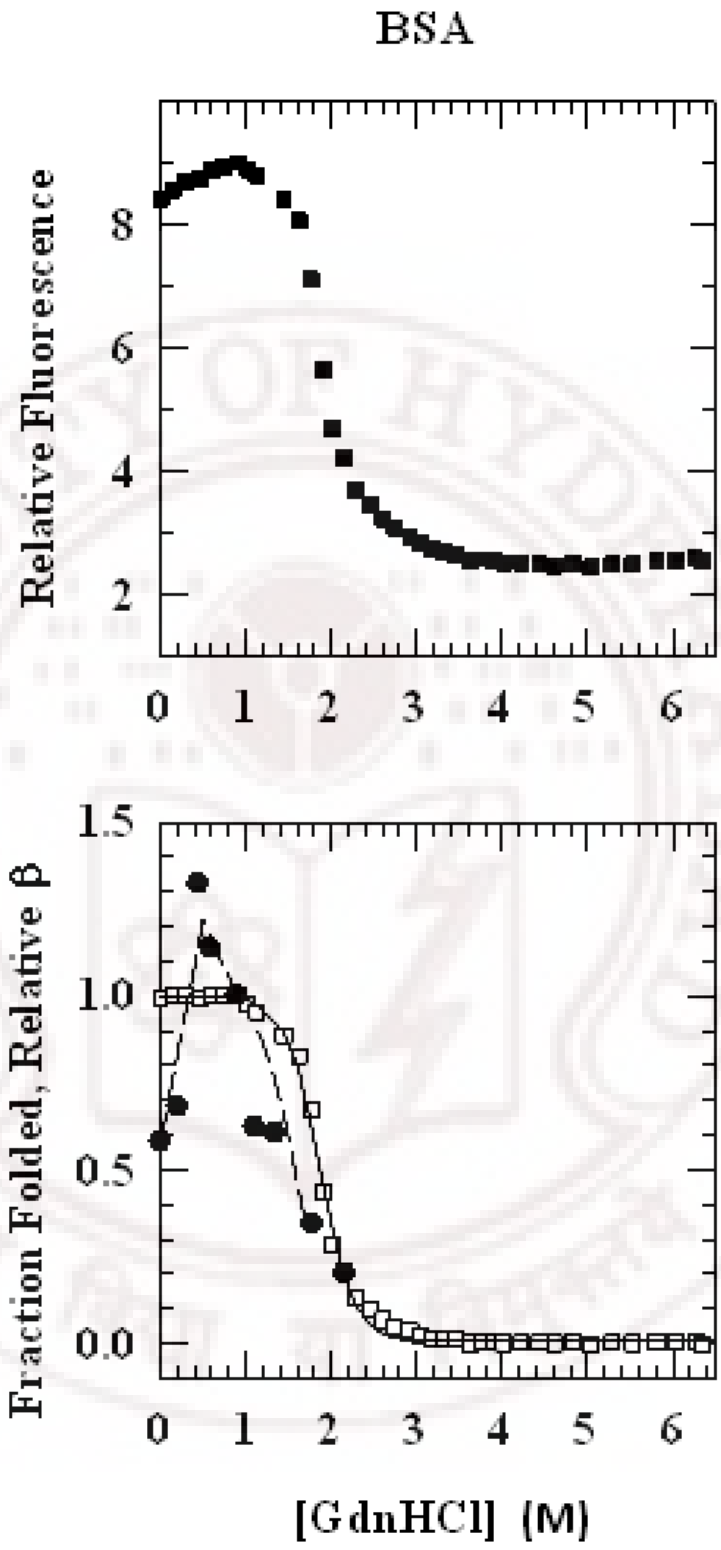

Figure 6.29: GdnHCl-induced equilibrium unfolding of BSA. The unfolding data normalized as fraction folded is compared with the variation of β. The continuous lines through the data represent least-squares fits using a two-state model according to equation 6.6

For the present purpose, we calculated the fraction folded for each protein, and

fitted the data to the two-state equation:

$$S_{obs} = \frac{(\mathrm{c}_f + \mathrm{m}_f[D]) + (\mathrm{c}_u + \mathrm{m}_u[D])\exp(\frac{-\Delta \mathrm{G}D^o + \mathrm{m}_g[D]}{\mathrm{RT}})}{1 + \exp(\frac{-\Delta \mathrm{G}D^o + \mathrm{m}_g[D]}{\mathrm{RT}})} \tag{6.6}$$

where S_{obs} is the observed emission signal, c_f and c_u, and m_f and m_u represent intercepts and slopes of native and unfolded baselines, respectively, ΔG_D is the free energy of unfolding, [D] is the denaturant concentration, and m_g represents the change in surface area during global unfolding of the protein. in principle, a two-state analysis, especially for BSA, may be a matter of subjective interpretation, but the purpose here is to map the observed features of β and τ_c onto the equilibrium melting transition and it is in this spirit that this analysis was attempted. All parameters were floated during fitting. The data show large-scale global transition setting in beyond $\sim$3 M GdnHCl for lysozyme and $\sim$1.5 M GdnHCl for BSA. This is consistent with the drop in β values at denaturant concentrations >3M for lysozyme and >1 M for BSA (Fig. 6.28 and 6.29). Fluorescence-monitored equilibrium data alone do not reveal any considerable alteration in the structure and dynamics of protein in the sub-denaturing to denaturing baseline region. However the increase of β in the pre-transition region appears to arise from changes in the orientational order parameter, S_I.

6.5 Discussion

To elucidate hydration dynamics in denaturant-induced protein unfolding, this study presents results of the variation of ^{1}H relaxation dispersion of lysozyme and BSA solutions containing GdnHCl in the 0-5 M and 0-2.15 M range, respectively. The three major results are:

- A slow variation in case of lysozyme, and a sudden fall in case of BSA, of the parameter α in the sub-denaturing limit, implying reduced contribution of the surface water molecules to the observed relaxation in the presence of lower concentrations of the denaturant.

- A distinctly biphasic variation of the dispersion amplitude β, apparent by an initial rise in the sub-denaturing limit (0-3 M GdnHCl for lysozyme and 0-0.45 M for BSA), followed by a sharp drop as unfolding conditions are approached.

- An apparent drop in the value of the effective correlation time (or the rotational correlation time) of the protein τ_r in the sub-denaturing limit, followed by its recovery and subsequent rise at higher concentrations of the denaturant.

The thermodynamic stability and the motional properties of the protein, as reflected in the characteristic variation of α, β and τ_c, under sub-denaturing to mild denaturing conditions is the central theme of the following discussion.

It is known that denaturants exert pronounced effect on the structure of water, and hence on the surface hydration of proteins *(Timasheff 1992, Breslow and Guo 1990)*. Water relaxation would be slower (lower α) when the protein is stripped off the surface waters, and the occupation of these sites by the ionic denaturant in its sub-denaturing limit is expected to perturb the surface electrostatics. In solution, GdnHCl exists as $GdnH^+$ cation and Cl^- anion, and both ion types can interact electrostatically with the surface ion binding sites, through Debye-Hückel charge-screening mechanism, for example. The resulting electrostatic interactions, either ion-pair type or charge-screening type, are known to stabilize proteins *(Pace and Grimsley 1988, Mayr and Schmid 1993)*. The stabilization of the acid molten globule state of cytochrome c at low concentrations of GdnHCl, due to the binding of Cl^- to the cationic sites *(Goto et al. 1990, Hagihara et al. 1983)*, provides a classic example. This protein stabilizing effect of GdnHCl is operative so long as the denaturant concentration is insufficient to exert its unfolding action. When the concentration of the denaturant is increased beyond the sub-denaturing limit, the stabilizing effect is overwhelmed by its own chaotropic effect.

We note that the NMR relaxation data provided here probe specifically into the displacement of surface waters by the denaturant. However, it should not be construed that the initial action of GdnHCl on proteins is through surface waters alone. Indeed, no particular type of amino acid or binding site appears to be a preferential target for denaturant binding *(Dunbar et al. 1997)*. The electrostatic influence of GdnHCl is felt by the buried, (or interior groups) as well, and all stabilizing interactions contribute to the thermodynamic equilibrium state of the protein.

Frequency dependent dispersion of ^1H relaxation in aqueous protein solution is known to arise from the buried water molecules in the protein interior and labile hydrogens *(Denisov and Halle 1996)*. All the dipolar interaction terms, intra and inter-molecular couplings between the water protons and the inter-molecular coupling between the water and protein protons that contribute to the longitudinal relaxation, are modulated by the reorientational motions of the protein molecules. Since sub-denaturing concentrations of GdnHCl are not expected to alter the native structure of the protein significantly, as was shown for lysozyme-urea solutions *(Lumb and Dobson 1992, Pike and Acharya 1994)*, the reorientational correlation time associated with global tumbling of the protein is not expected to vary substantially due

to the presence of denaturant in low doses. Then the increase in the dispersion amplitude in the presence of lower concentrations of the denaturant is naturally expected to originate largely from changes in the dynamics of the internal waters. These processes, considered under the generalized order parameter S_I, include reorientational motions of the water molecules that are fast relative to the isotropic global tumbling of the protein.

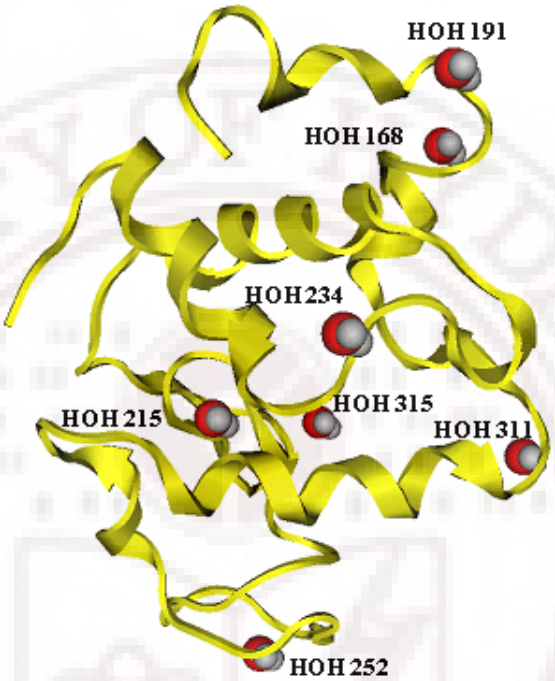

Figure 6.30: Ribbon diagram of lysozyme showing the crystallographically defined buried waters. In the presence of sub-denaturing amounts of denaturant, the water, HOH 191, interacts directly with denaturant.

Although the mode of action of denaturants on proteins is still unclear there is considerable evidence for direct protein-denaturant interactions *(Robinson and Jencks 1965, Makhatadze and Privalov 1992)*. An earlier crystallographic study of α-chymotrypsin crystals soaked in lower concentrations of urea and GdnHCl indicated direct interactions of $GdnH^+$ ions and urea with protein groups *(Hibbard and Tulisky 1978)*. Crystal structures of lysozyme with urea *(Pike and Acharya 1994)*, and ribonuclease A with GdnHCl, and dihydrofolate reductase with urea *(Dunbar et al. 1997)* also showed denaturant binding to proteins mediated by multiple hydrogen bonding and van der Waals interactions. The change in the solvent structure after the addition of denaturants is rather small *(Dunbar et al. 1997)*. However, lysozyme structures with sub-denaturing amount of urea clearly show one of the seven internal waters, HOH 191 (Fig. 6.30), directly interacting with a urea molecule, urea 256, through a pair of hydrogen bonds *(Pike and Acharya 1994)*. Involvement of internal water molecules in the interaction of GdnHCl (1.2 M) with lysozyme was not noticed

though *(Mande and Sobhia 2000)*. In spite of this, the influence of $GdnH^+$ ions on the cavity waters cannot be ruled out. Even if the denaturants do not engage the internal water molecules directly, polyfunctional interactions between denaturants and the protein can affect the waters through indirect modes, through a decrease in the volumes of internal cavities. An immediate consequence of denaturant binding is a decrease in the motional freedom of all components that are bonded into. As a result, fluctuations in the positions of individual, or cluster of, atom(s) around their average are attenuated. Evidence for this conjecture comes from a significant decrease in the crystallographic B-factor of side-chain and backbone atoms of proteins, including lysozyme, in the presence of lower concentrations of denaturants *(Pike and Acharya 1994, Dunbar et al. 1997)*. Lower dynamic mobility favours greater stability in the sub-denaturing limit. In such a "stiffened state of the protein "the libration dynamics of the buried waters are also affected. It follows that sub-denaturing amounts of denaturants have the potential to bring about a "disorder-to-order" transition of the internal waters, an entropy expensive process. Libration amplitudes of cavity waters were described within the formalism of the anisotropic harmonic libration (AHL) model *(Halle et al. 1999, Denisov et al. 1997)*. For ^{1}H, the generalized order parameter, S_I, if affected by rocking and twisting motions of the water *(Halle et al. 1999)*. We are thus led to conclude that in the presence of lower concentrations of GdnHCl it is the higher S_I for one or more cavity waters that dominates, and consequently the value of β increases (Figs 6.14 and 6.26). Under strongly unfolding conditions, achieved with further increments in GdnHCl, the structure-ordering effect of the denaturant is overwhelmed by its own structure-unfolding effect. The consequent disappearance of water cavities is reflected in the sharp drop in β (Fig. 6.14 and 6.26).

6.6 Conclusions

Stoichiometric binding theory for direct protein-denaturant interaction affords a satisfactory interpretation of protein unfolding transitions *(Schellman 1978, Schellman 1987)*. However, the effect of lower concentrations of denaturants on structural, dynamic, and thermodynamic properties of proteins has not received as much attention. The present work reveals the modulation of surface hydration, and the dynamical constraints imposed by GdnHCl on the buried waters of lysozyme and BSA. These binding-mediated effects appear general for all proteins. For example, energetic stabilization by denaturant binding was demonstrated for RNAse T_1 *(Mayr and Schmid 1993)*, protein disulfide isomerase *(Morjana et al. 1993)*, and cytochrome c *(Bhuyan 2002, Kumar and Bhuyan 2004)*. These effects often escape detection be-

cause either the change in the magnitude of the property measured is small or the sensitivity of the measuring probe is inadequate. The dispersion amplitude of ^{1}H relaxation in protein solutions is sensitive enough to detect the denaturant-induced constraints on the internal dynamics.

Similar trend in the variation of β, as shown here for lysozyme and BSA (Fig. 6.14 and 6.26), were reported earlier for a β-barrel protein, namely, intestinal fatty acid-binding protein *(Modig et al. 2003)* Although the data were interpreted in terms of accumulation of an equilibrium folding intermediate, the authors mentioned in this connection the possibility of trapping of one or two previously short-lived water molecules by urea molecules in long-lived association with the protein *(Modig et al. 2003)*. Our studies strongly indicate that it is the effect of the denaturant on S_I, rather than the accumulation of folding intermediates, that is reflected by the data. Lysozyme is one of most well studied proteins, and there is no evidence for the accumulation of a folding intermediate at equilibrium. Similar pattern of variation of β with GdnHCl observed for other protein systems (unpublished results) provides a reasonable basis for the suggestion that protein stabilization mediated by the intra-molecular protein cross-linking action at low concentrations of denaturants is a general phenomenon. Relaxation dispersion measurements extended to other protein systems seem to be a rewarding exercise with a demonstrated potential to shed more light into the mode of action of denaturants.

Chapter 7

Summary and Conclusions

Advances in measuring relaxation rates at very low frequencies through innovative methodologies like field cycling technique have made the dynamic range of these experiments cover nearly five decades of frequency especially making it possible to focus on very low frequency dynamic processes. This work takes advantage of this capability to investigate slow dynamic processes. These investigations yielded profitably on various molecular processes like order director fluctuations (ODF), self diffusion (SD), and molecular reorientations (R) in the nematic phase, pre-transitional effects just below and above isotropic nematic transition in certain liquid crystals. An attempt is made to probe ^{19}F spin relaxation paths which are qualitatively different from proton by an appropriate choice of the liquid crystal system. This seems to be the first attempt to carry out NMRD study with different nuclei reporting differently about the dynamics of the same molecule. Further this technique is used to probe protein-denaturant interactions to understand protein folding paths and their stability.

In general terms, the results provided reasonable insight into the role of molecular structure on the dynamic organization of liquid crystals, sensitivity of spin-rotation interactions in probing novel slow processes in liquid crystals not reported by dipolar couplings, and finally the role of denaturants in initially stabilizing the tertiary structure of protein xxx earlier by other investigations.

The tow systems chosen for this purpose have interesting and fairly charecteristic and well time-scale separated dynamic phenomena. The interpretation of these detailed results require equally elaborate molecular dynamic models, whose applications can be satisfactorily tested by demands. Consistency of the experimental data with model parameters are the two dimensional space of both frequency and temperature. The present studies thus report such xxx in liquid crystal and protein solutions making use of the state of the art NMR methodology tailored for slow processes, and

applying very interesting models to interpret this data.

The PMRD studies on 4O.m liquid crystals proved to be successful in bridging the earlier high frequency studies in these systems with complimentary results. It is found that the cutoffs of ODF modes are sensitive to the end chain length (m) and lower cutoff wavelengths increase as the alkyl chain length increases. These studies bring out the effect of underlying layered smectic phases on the dynamic organization of nematic medium. The signatures of the presence of layered structure diminish as the order of the underlying smectic phase increases. It becomes transparent from the observations that in 4O.2, where the underlying S_B did not form cybotactic clusters in the nematic medium, unlike liquid crystals like 8OCB with underlying S_A phase, on the other hand it showed a R_1 dispersion similar to the case where there is no underlying smectic phase. In general in the homologous series the observed anisotropic physical properties show odd-even effects, but in the present case the cutoffs did not show such effect where as a monotonic variation of lower cutoff wavelength is observed as m-value goes from 2 to 4. The cutoffs observed in 4O.4 and the mixture of 4O.2 and 4O.4 are represented the nature of the underlying smectic phases in these samples.

Just below T_{NI} the fluctuations in the nematic order parameter are caused by the fluctuations in the magnitude of the long-range orientational order. The time scales of these nematic order parameter fluctuations and their slowing down, as the nematic phase stabilizes, are observed in 4O.m liquid crystals.

While the ^{1}H studies on 4OTOLFm and 4OFTOL are consistent with earlier studies in the isotropic phase showing the critical slowing down of short range nematic order fluctuations as T_{NI} is reached, the ^{19}F relaxation studies disclose a slow mechanism, which has qualitatively different temperature dependence in the experimental frequency range. In this context the emphasis is made on the presence of *single fluorine* on the core of liquid crystal molecule, noting that the only effective relaxation mechanism is due to the spin-rotation interaction. Data were analyzed classifying the dispersions into conventional region and overlapping region (altra low freqency, ¡0.5 MHz).

In the conventional region dispersion is sensitive to short range nematic order fluctuations in addition to a slower process modeled as cage dynamics (slowly relaxing local structures). Nuclear spins, coupled with lattice by Spin-rotation interaction, modulated by fluctuating torques provides the relaxation path in this case. Whereas the critical fluctuations of short range nematic order are prone to both the nuclei

^{1}H and ^{19}F. It is confirmed from the consistent data at different temperatures with comparable time scales obtained for this mechanism.

The two nuclei have nearly equal gyromagnetic ratios, and hence their line shapes overlap at low enough Larmor frequencies providing a cross relaxtion path. Such effects are clearly seen in the dispersion profiles below 500 kHz. This observation provides an opportunity to infer at least qualitatively about the changes in spectral line-widths near the phase transition. The temperature dependent studies of the relaxation rates further lend support to the models proposed in connection with the dispersion behaviour of the respective nuclei. In conclusion, singly fluorinated molecules in such complex fluids are seen to be exclusively sensitive to angular momentum time-correlations directly, and seem to offer a unique opportunity to probe very slow molecular processes, arising out of other cooperative modes in the system. The temperature dependant data showed in these results shows that below T_{NI} also this cooperative phenomenon provides the relaxation paths to 19F nuclei. This initial comparative study of the dynamics with multinuclear NMRD technique seems to indicate a new potential to probe new dynamic process which were not reflected in in the time modulation of dipolar interaction as is evidenced by the proton relaxation data.

The PMRD investigations, made on aqueous solutions of lysozyme and bovine serum albumin (BSA), in the presence of mild dosages of guanidine hydrogen chloride (GdnHCl), point out the increased orientational order of the interior waters in the protein. And further, in support of the well-known hydrophobic effect, these results seem to support the hypothesis of initial stiffening and stability of the protein at these small concentrations of denaturants. These results are inferred from a model dependent analysis of relaxation data, where the protein-water system is dynamically classified into three different time scales. The consistent correlation times obtained in the analysis and matching of these results with those obtained by complementary probes strongly support this hypothesis. The similar observations made on two different prototypes of protein samples here, in support of recent studies on protein-denaturant interactions, enforcing to conclude that the protein stiffening effect is general behaviour of all globular proteins.

In conclusion, nuclear spin-lattice relaxation measurements carried out over a wide frequency range, and supplemented with appropriate temperature dependent studies, seem to provide a powerful experimental probe to directly probe low frequency features of spectral densities of molecular dynamics in different soft materials. These experiments, supported by theoretical models of various molecular processes, prove

to be very valuable in informing on a variety of phenomena, characteristic of the materials investigated. In particular, the work reports a contrasting experiment wherein two very similar nuclei located on the same molecule report differently on the underlying processes, due to their differing sensitivity to the time correlation functions. These experiments indicate the possibility of exploring dynamic processes in different phase of the liquid crystal via angular momentum time correlations, and possibly uncovering molecular processes hitherto not reported through NMR techniques. In conclusion it is evidenced that the wide-dynamical range offered by NMR methods, coupled with detailed temperature dependent studies or in certain cases in support with the structural information are rich sources of dynamics in complex fluids. Correlating the physical properties with dynamics under the influence of external variable is a rewarding exercise. The strength of NMRD powered by field-cycling technique is highly appreciated in this context.

Bibliography

Abragam, A.: 1961, *The principles of nuclear magnetism*, Clarendon Press, Oxford.

Ahmad, A., Millett, I. S., Doniach, S., Uversky, N. V. and Flink, A. L.: 2004, Stimulation of insulin fibrillation by urea-induced intermediates, *J. Biol. Chem.* **279**, 14999–15013.

Ailion, D. C.: 1983, *Methods of Solid State Physics*, Vol. 21, Acadamic Press.

Alapati, P. R., Potukuchi, D. M., Rao, N. V. S., Pisipati, V. G. K. M., Paranjpe, A. S. and Rao, U. R. K.: 1988, Phase transition and structural investigations in 5O.5, 5O.6 and 5O.7, *Liq. Cryst* **3**, 1461.

Alben, R.: 1973, Phase transitions in a fluid of biaxial particles, *Phys. Rev. Lett.* **30**, 778.

Anoardo, E., Galli, G. and Ferrante, G.: 2001, Fast field cycling NMR: Applications and instrumentation, *Appl. Magn. Reson.* **20**, 365.

Bermann, A., Gelerinter, E., Frybury, G. C. and Brown, G. H.: 1973, *Liquid crystals and ordered fluids* **2**, 23.

Bhuyan, A. K.: 2002, Protein stabilization by urea and guanidine hydrochloride, *Biochemistry* **41**, 13386–13394.

Blicharska, B., Florkowski, Z., Hennel, J. W., Held, G. and Noack, F.: 1970, Investigation of protein hydration by proton spin relaxation time measurements, *Biochim. Biophys. Acta* **207**, 381.

Blinc, R., Hogenboom, D. L., O'Reilly, D. E. and Peterson, E. M.: 1969, Spin relaxation and self-diffusion in liquid crystals, *Phys. Rev. Lett.* **23**, 969.

Blinc, R., Luzar, M., Vilfan, M. and Burgar, M.: 1975, Proton spin lattice relaxation in smectic TBBA, *J. Chem. Phys.* **63**, 3445.

Blinc, R., Pirs, J. and Zupancic, I.: 1973, Measurements of self-diffusion in liquid crystals by a multi-pulse NMR method, *Phys. Rev. Lett.* **30**, 546.

Blinc, R., Vilfan, M., Luzar, M., Seliger, J. and Zagar, V.: 1978, Spin-lattice relaxation mechanisms in the smectic phases of TBBA, *J. Chem. Phys.* **68**, 303.

Blink, R.: 1976, NMR basic principles and progress, *Pintar M.M.* **13**, 97.

Bloch, F.: 1946, Nuclear induction, *Phy. Rev.* **70**(14), 460–474.

Bloembergen, N., Purcell, E. M. and Pound, R. V.: 1948, Relaxation effects in nuclear magnetic resonance absorption, *Pys. Rev* **73**, 679.

Breslow, R. and Guo, T.: 1990, Surface tension measurements show that chaotroppic salting in denaturants are not just water structure breakers, *Proc. Natl. Acad. Sci. USA* **87**, 167–169.

Brown, R. J. C., Gutowsky, H. S. and Shimomura, K.: 1963, *J. Chem. Phys.* **38**, 76.

Bruce, A., Johnson, A., Lewis, J., Raff, M., Roberts, K. and Walters, P.: 2002, *Molecular Biology of the Cell*, number ISBN 0-8153-3218-1., 4 edn, Garland Science, a member of the Taylor & Francis Group, New York and London.

Burrough, W. S.: 1961, *The soft mechine*, Nova trilogy, Olympia press, US.

Cabane, B.: 1972, *Adv. Vol. Relaxation Processes.* **3**, 341.

Cantor, R. C. and Schimmel, P. R.: 1980, *Biophysical Chemistry*, Vol. Vol.II, Freeman and Company, New York.

Carr, H. Y. and Purcell, E. M.: 1964, Effects of diffusion on free precession in nuclear magnetic resonance experiments, *Phys. Rev* **94**, 630.

Castellano, J. A.: 1991, Liquid crystal display applications past present & future, *Liquid crystals today* **1**, 1–4.

Catanescu, C. O., Chien, L. C. and Wu, S. T.: 2004b, High birefringence nematic liquid crystlas for display and telecom applications, *Mol. Cryst. Liq. Cryst.* **411**, 93–102.

Catanescu, C. O., Wu, S. T. and Chein, L. C.: 2004a, Tailoring the physical properties of some high birefringent isothiocyanato-based liquid crystals, *Liquid Crystals* **31**(4), 541–555.

Chandrasekar, S.: 1943, Liquid crystals, *Rev. Mod.Phys.* **15**, 1.

Chavez, F. V., Bonetto, F. and Pusiol, D. J.: 2000, Time scale of short range order fluctuation in the isotropic phase of butylcyano-phenylcyclohexane liquid crystal, *Chem. Phys. Lett.* **330**, 368–372.

Chenug, L., Mayer, R. B. and Gruler, H.: 1973, Measurements of nematic elastic constants near a second order nematic-smectic a phase change, *Phys. Rev. Lett.* **31**, 349.

Collings, P. J. and Patel, J. S.: 1997, *Handbook of Liquid Crystal Research*, Oxford Univ. Press, Oxford.

Company, M. W. T.: 1936, *British Patent* **441**, 274.

Cotter, M. A.: 1977, Consistency of mean field theories of nematic liquid crystals, *Mol. Cryst. Liq. Cryst.* **39**, 173.

Czub, J., Urban, S., Dabrowski, R. and Gestblom, B.: 2005, Dielectric properties of liquid crystalline isothiocyanato-tolane derivatives with fluorine atom at various lateral positions, *Acta Physica Polonica A* **107**, 947.

Dabrowski, R., Dziaduszck, J., ziolek, A., Szczucinski, L., Stolarz, Z., Sasnonski, G., Bezborodov, V., Lapanik, W., Gauza, S. and Wu, S. T.: 2007, Low viscosity high birefringence liquid crystalline compunds and mixtures, *Optoelectronics Review* **15**(1), 47.

de Gennes, P. G.: 1969, *J. Phys. Paris* **30**, C4.65.

de Gennes, P. G.: 1972, *Solid State Comm.* **10**, 753.

de Gennes, P. G.: 1974, *The Physics of Liquid Crystals*, Oxford University, New York.

Denisov, V. P. and Halle, B.: 1994, Dynamics of the internal and external hydration of globular proteins., *J. Am. Chem. Soc.* **116**, 10324.

Denisov, V. P. and Halle, B.: 1995a, Protein hydration dynamics in aqueous solution. a comparison of bovine pancreatic trypsin inhibitor and ubiquitin by ^{17}O spin relaxation dispersion, *J. Mol. Biol.* **245**, 682.

Denisov, V. P. and Halle, B.: 1995b, Hydrogen exchange and protein hydration. the deuteron spin relaxation dispersion of bpti and ubiquitin, *J. Mol. Biol.* **245**, 698.

Denisov, V. P. and Halle, B.: 1995c, Direct observation of calcium-coordinated water in calbindin D9k by nuclear magnetic relaxation dispersion, *J. Am. Chem. Soc.* **117**, 8456–8465.

Denisov, V. P. and Halle, B.: 1996, Protein hydration dynamics in aqueous solution, *Faraday Discuss.* **103**, 227–244.

Denisov, V. P., Jonsson, B. H. and Halle, B.: 1999, Hydration of denatured and molten globule proteins, *Nature structural biology* **6**, 253.

Denisov, V. P., Venu, K., Horlein, J. P. H. D. and Halle, B.: 1997, Orientational order and entropy of water in protein cavities, *J. Chem. Phys.* **101**, 9380–9389.

Deverell, C.: 1969, 31p nmr chemical shifts spin spin -rotation interaction and the absolute shielding of the 31p nucleus, *Molec. Phys.* **17**, 551.

Deverell, C.: 1970, Nuclear magnetic relaxation by spin-rotation interaction. determination of spin-rotation interaction constants from nuclear magnetic shielding constants, *Molec. Phys.* **18**, 319.

Doane, J. W., Golemme, A., Wats, J. L., Jr, J. G. W. and Wu, B. G.: 1987, Polymer dispersed liquid crystals for display applicaiton, *Mol. Cryst. Liq. Cryst.* . Papers in Honor of The 100th Anniversary of Liquid Crystal Research.

Dobson, C. M.: 1992, Unfolded proteins, compact states and molten globules, *Curr. Opin. Struct. Biol.* **2**, 6–12.

Dong, R. Y.: 1983, *Israel J. Chem.* **23**, 370.

Dong, R. Y.: 1994, *Nuclear magnetic resonance of liquid crystals*, Springer Verlag, New York.

Dunbar, J. H. P., Yennawar, S., Banerjee, J., Luo and Farbr, G. K.: 1997, The effect of denaturants in protein structure, *Protein Sci.* **6**, 1272–1733.

Efimova, Y. M., Haemers, S., Wierczinski, B., Norde, W. and vanWell, A.: 2007, Stability of globular proteins in h_2o and d_2o, *Biopolymers* **85**, 264–273.

Eigen, M.: 1964, Proton transfer, acid-base catalysis, and enzymatic hydrolysis. part 1:elementary processes., *Angew. Chemie (int. Ed.)* **3**, 1.

Elkadi, N., Taulier, N., LieHuerou, J. Y., Gindre, M., Urbach, W., Nwigwe, I., Khan, P. C. and Waks, M.: 2006, Unfolding and refolding of bovine serum albumin at acid ph: altra sound and structural studies, *Biophys. J* **106**, 088963.

Evans, P. A., Topping, K. D., Woolfson, D. N. and Dobson, C. M.: 1991, Hydrophobic clustering in nonnative states of a protein: interpretation of chemical shifts in NMR spectra of denatured states of lysozyme, *Proteins: Struct. Funct. Genet.* **9**, 248–266.

Faber, T. E.: 1982, *Proc. Roy. Soc. London Ser.* **A 375**, 579.

Fakushima, E. and Roeder, S. B. W.: 1981, *Experimental Pulsed NMR: A Nuts and Bolts Approach Reading*, Addision-Wesley, Massachusetts.

Farrar, T. C. and Becker, E. D.: 1971, *Pulsed and Fourier Transform NMR*, Academic Press, New York.

Flannery, J. B. J. and Haas, W.: 1970, Low-temperature mesomorphism in terminally substituted benzylidene anilines, *J. Phys. Chem.* **74**, 3611.

Frank, F. C.: 1958, *Disc. Faraday Soc.* **59**, 958.

Freed, J. H.: 1977, Stochastic-molecular theory of spin-relaxation for liquid crystals, *J. Chem. Phys.* **66**, 4183.

Freed, J. H.: 1994, *Molecular Dynamics of Liquid Crystals*, NATO Advancd Summer School. Edited by Luckhurst, G.R., and Veracini, C.A. (Kluwer, 1994), chap.12; J.H. Freed, A. Nayeem, and S.B. Rananavare, ibid., Chap.15. 1.

Freiser, M. J.: 1970, *Phys. Rev. Lett.* **24**, 1041.

Fryburg, G. C., Gelerinter, E. and Fishel, D. L.: 1972, *Mol. Cryst. Liq. Cryst.* **16**, 39.

Garland, C. W. and Stine, K.: 1987, *Proceedings of XII Liq. Cryst. Conf. Berkely.*

Gauza, S., Du, F., Wu, J. R., Wu, S. T., ad R Dabrowski, A. S., Janarthanan, N. and Hsu, C. S.: 2003b, High birefringence and low viscosity liquid crystal mixtures, *SID Symposium, Digest of Technical papers*, Vol. 34, p. 1054.

Gauza, S., Du, F., Wu, J. R., Wu, S. T. and Dabrowski, R.: 2003c, High birefringence and wide nematic range liquid crystal mixture, *Proc. SPIE* **5213**, 1.

Gauza, S., Parish, A., Wu, S. T., Spadlo, A. and Dabrowski, R.: 2008b, Fast switching near a s-n phase transition, *Liquid Crystal* **35**(6), 711–717.

Gauza, S., Parish, A., Wu, S. T., Spado, A. and Dabrowski, R.: 2008a, Physical properties of laterally flourinated isothiocynato phenyl-tolane liquid crystals, *Liquid Crystals* **35**, 4483.

Gauza, S., Wang, G., Wen, C. H. and Wu, S. T.: 2003a, High birefringence isothiocyanato tonlane liquid crystals, *Jap. J. App. Physics* **42**(64), 3463.

Gauza, S., Wen, C. H., Tan, B. and Wu, S. T.: 2004a, Uv stable high birefringence liquid crystals, *Jap. J. Appl. Phys.* **43**, 7176–7180.

Gauza, S., Wen, C. H., Wu, S. T., Dabrowski, R., Catanescu, C. S. H. C. O. and Chien, L. C.: 2005b, High birefringence liquid crystals for photonic applications, *Proceedings of SPIE* **5947**(594706), 1–14. International Society for optical engineering.

Gauza, S., Wu, J. R., Spadlo, A., Dabrowski, R., Janarthanan, N., Hsu, C. S., Catanescu, O. C. and Chien, L. C.: 2004b, Molecular engineering of high-birefringence liquid crystlas, *Proceedings of SPIE,* **5565**, 159.

Gauza, S., Zhu, X., Wu, S. T., Piecek, W. and Dabrowski, R.: 2007b, High birefringence liquid crystals for colour-sequential lcds, *SID international Symposium, Digest of technical papers*, Vol. 38, pp. 142–145.

Gauza, S., Ziao, Y., Lecor, T. and Wu, S. T.: 2007c, High figure of merit laterally fluorinated biphenyl tolane-isothiocyanates, *Mol. Cryst. Liq. Cryst.* **479**, 169/1207 – 179/1217.

Gay, J. G. and Berne, B. J.: 1981, Modification of the overlap potential to mimic a linear site-site potential, *J. Chem. Phys.* **74**, 3316–3319.

Ghosh, S. K., Tettamanti, E. and panatta, A.: 1980, Dynamic critical behaviour in nematic liquid crystals above the nematic-isotropic transition, *Phys. Rev. B.* **21**, 1194.

Goldman, M.: 1970, *Spin temperature and nuclear magnetic resonance in solids*, Vol. 51, Oxford, England.

Goodby, J. W., Gray, G. W., Leadbetter, A. L. and Mazid, M. A.: 1980, *Liquid crystals of one and two dimensional order*, Springer Verlag,New York.

Gordon and Breach: 1967, *Collected papers of L. D. Landau*, Science Publisher, 2nd Edition, New York.

Goto, Y., Takahashi, N. and Fink, A. L.: 1990, Mechanism of acid-induced folding of proteins, *Biochemistry* **29**, 3480–3488.

Gramsbergen, E. F., Longa, L. and de Jeu, W. H.: 1986, *Phys. Rep.* **135**, 195.

Gray, G. W.: 1979, *The molecular physics of liquid crystals Ed Luckhurst G R and Gray G W*, Academic Press.

Green, D. K. and Powles, J. G.: 1965, Nuclear spin-lattice relasation, including the spin-rotation interaction, in liquid benzene and several benzene derivatives up to the critical temperature, *Proc. Phys. Soc.* **85**, 87.

Greenfield, S., Coates, D., Brown, E. and Hittich, R.: 1993, Laterally fluorinated tolanes of low melting point liquid crystals, *Liquid Crystals* **13**(2), 301.

Grosch, L. and Noack, F.: 1976, Nmr relaxation investigation of water mobility in aqueous bovine serum albumin solutions, *Biochimica et Biophysica Acta.* **453**, 218–232.

Group, L. C. O.: 1971, Simplified elastic theory for smectic c, *Solid state commun.* **9**, 653.

Gupta, C. D.: 1995, Numerical studies of phase transitions and critical phenomena in liquid crystals, *Int. J. Mod Phys. 9B* **48**, 2219.

Hagihara, Y., Aimoto, S., Fink, A. L. and Goto, Y. J.: 1983, Guanidine-hydrochloride induced foldig of proteins, *J. Mol. Biol.* **231**, 180–184.

Hahn, E. L.: 1950, *Phys. Rev.* **B80**, 580.

Halle, B. and Denisov, V. P.: 2001, Magnetic relaxation dispersion studies of biomolecular solutions, *Methods Enzymol.* **338**, 178–201.

Halle, B., Denisov, V. P. and Venu, K.: 1999, Multinuclear relaxation dispersion studies of protein hydration, *Biological Magnetic Resonance (Krishna, N.R. and Berliner, J.Jl, Eds.)* **17**(Kluwer Academic/Plenum Publisher, New York), 419–484.

Halle, B., Johannesson, H. and Venu, K.: 1998, Model free analysis of stretched relaxation dispersions, *J. Magn. Reson.* **135**, 1–13.

Halle, B. and Wennerstrom, H.: 1981, *J. Magn. Reson.* **44**, 89.

Haller, I. and Litster, J. D.: 1970, Temperature dependence of normal modes in a nematic liquid crystal, *Phys. Rev. Lett.* **25**, 1550.

Harmon, J. F. and Muller, B. N.: 1969, Nuclear spin relaxation by translational diffusion in liquid ethane, *Phys. Rev.* **182**, 400.

Heilmeier, G. H., Barton, L. A. and Zanoni, L. A.: 1968, *Appl. Phys. Lett.* **13**, 46.

Heilmeier, G. H., Castellano, G. A. and Zanoni, L. A.: 1969a, *Mol. Cryst. Liq. Cryst.* **8**, 293.

Heilmeier and Goldmacher, J. E.: 1969b, *Proc. IFEEE* **57**, 34.

Hibbard, L. S. and Tulisky, A.: 1978, Expression of functioality of alpha-chimotripsin. E ffects of guanidine hydrochloride and urea on the onset of denaturation, *Biochemistry* **17**, 5460–5468.

Hsu, C. S., Gauza, S. and Wu, S. T.: 2006, Synthesis and mesomarphic properties of fluoro and isothiocyanato biphenyl tolane liquid crystals, *Liquid Crystals* **33**, 1199.

Hubbard, P. S.: 1963, Theory of nuclear magnetic relaxation by spin-rotational interactions in liquids, *Phys. Rev* **131**, 1155.

Ibarra-Molero, B., Loladze, V. V., Makhatadze, G. I. and Sanchez-Ruiz, J. M.: 1999a, Thermal versus guanidine-induced unfolding of ubiquitin: An analysis in terms of the contributions from chargecharge interactions to protein stability., *Biochemistry* **38**, 8138–8149.

Ibarra-Molero, B., Makhatadze, G. I. and SanchezRuiz, J. M.: 1999b, Cold denaturation of ubiquitin., *Biochim. Biophys. Acta.* **1429**, 384.

Kiihne, H. and Bryant., R. G.: 2000, Protein-bound water molecule counting by resolution of ^{1}H spin-lattice relaxation mechanisms, *Bio. Phys. J.* **78**, 2163.

Kimmich, R. and Anardo, P.: 2004, Field cycling nmr relaxometry, *Prog.Nulcl. Magn. Reson. Spectrosc.* **44**, 257.

Kimmich, R. and Noack, F.: 1970, Kernmagnetische relaxation in proteinlsungen(nuclear magnetic relaxation in protein solutions), *Z. Natureforsch* **25a**, 299–301.

Knubovets, T., Osterhout, J. J., Connolly, P. J. and Klibanov, A. M.: 1999, Structure, thermostability, and conformational flexibility of hen egg-white lysozyme dissolved in glycerol, *Proc. Natl. Acad. Sci. USA* **96**, 1262–1267.

Koenig, S. H.: 1969, Classes of hydration sites at protein-water interfaces: The source of contrast in magnetic resonance imaging, *Biophys. J.* **69**, 593.

Koenig, S. H. and Brown, R. D. I.: 1992, Molecular theory of relaxation and magnetization transfer: Appication to cross-linked bsa, amodel fro tissue, *Magn. Reson. Medicine* **30**, 685–695.

Kovrigin, E. L. and Potekhin, S. A.: 1999, On stabilizig action of protein denaturants: acetonitril effects on stability of lysozyme in aqueous solutions, *Biophysical Chemistry* **83**, 45.

Krieger, T. J. and James, H. M.: 1954, Successive orientational transitions in crystals, *J. Chem. Phys.* **22**, 796.

Kruger, G. J.: 1982, *Phys. Rep.* **82**, 229.

Kruger, G. J. and Spiesecke, H.: 1973, *Z. Natureforsch.* **28a**, 964.

Kubo, R. and Tomita, K.: 1954, *J.Phys. Soc. Jpn.* **9**, 888.

Kumar, R. and Bhuyan, A. K.: 2004, Two state folding of horse ferrocytochrome c: analyses of linear free energy relationship, chevron curvatture, and stopped flow burst relaxation kinetics, *Biochemistry* **44**, 3024–3033.

Kuwajima, K., Hiraoka, Y., Ikeguchi, M. and Sugai, S.: 1985, Comparison of the transient folding intermediates in lysozyme and alpha lactalbumin, *Biochemistry* **24**, 874–881.

Landau, L. D.: 1937, *Phys. Z Sowjefunion* **11**, 26.

Landau, L. D. and Lifshitz, E. M.: 1980, *Statistical Physics*, Vol. 1, 3rd edition edn, Pergamon, Oxford.

Lebwohl, P. A. and Lasher, G.: 1972, Nematic liquid crystal ordera monte carlo calculation, *Phys. Rev. A* **6**, 426–429.

Lei, L.: 1982, *Jphysis (paris)* **43**, 251.

Leslie, F. M.: 1968., *Arch. Ration. Mech. Anal.* **28**, 265–283.

Liepinsh, E. and Otting, G.: 1996, Proton exchange rates from amino acid side chains-implications for image contrast, *Magn. Reson. Med.* **35**, 30–42.

Limmer, S., Schiffler, J. and Findeison, M.: 1984, Proton NMR studies of smectic phases of three n-(4-n-alkyloxy benzylidene)-4'-alkylanilines(nO.m's), *J. de Phys.* **45**, 1149.

Lipari, F. and Szabo, A.: 1982, *J.Am. Chem. Soc.* **104**, 4546–4559.

Lu, Y. Q., Du, F., Lin, Y. H. and Wu, S. T.: 2004, Variable optical attenuator based on polymer stabilized twisted nematic liquid crystal, *Optics Express* **12**(7), 1221.

Luckhurst, G. R.: 1979, *Molecular field theories of nematics*, Acad. Press, New York,. Molecular Physics of Liquid Crystals Ed. G R Luckhurst and G W Gray.

Luckhurst, G. R. and Zannoni, C.: 1977, Why is the maier-saupe theory of nematic liquid crystals so successful, *Nature* **267**, 412.

Lumb, K. J. and Dobson, C. M.: 1992, ^{1}H nuclear magnetic resonance studies fo the interaction of urea with hen lysozyme, *J. Mol. Biol.* **227**, 9–14.

Mahmood, R., Khan, I., Gooden, C., Baldwin, C., Johnson, D. L. and Neubert, M. E.: 1985, Light - scattering study of director dynamics above the nematic - smectic - A phase transition, *Phys. Rev. A* **32**, 1286.

Maier, W. and Saupe, A.: 1959, *Z. Naturforsch.* **14a**, 882.

Maier, W. and Saupe, A.: 1960, *Z. Naturforsch.* **15a**, 287.

Makhatadze, G. I., Lopez, M. M., Richardson, J. M. and Thomas, S. T.: 1998, Anion binding to ubiquitin molecule, *Protein Sci.* **7**, 689–697.

Makhatadze, G. I. and Privalov, P. L.: 1992, Protein interactions with urea and guanidinium chloride, *J.Mol.Biol.* **226**, 491–505.

Mande, S. C. and Sobhia, M. E.: 2000, Structural characterization of protein denaturant interactions: crystal structures of hen egg-white lysozyme in complex with DMSO and guanidinium chloride, *Protein Engineering* **13**, 133–141.

Mauguin, C.: 1911, *Bull. Soc. fr. Min.* **34**, 71.

Mayr, L. M. and Schmid, F. X.: 1993, Stabilization of a protein by guanidine chloride, *Biochemistry* **32**, 7994–7998.

Meiboom, S. and Gill, D.: 1958, *Rev. Sci. Instrum.* **29**, 6881.

Miechle, M. and Garland, C. W.: 1983, calorimetric study of the smectic-A - smetic-C phase transition in liquid crystals, *Phs. Rev. A* **27**, 2624.

Mitra, S., Mukhopadhyay, R. and Venu, K.: 2000, Molecular motions in a liquid crystal BBBA (4O.4): QENS study, *Chem. Phys.* **261**, 149.

Mitra, S., Venu, K., Tsukushi, I., Ikeda, S. and Mukhopadhyay, R.: 2004, Molecular reorientations in liquid crystals pentyloxy benzylidine hexylanilene (PBHA) and butyloxy benzylidine octylanilene (BBOA), *Phys. rev. E.* **69**, 061709.

Modig, K., G, E. K. F., Prendergast and Halle, B.: 2003, Water and urea interactions with the native and unfolded forms of a beta-barrel protein, *Protein Sci.* **12**, 2768–2781.

Monera, O. D., Kay, C. M. and Hodges, R. S.: 1994, Protein denaturation with guanidine hydrochloride or urea provides different estimates of stability depending on the contribution of electro static interactions, *Protein Sci.* **3**, 1984–1991.

Moore, T. C., Kubo, A. L., Mathews, R. C., Wade, C. G., Tarr, C. E. and field, M. E.: 1980, *J. Magn. Reson.* **38**, 135.

Morjana, N. A., Mckeone, B. J. and Gillbert, H. F.: 1993, Guanidine hydrochoride stabilization of partially unfolded intermediate during the reversible denaturation of protein disulfide isomerase, *Proc. Natl. Acad. Sci. USA* **90**, 2107–2111.

Morozova, L. A., Haynie, D. T., AricoMuendel, C., Dael, H. V. and Dobson, C. M.: 1995, Structural basis of the stability of a lysozyme molten globule, *Nat. Struct. Biol* **2**, 871–875.

Mugele, T., Graff, V., Wolfel, W. and Noack, F.: 1980, *Springer ser.Chem.Phys.* **11**, 88.

Murase, K.: 1971, *Bull. Chem. Soc. Jpn.* **45**, 1772.

Nagabhushan, C., Geetha, G., Nair, R. and Ratna, R.: 1988, dielectric studies of the hexatic B-smecticA and crystals B-smecticA transitions, *Liq. Cryst* **3**, 175.

Nagel, G., Wolfel, W. and Noack, F.: 1983, *Ksrael J. Chem.* **23**, 380.

Noack, F.: 1984, Nmr studies of self - diffusion in some hologous nematic liquid crystals, *Mol. Cryst. Liq. Cryst.* **113**, 247.

Noack, F.: 1986, NMR field cycling spectroscopy principles and applications, *Prog. Nucl. Mag. Reson. Spectrosc.* **18**, 171.

Norrido, P. L. and Segre, V.: 1979, *The Molecular Physics of liquid crystals*, Academic press,New York.

Onsager, L.: 1949, *Ann. N.Y. Acad. Sci* **51**, 627.

Pace, C. N., Alston, R. W. and Shaw, K. L.: 2000, Charge-charge interactions influence the denatured state ensemble and contribute to protein stability, *Protein Sci.* **9**(7), 1395–1398.

Pace, C. N. and Grimsley, G. R.: 1988, Ribinuclease t1 is stabilized by cation and anion binding, *Biochemistry* **27**, 3242–3246.

Pacini, P. and Zannoni, C.: 1998, *Advances in the Computer Simulations of Liquid Crystals*, Vol. 545 of *NATO Science series*, Proceedings of the NATO Advanced Study Institute.

Pauling, L. and Corey, R. B.: 1951, Configurations of polypeptide chains with favored orientations of the polypeptide around single bonds: Two pleated sheets, *Proc. Natl. Acad. Sci. Washington* **37**, 729–740.

Pauling, L., Corey, R. B. and Branson, H. R.: 1951, Two hydrogen-bonded helical configurations of the polypeptide chain, *Proc. Natl. Acad. Sci. Washington* **37**(205), 211.

Phanikumar, B. V. N.: 2003, *Ph.D.Thesis*, University of Hyderaabad, India.

Phanikumar, B. V. N., Satheesh, V., Venu, K., Sastry, V. S. S. and Dabrowski, R.: 1998, Study of nematic and smectic order fluctuations in the nematic phase through proton magnetic relaxometry, *Phase transitions* .

Piculell, L. and Halle, B.: 1986, Water spin relaxation in colloidal systems part2: ^{1}7O ^{2}H relaxation in protein solutions, *J. Chem. Soc., Faraday Trans. 1* **82**, 401.

Pike, W. C. A. and Acharya, R.: 1994, A structural basis for the interaction of urea with lysozyme, *Protein Sci.* **3**, 706–710.

Pincus, P.: 1969, Nuclear relaxaqtion in nematic liquid crystals, *Solid State Commun.* **7**, 415.

Pisipati, V. G. K. M., Rannavare, S. B. and Freed, J. H.: 1987, *Mol. Cryst. Liq. Cryst.* **4**, 181.

Pohl, L., Eidenschink, R., Krause, G. and Erdmann, D.: 1977, *Phys. Lett. A.* **60**, 421–23.

Pohl, L., Eidenschink, R., Krause, G. and Weber, G.: 1978, *Phys. Lett. A* **65**, 169–172.

Potukuchi, D. M.: 1989, *Ph.D.Thesis*, Nagarjuna University,India.

Press, W. H., Teukolsky, S. A., Vetterling, W. T. and Flannery, B. P.: 1992, *Numerical Recipes in C: the art of scientific computing*, 2nd edn, Cambridge University Press.

Priestly, E. B., Wojtowicz, P. J. and Sheng, P.: 1975, *Introduction to liquid crystals*, Plenum Press, New York.

Pushnik, F. and Schara, M.: 1976, *Chem. Phys. Lett.* **37**, 106.

Pushnik, F., Schara, M. and Sentjure, M.: 1975, EPR study of thge orientational order and molecular dynamics in the smectic-A and smectic-B phase of a liquid crystal, *J.Phys.(Paris)* **35**, 665.

Pusiol, D. J. and Chavez, F. V.: 1999, Nmr study of the director fluctuations coherence length in the nematic phase of butylcyano-phenyl chclohexane, *Chem. Phys. Lett.* **312**, 91–95.

Radford, S. E., Dobson, C. M. and Evans, P. A.: 1992, The folding of hen lysozyme inv9olves partially structured intermediates and multiple pathways, *Nature* **358**, 302–307.

Ramsey, N. F.: 1950, *Phys. Rev.* **78**, 699.

Ramsey, N. F.: 1956, *Molecular beams*, Oxford University Press, New York.

Ramsey, N. F.: 1961, *Am. Scient.* **49**, 509.

Rannavare, S. B., Pisipati, V. G. K. M. and Freed, J. H.: 1987, *Chem. Phys. Lett.* **140**, 225.

Rannavare, S. B., Pisipati, V. G. K. M. and Freed, J. H.: 1988, ESR. and DSC investigation of phase transitions in polymorphic 4-n-alkoxybenzylidene-4-n-alkylanilines, *Liq. Cryst* **3**, 957.

Ravindranath, G.: 1991, *Ph.D. Thesis*, Uiversity of Hyderabad,India.

Rebeirio, A. C.: 1987, Molecular dynamics in a partial bilayer smectic a phase by proton nmr relaxation, *Mol. Cryst. Liq. Cryst.* **151**, 261.

Redfield, A. G.: 1965, *Adv. Magn. Reson.* **1**, 1.

Ren, H., Lin, Y. H., Fan, Y. H. S. and Wu, S. T.: 2004, In plane switching liquid crystal gel for polarization independent light switch, *J. App.Phys.* **96**, 3609.

Richardson, R. M., Leadbetter, A. J., Hayter, J. B., Sterling, W. G., Gray, G. W. and Tajbadhsh, A.: 1984, *J. d. Phys.* **45**, 106.

Robinson, D. R. and Jencks, W. P.: 1965, The effect of compunds of urea-duanidinium class on the activity coefficient of acetyltetraglycine ethyl ester and related compounds, *J.Am. Chem. Soc.* **87**, 2462–2470.

Rosenblatt, C. and Ho, J. T.: 1983, *J. Phys.* **44**, 1383.

Sailaja, A. S.: 1994, *Ph.D. Thesis*, University of Hyderabad,India.

Sastry, V. S. S., Polimeno, A., Crepeau, R. H. and Freed, J. H.: 1996a, Studies of spin relaxation and molecular dynamics in liquid crystals, *J. Chem. Phys.* **105**, 5753.

Sastry, V. S. S., Polimeno, A., Crepeau, R. H. and Freed, J. H.: 1996b, Studies of spin relaxation and molecular dynamics in liquid crystals, *J. Chem. Phys.* **105**, 5773.

Satheesh, V.: 2000, *Ph.D.Thesis*, University of Hyderabad.

Satheesh, V., PhaniKumar, B. V. N., Venu, K. and Sastry, V. S. S.: 1999, *Solid State Physics, India* **41**, 167.

Schellman, J. A.: 1978, Solvent denaturation, *Biopolymers* **17**, 1305–1322.

Schellman, J. A.: 1987, The thermodynamic stability of proteins, *Annu. Rev. Biophys. chem.* **15**, 115–137.

Schmiedel, H., Hillner, B., Grande, S., Losche, A. and Limmer, S.: 1980, *J. Mag. Reson.* **40**, 369.

Schweikert, K. H. and Noack, F.: 1989, *Z. naturforsch* **44a**, 597.

Sheng, P. and Priestley, E. B.: 1974, *Introduction to Liquid Crystals*, Plenum, New York.

Shortle, D.: 1993, Denatured states of proteins and their roles in folding and stability, *Curr. Opin. Struct. Biol.* **3**, 66–74.

Singh, S.: 2000, Phase transitions in liquid crystals, *Physics Reports* **324**, 107–269.

Singh, Y.: 1991, *Phys. Rep.* **207**, 351.

Slichter, C. P.: 1978, *Principles of Magnetic Resonance*, 2nd edn, Springer-Verlag, Berlin.

Smith, G. W. and Gardlund, Z. G.: 1973, Liquid crystalline phases in a doubly homologous series of benzeledene anilines-textures and scaning calorimetry, *J. Chem. Phys.* **59**, 3214.

Solomon, I.: 1955, relaxation processes in a system of two spins, *Phys. Rev.* **99**, 559.

Stegemeyer, H., Blumel, T., Hiltrop, K., Onusseit, H. and Porsch, F.: 1986, Thermodynamic structural and morphological studies on liquid - crystalline blue phases, *Liq. Cryst.* **1**, 3.

Stephen, M. J. and Stratey, J. P.: 1974, Physics of liquid crystals, *Rev. Mod. Phys.* **46**, 617.

Stinson, T. W. I. and Lister, J. D.: 1973, Correlation range of fluctuations of short - range order in the isotropic phase of a liquid crystal, *Phys. Rev. Lett.* **30**, 688.

Stinson, T. W. I. and Litster, J. D.: 1970, Pretransitional phenomena in the isotropic phase of a nematic liquid crystal, *Phys. Rev. Lett.* **25**, 503.

Struppe, J. and Noack, F.: 1996, Angular and frequency dependent spin relaxation study of liquid crystalline cyanobiphenyls, *Liq. Cryst.* **20**, 595.

Suzanne, K. and Bryant, R. G.: 2000, Protein-bound water molecule counting by resolution of ^{1}H spin-lattice relaxation mechanism., *Biophysical Journal* **78**, 2613–2169.

Takahashi, M., Mita, S. and Kondo, S.: 1987a, On the even-odd effect of volume changes at I/N and N/S_A transitions, *Mol. Cryst. Liq. Cryst.* **147**, 99.

Takahashi, M., Mita, S. and Kondo, S.: 1987b, Birefringence study of the nematic-smectic a phase transition of n-(4-n-pentyloxybenzylidene)-4-n-alkylaniline (5O.m), *Phase Transitions* **9**, 1–10.

Tanford, C., Aune, D. C. and Ikai, A.: 1973, Kinetics of unfolding and refolding of proteins. iii. Results for lysozyme, *J. Mol. Biol.* **73**, 185–197.

Thompson, R. T., Kydon, D. W. and Pintar, M. M.: 1977, Study of molecular dynamics in a homologous liquid crystal series by nuclear spin thermodynamics, *J. Chem. Phys.* **67**, 5914.

Timasheff, S. N.: 1992, Water as ligand: preferential binding and exclusion of denaturants in protein unfolding, *Biochemistry* **31**, 9857–9864.

Torrey, H. C.: 1953, Nuclear spin relaxation by translational diffusion, *Phys. Rev.* **92**, 962.

van der Klink, J. J., Schriever, J. and Leyte, J.: 1974, *Ber. Bunsenges. Phys. Chem.* **78**, 369.

Venu, K.: 1985, *Ph.D.Thesis*, University of Hyderabad, India.

Venu, K., Denisov, V. P. and Halle, B.: 1997, Water ^{1}H magnetic relaxation dispersion in protein solutions. a quantitative assessment of internal hydration, proton exchange and cross relaxation, *J. Am. Chem. Soc.* **119**, 3122–3134.

Venu, K. and Sastry, V. S. S.: 1998, *Symposium on Field Cycling Relaxometry (Techniques, applications and Theories).*

Venu, K. and Sastry, V. S. S.: 1999, Smectic order fluctuations and nematic phase stability: Nuclear magnetic relaxation dispersion studies, *Solid State Physics, India* **42**, 15.

Vilfan, M. and Zumer, S.: 1980, Theory of nuclear - spin relaxation by translational self-diffusion in liquid crystals: Smectic-a phase, *Phys. Rev.* **A21**, 672.

Vold, R. R. and Vold, R. L.: 1988, *J. Chem. Phys.* **88**.

Vold, R. R. and Vold, R. L.: 1989, *Molecular dynamics of Liquid Crystals*, NATO Advancd Summer School.

Wade, C. G.: 1977, Nmr relaxation in thermotropic liquid crystals, *Ann.Rev.Phus.Chem.* **28**, 47. and the references given therein.

Wagsness, R. K. and Bloch, F.: 1953, The dynamical theory of nuclear induction, *Phys. Rev.* **89**, 728.

Wen, C. H., Fan, Y. H., Wu, S. T., Dabrowski, R., Catanescu, C. O. and Chien, L. C.: 2003, Side chain effects on high birefringence liquid crystals, *Proc.SPIE* **4658**, 28.

Wen, C. H., Gauza, S., Li, J., Wu, S. T., Wang, H. and Liang, X.: 2005, High contrast homeotropic allignment of difluoro tolane, *SID international Symposium, Digest of technical papers*, Vol. 36, pp. 1466–1469.

Widom, B.: 1963, Some topics in the theory of fluids, *J. Chem. Phys.* **39**, 2808.

Wildegger, G. and Kiefahber, T.: 1997, Three state model for lysozyme folding; triangular folding mechanism with an energetically trapped intermediate, *J. Mol. Biol.* **270**, 294–304.

Woessner, D. E. and Snowden, B. S.: 1970, Pulsed nmr study of water in agar gels, *Colloid Interface Sci.* **34**, 290.

Wolf, D.: 1979, *Spin temperture and nuclear spin lattice relaxation in matter*, Clarendon Press, Oxford.

Wolfel, W., Noack, F. and Stohrer, M.: 1975, *Z. naturforsch* **30a**, 437.

Wright, D. C. and Mermin, N. D.: (1989), Crystalline liquids: the blue phases, *Rev. Mod. Phys.* **61**, 385.

Wu, S. T.: 1997, Laterally fluorinated liquid crystals for display applications, *SPIE* **3015**, 8.

Wu, S. T.: 1998, Fast response liquid crystals for electro optic applications, *SPIE* **3421**, 142.

Wu, S. T.: 2001, High birefringence liquid crystals for laser beam stearing, *The annual AIAA/BMDO technology conference[10th], Unclassified Proceedings*, Vol. 1, Williamsburg, Virginia.

Wu, S. T.: 2002, Molecular design strategies for high birefringence liquid crystals, *Material Research Society Symposium - Proceedings*, Vol. 709, pp. 219–228.

Zumer, S. and Vilfan, M.: 1978, Theory of nuclear spin relaxation by translational self - diffusion in liquid crystals: Nematic phase, *Phys. Rev.* **A17**, 424.

Zupancic, I., Pirs, I., Luzar, M., Blicn, R. and Doane, J. W.: 1974, Anisotropy of the self - diffusion tensor in nemcatic MBBA, *Solid State Commun.* **15**, 227.